3-1-96 JSC

December 1995 • NREL/TP-442-6474

Effects of Surface Roughness and Vortex Generators on the LS(1)-0417MOD Airfoil

R. L. Reuss
M. J. Hoffman
G. M. Gregorek
The Ohio State University
Columbus, Ohio

National Renewable Energy Laboratory
1617 Cole Boulevard
Golden, Colorado 80401-3393
A national laboratory of the U.S. Department of Energy
Managed by Midwest Research Institute
for the U.S. Department of Energy
under Contract No. DE-AC36-83CH10093

MASTER

DISTRIBUTION OF THIS DOCUMENT IS UNLIMITED

NREL/TP-442-6474 • UC Category: 1211 • DE96000495

Effects of Surface Roughness and Vortex Generators on the LS(1)-0417MOD Airfoil

R. L. Reuss
M. J. Hoffman
G. M. Gregorek
The Ohio State University
Columbus, Ohio

NREL Technical Monitor:
C. P. Butterfield

MASTER

National Renewable Energy Laboratory
1617 Cole Boulevard
Golden, Colorado 80401-3393
A national laboratory of the U.S. Department of Energy
Managed by Midwest Research Institute
for the U.S. Department of Energy
under contract No. DE-AC36-83CH10093

Prepared under Subcontract No. XF-1-11009-3

December 1995

DISTRIBUTION OF THIS DOCUMENT IS UNLIMITED

NOTICE

This report was prepared as an account of work sponsored by an agency of the United States government. Neither the United States government nor any agency thereof, nor any of their employees, makes any warranty, express or implied, or assumes any legal liability or responsibility for the accuracy, completeness, or usefulness of any information, apparatus, product, or process disclosed, or represents that its use would not infringe privately owned rights. Reference herein to any specific commercial product, process, or service by trade name, trademark, manufacturer, or otherwise does not necessarily constitute or imply its endorsement, recommendation, or favoring by the United States government or any agency thereof. The views and opinions of authors expressed herein do not necessarily state or reflect those of the United States government or any agency thereof.

Available to DOE and DOE contractors from:
Office of Scientific and Technical Information (OSTI)
P.O. Box 62
Oak Ridge, TN 37831
Prices available by calling (615) 576-8401

Available to the public from:
National Technical Information Service (NTIS)
U.S. Department of Commerce
5285 Port Royal Road
Springfield, VA 22161
(703) 487-4650

Printed on paper containing at least 50% wastepaper, including 10% postconsumer waste

Foreword

Airfoils for wind turbines have been selected by comparing data from different wind tunnels, tested under different conditions, making it difficult to make accurate comparisons. Most wind tunnel data sets do not contain airfoil performance in stall commonly experienced by turbines operating in the field. Wind turbines commonly experience extreme roughness for which there is very little data. Finally, recent tests have shown that dynamic stall is a common occurrence for most wind turbines operating in yawed, stall or turbulent conditions. Very little dynamic stall data exists for the airfoils of interest to a wind turbine designer. In summary, very little airfoil performance data exists which is appropriate for wind turbine design.

Recognizing the need for a wind turbine airfoil performance data base, the National Renewable Energy Laboratory (NREL), funded by the U.S. Department of Energy, awarded a contract to Ohio State University (OSU) to conduct a wind tunnel test program. Under this program, OSU tested a series of popular wind turbine airfoils. A standard test matrix was developed to assure that each airfoil was tested under the same conditions. The test matrix was developed in partnership with industry and is intended to include all of the operating conditions experienced by wind turbines. These conditions include airfoil performance at high angles of attack, rough leading edge (bug simulation), steady and unsteady angles of attack.

Special care has been taken to report as much of the test conditions and raw data as practical so that designers can make their own comparisons and focus on details of the data relevant to their design goals. Some of the airfoil coordinates are proprietary to NREL or an industry partner. To protect the information which defines the exact shape of the airfoil, the coordinates have not been included in the report. Instructions on how to obtain these coordinates may be obtained by contacting C.P. (Sandy) Butterfield at NREL.

C. P. (Sandy) Butterfield
Wind Technology Division
National Renewable Energy Laboratory
1617 Cole Boulevard
Golden, Colorado 80401 USA
Internet Address: Sandy_Butterfield@NREL.GOV
Phone: 303-384-6902
FAX: 303-384-6901

Abstract

Wind turbines in the field can be subjected to many and varying wind conditions, including high winds with the rotor locked or with yaw excursions. In some cases, the rotor blades may be subjected to unusually large angles of attack that possibly result in unexpected loads and deflections. To better understand loadings at unusual angles of attack, a wind tunnel test was performed.

An 18-inch constant-chord model of the LS(1)-0417MOD airfoil section was tested under two dimensional steady state conditions in the Ohio State University Aeronautical and Astronautical Research Laboratory 7x10 Subsonic Wind Tunnel. The objective of these tests was to document section lift and moment characteristics under various model and air flow conditions. Surface pressure data was acquired at -60° through +230° geometric angles of attack, at a nominal 1 million Reynolds number. Cases with and without leading edge grit roughness were investigated. The leading edge roughness was used to simulate blade conditions encountered on wind turbines in the field. Additionally, surface pressure data were acquired for Reynolds numbers of 1.5 and 2.0 million, with and without leading edge grit roughness; the angle of attack was limited to a -20° to 40° range.

In general, results showed lift curve slope sensitivities to Reynolds number and roughness. The maximum lift coefficient was reduced as much as 29% by leading edge roughness. Moment coefficient showed little sensitivity to roughness beyond 50° angle of attack, but the expected decambering effect of a thicker boundary layer with roughness did show at lower angles.

Tests also were conducted with vortex generators located at the 30% chord location on the upper surface only, at 1 and 1.5 million Reynolds numbers, with and without leading edge grit roughness. In general, with leading edge grit roughness applied, the vortex generators restored 85 percent of the baseline level of maximum lift coefficient but with a more sudden stall break and at a higher angle of attack than the baseline.

Table of Contents

Page

List of Symbols vii

Acknowledgements viii

Introduction 1

Test Facility 2

Model Details 3

Test Equipment and Procedures 6
- Data Acquisition 6
- Data Reduction 7
- Test Matrix 7

Results and Discussion 8

Summary 12

Appendix A: Model and Surface Pressure Tap Coordinates A-1

Appendix B: Integrated Coefficients and Pressure Distributions B-1

List of Figures

Page

1. OSU/AARL 7x10 Subsonic Wind Tunnel 2
2. LS(1)-0417MOD Airfoil Section 3
3. Model Design 3
4. Roughness Pattern 4
5. Vortex Generator Geometry 5
6. Data Acquisition Schematic 6
7. C_l vs α, Extended Range 8
8. $C_{m\frac{1}{4}}$ vs α, Extended Range 8
9. C_{dp} vs α, Extended Range 9
10. C_l vs α, Clean 9
11. C_l vs α, LEGR, k/c=0.0019 9
12. $C_{m\frac{1}{4}}$ vs α, Clean 10
13. $C_{m\frac{1}{4}}$ vs α, LEGR, k/c=0.0019 10
14. C_l vs α, Vortex Generators 10
15. $C_{m\frac{1}{4}}$ vs α, Vortex Generators 10
16. Drag Polar, Vortex Generators, C_l vs C_{dp} 10
17. C_p vs x/c, α=0° 11
18. C_p vs x/c, α=15° 11
19. C_p vs x/c, α=184° 11

List of Tables

Page

1. LS(1)-0417MOD Aerodynamic Parameters Summary 12

List of Symbols

AOA	Angle of Attack, degrees
α	Angle of Attack, degrees
c	Chord Length, inches
C_{dmin}	Minimum Drag Coefficient
C_{dp}	Section Pressure (Form) Drag Coefficient
C_{dw}	Section Drag Coefficient, calculated from Wake momentum deficit
C_l	Section Lift Coefficient
C_{lmax}	Section Maximum Lift Coefficient
C_m	Section Pitching Moment Coefficient
C_{mo}	Section Pitching Moment Coefficient at zero degrees angle of attack
$C_{m1/4}$	Section Pitching Moment Coefficient about the quarter chord
C_p	Pressure Coefficient
C_{pmin}	Minimum Pressure Coefficient
k	Roughness element height, inches
psi	Units of pressure, pounds per square inch
q	Dynamic pressure, psi
Re	Reynolds number
x	Axis parallel to airfoil reference line, Coordinate in inches
y	Axis perpendicular to airfoil reference line, Coordinate in inches

Acknowledgements

This work was made possible by the efforts and financial support of the National Renewable Energy Laboratory which provided major funding and technical monitoring; the U.S. Department of Energy, which is credited for its funding of this document through the National Renewable Energy Laboratory under contract number DE-AC36-83CH10093 and U.S. Windpower Incorporated which provided funding for models and provided technical assistance. The staff of the Ohio State University Aeronautical and Astronautical Research Laboratory appreciate the contributions made by personnel from both organizations.

Introduction

Wind turbines in the field can be subjected to many and varying wind conditions, including high winds with the rotor locked or with yaw excursions. In some cases the rotor blades may be subjected to unusually large angles of attack that possibly result in unexpected loads and deflections. To better understand loadings at unusual angles of attack, a wind tunnel test was performed. An 18-inch constant-chord model of the LS(1)-0417MOD airfoil section was tested under two-dimensional, steady state conditions in the Ohio State University Aeronautical and Astronautical Research Laboratory (OSU/AARL) 7x10 Subsonic Wind Tunnel (7x10). The objective of these tests was to document section lift and moment characteristics under various model and air flow conditions. These included a normal angle of attack range of -20° to +40°, an extended angle of attack range of -60° to +230°, applications of leading edge grit roughness (LEGR), and use of vortex generators (VGs), all at chord Reynolds numbers as high as possible for the particular model configuration. To realistically satisfy these conditions the 7x10 offered a tunnel-height-to-model-chord ratio of 6.7, suggesting low interference effects even at the relatively high lift and drag conditions expected during the test. Significantly, it also provided chord Reynolds numbers up to 2.0 million.

Knowing the LS(1)-0417MOD model would later be run in the OSU/AARL 3x5 Subsonic Wind Tunnel (3x5), the present test setup and methods were kept as similar as possible to those for the 3x5. This will allow a direct comparison of data obtained in the two wind tunnels. Consequently, most of the data acquisition equipment was moved from the 3x5 to the 7x10. Minor changes were made to the system in order to adapt the equipment to the larger facility. Also, so that the LS(1)-0417MOD model could be used in both tunnels, it was specially designed to include a central 3-foot span sensing section with removable, contoured, spanwise extensions.

A "standard" grit pattern was applied in all LEGR cases. The grit pattern was developed by U.S. Windpower, OSU/AARL, and the University of Texas, Permian Basin. The VGs were provided to OSU/AARL by U.S. Windpower. Detailed discussion of the grit pattern and VGs can be found in the Section , Model Details.

Reynolds numbers of 1, 1.5, and 2 million were tested for normal angle of attack range cases (-20° to +40°). At 1 million Reynolds number, the model was additionally swept through the extended angle of attack range. The model buffeted at higher dynamic pressures, thus precluding higher Reynolds number data for extended angle of attack range. However, both clean and LEGR data were taken for all useable tunnel conditions. Finally, VG effects were evaluated over the normal angle of attack range, for Reynolds numbers of 1 and 1.5 million, and for clean and LEGR cases. The VGs were tested at the 30% chord upper surface station only; any attempt at higher Reynolds numbers with VGs consistently result in VGs separating from the model. Scheduling constraints precluded any significant effort to alleviate the VG attachment problem.

Test Facility

Tests described here were performed in the OSU/AARL 7x10 subsonic wind tunnel. A schematic of the tunnel is shown in figure 1. There are two test sections in this tunnel: a 7-foot by 10-foot section in which these tests were conducted, and a 16-foot by 14-foot section in which very low speed and high angle of attack testing is performed with large models. The wind tunnel is a closed-circuit, single-return, continuous-flow system. A velocity range of 35 to 180 knots is developed in the 7x10 test section by a six-blade, fixed-pitch, 20-foot diameter fan directly driven by a 2000-horsepower, variable-speed motor. The tunnel's steel outer shell is water spray cooled to control internal air temperature. Its test section floor contains a rotating table which allows adjustment of the model angle of attack through a 290° range about a vertical axis. A large, long traverse, wake survey probe was not available; consequently, none was installed in the test section.

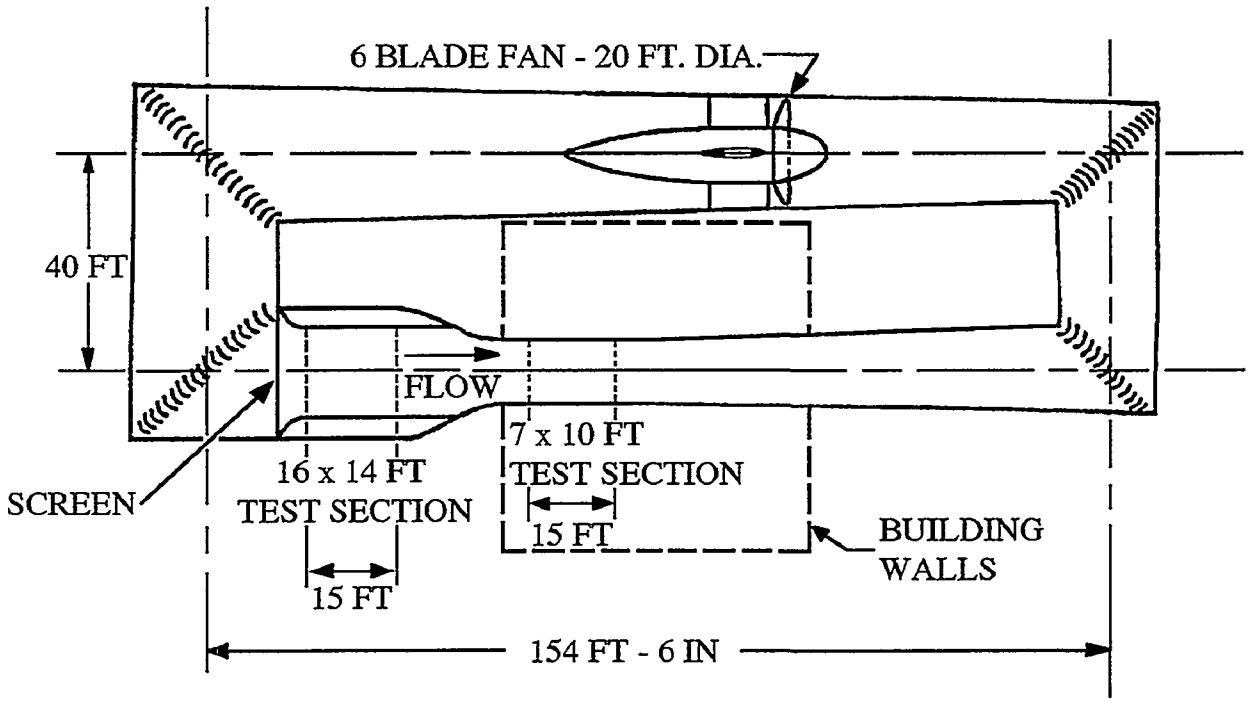

Figure 1. OSU/AARL 7x10 Subsonic Wind Tunnel

Model Details

An 18-inch constant-chord LS(1)-0417MOD airfoil model was designed by OSU/AARL personnel and manufactured by others. Figure 2 shows the airfoil section; the section's measured coordinates are given in Appendix A. The model was made of a carbon composite skin over a foam core. The main load bearing member is a 1½-inch diameter steel tube that passes through the foam core at the airfoil quarter chord station. Steel and composite ribs and end plates transfer loads from the composite skin to the steel tube. The final surface was hand worked using templates to attain given coordinates within a tolerance of ±0.01 inches.

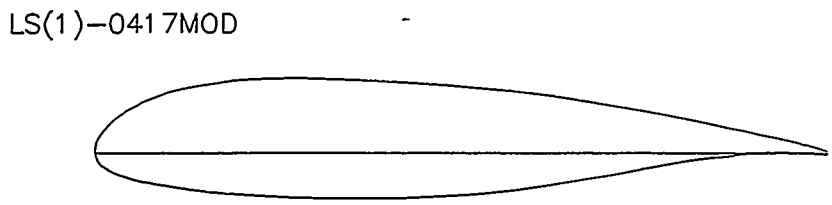

Figure 2. LS(1)-0417MOD Airfoil Section

Since the model also had to be used in the 3x5 subsonic wind tunnel for additional tests, it was designed with a 3-foot span main sensing section and 2-foot extension panels for each end, shown in figure 3. The extensions, used for 7x10 tunnel testing, were fabricated with the same contour as the main section. They slide over the steel tube and fasten to the endplates of the main section. Other minor model features were included, such as an extension to the model support tube and an adaptation of the support tube end to accommodate the different angle of attack potentiometer mountings in each facility.

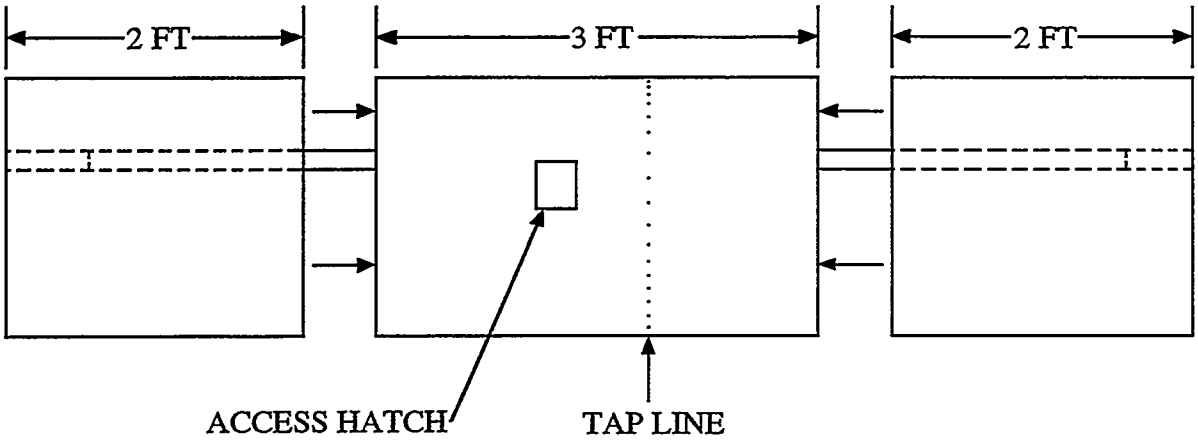

Figure 3. Model Design

To minimize pressure response times, the lengths of surface pressure tap leadout lines were made as short as possible. Although response time was not particularly important for the present test, it was important for the unsteady testing to be done later in the 3x5 wind tunnel. Therefore, a compartment was built into the model to hold the pressure scanning modules. This compartment can be accessed through a panel door fitted flush with the model contour on the lower (pressure) surface.

For test cases involving roughness, to have a standard, repeatable pattern with grit as roughness elements was desired. Prior to these tests, grit was lightly blown into a thin layer of spray adhesive or a tape adhesive to obtain a roughened surface on models. A different method was developed and used here. OSU/AARL and U.S. Windpower personnel jointly developed a roughness pattern using a molded insect pattern taken from a wind turbine in the field by personnel at the University of Texas, Permian Basin.

The resultant particle density was 32 particles per square inch in the middle of the pattern, and thinning to 8 particles per square inch at the edge of the pattern. Figure 4 shows the pattern template produced by U.S. Windpower from these specifications. The pattern was repeatedly cut into a steel sheet 4-inches wide and 3-feet long with holes just large enough for one piece of grit. Based on average particle size from the field specimen, standard #40 lapidary grit was chosen for the roughness elements, giving k/c=0.0019 for an 18 inch chord model.

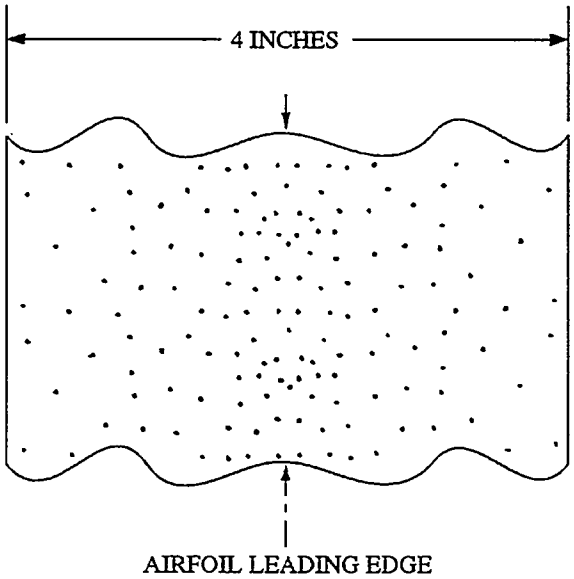

Figure 4. Roughness Pattern

To use the template, 4-inch wide double-tack tape was stuck to one side of the template and grit was poured and brushed from the opposite side. The tape was then removed from the template and transferred to the model. This scheme allowed the same roughness pattern to be replicated for any test.

VGs were applied to the model for some data points. U.S. Windpower provided the VGs with the geometry shown in figure 5. The VGs were pairs of right isosceles triangular shapes set on their longest sides at 30° included angle to each other and 15° to the chord line. The pairs were repeated every 1.61 inches in the spanwise direction. This VG configuration was fabricated in 1.53-inch wide injection-molded plastic strips with a 0.036-inch base-plate thickness. For ease of installation and to minimize damage to the model surface, these strips were fastened at the 30% chord upper surface station

using rubber cement between the VG base-plate and model, and thin tape (0.003-inch thick) over the base plate leading and trailing edges.

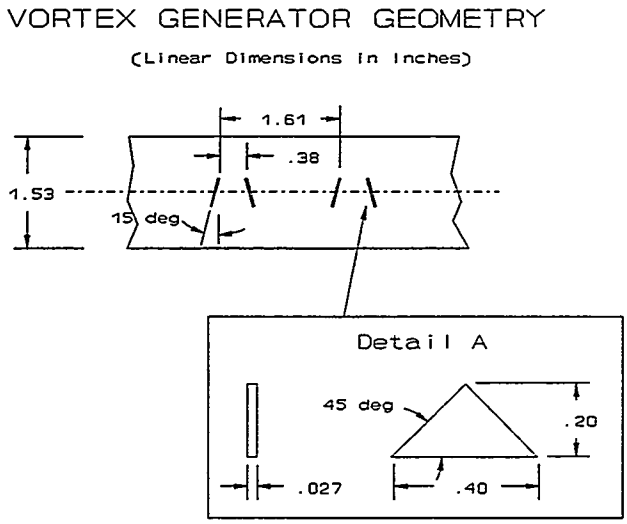

Figure 5. Vortex Generator Geometry

Test Equipment and Procedures

Data Acquisition

Data was acquired and processed from up to 60 surface pressure taps, three individual tunnel pressure transducers, and an angle of attack potentiometer. The data acquisition system included an IBM PC compatible 80386-based computer connected to a Pressure Systems Incorporated (PSI) data scanning system. The PSI system included a 780B Data Acquisition and Control Unit (DACU), 780B Pressure Calibration Unit (PCU), 81-IFC scanning module interface, two ESP-32 5-psid range pressure scanning modules (ESPs), and a 30-channel Remotely Addressed Millivolt Module (RAMM-30). Figure 6 shows the data acquisition system schematic.

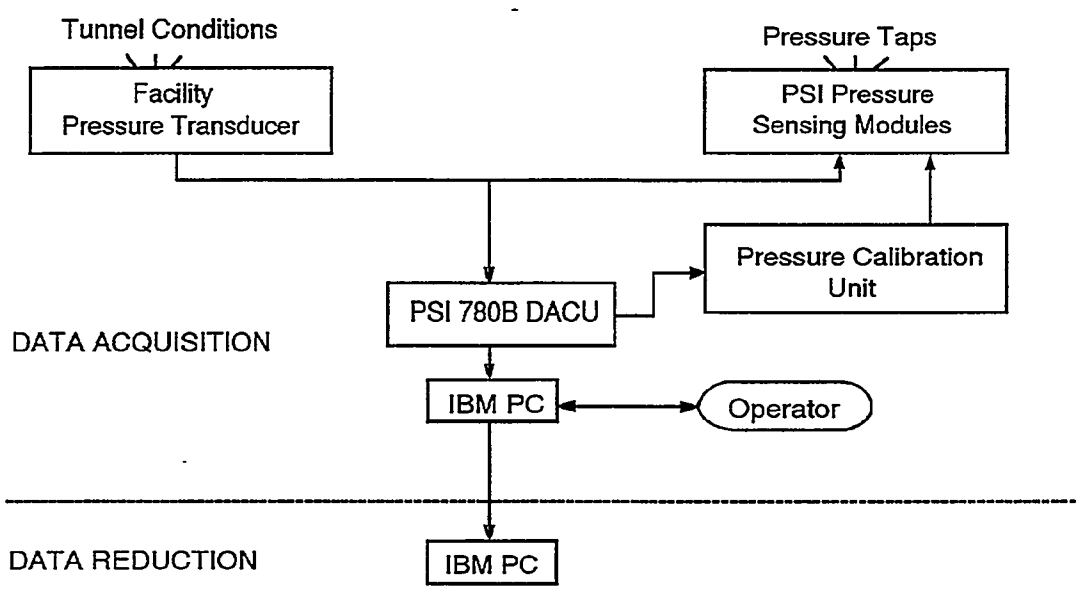

Figure 6. Data Acquisition Schematic

Three individual pressure transducers read tunnel total pressure, tunnel east static pressure, and tunnel west static pressure. Before the test began, these transducers were bench calibrated using a water manometer to determine their sensitivities and offsets. Related values were entered into the data acquisition and reduction program so the transducers could be shunt-resistor calibrated before each series of wind tunnel runs.

The angle of attack potentiometer was a linear rotary potentiometer and was regularly calibrated during the tunnel pressure transducers shunt calibration. The angle of attack calibration was accomplished by taking voltage readings at known values of set angle of attack. This calibration method gave angle of attack readings within ±0.25° of actual over the entire angle range.

Two ESPs were calibrated simultaneously using the DACU and PCU. At operator request, the DACU commanded the PCU to apply known regulated pressures to the ESPs and read the output voltages from each integrated pressure sensor. From these values, the DACU calculated the calibration coefficients and stored them internally until the coefficients were requested by the controlling computer. This calibration

was done several times during a run set because the ESPs were installed inside the model and their outputs tended to drift with temperature changes during a test sequence. Frequent online calibrations minimized the effect.

Finally, at operator request, pressure measurements from the airfoil surface taps and all other channels of information were acquired and stored by the DACU and subsequently passed to the controlling computer for final processing.

Data Reduction

The data reduction routine was incorporated as a section of the data acquisition program. This combined data acquisition and reduction routines allowed data to be reduced online during a test. By quickly reducing selected runs, integrity checks could be made to insure the equipment was working properly and to enable timely decisions about the test matrix.

The ambient pressure and tunnel air temperature were manually input into the computer and were updated regularly. These values, as well as the measurements from the tunnel pressure transducers, were used to calculate tunnel airspeed. As a continuous check of readings, both the tunnel individual pressure transducers and the ESPs read the tunnel total and static pressures.

A typical data point was derived by acquiring twenty data scans of all channels over a 1-second window at each angle of attack and tunnel condition. The reduction portion of the program processed each data scan to coefficient forms C_p, C_l, $C_{m¼}$, and C_{dp} using the measured surface pressure voltages, calibration coefficients, tap locations and wind tunnel conditions. All scan sets for a given condition were then ensemble averaged to provide one set. All data were saved in electronic form. The data were not corrected for any tunnel wall effects, etc.

Test Matrix

The test was designed to allow an extended angle of attack range of -60° to 230° and Reynolds numbers of 1, 1.5, and 2 million with and without LEGR. The tabular data in Appendix B contains the actual Reynolds number for each angle of attack. The angle of attack increment was 4-degrees when $\alpha<-20°$ or $\alpha>40°$, 2-degrees when $-20°< \alpha <10°$ or $20°< \alpha <40°$, and 1-degree when $10°< \alpha <20°$. All test speeds and angles of attack were set for model clean and LEGR conditions.

For some cases, VGs were mounted at the 30% chord position on the model's upper surface only. The VG strips were provided by U.S. Windpower and were the exact type used on wind turbines in the field. Test conditions while the VGs were applied included clean and LEGR data at 1 and 1.5 million Reynolds numbers over an angle of attack range of -20° to 40°.

Unexpected complications during testing forced adjustments to this desired test matrix. Those complications and their effects are elaborated in the next section, Results and Discussion.

Results and Discussion

The LS(1)-0417MOD airfoil model was tested at three Reynolds numbers in the 7x10. Unfortunately, due to less than expected model rigidity, the model flexed and fluttered when near perpendicular to the flow at the higher test airspeeds. The tunnel airspeed was reduced for those conditions to reduce dynamic effects and to preserve the model's structural integrity. Consequently, the Reynolds number was not constant for the entire extended angle of attack sweeps and only the nominal 1 million Reynolds number condition was obtained. The Reynolds number was as low as 0.6 million during the nominal 1 million Reynolds number extended angle of attack cases. Also, no wake survey probe was available for the test; only pressure drag from surface pressure integrations is presented.

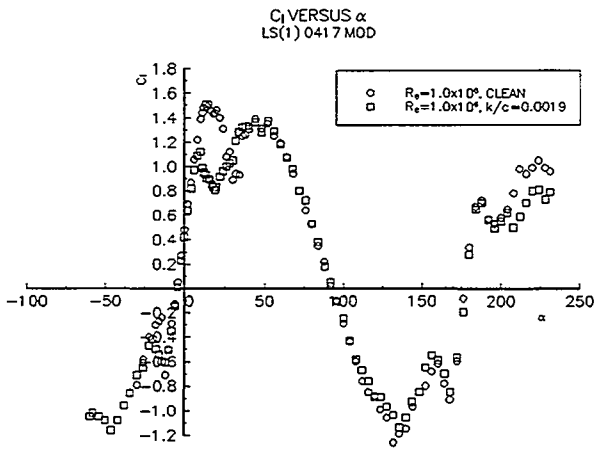

Figure 7. C_l vs α, Extended Range

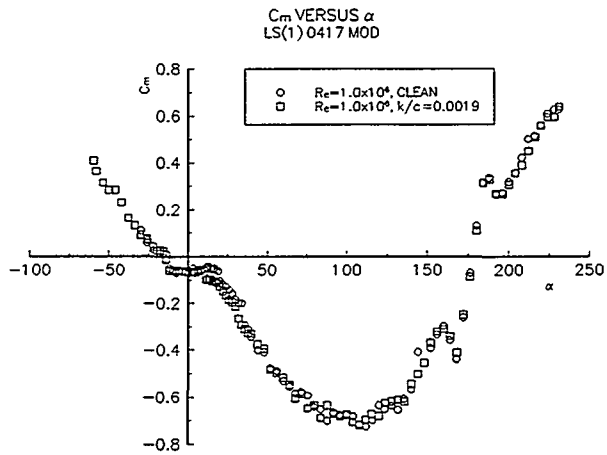

Figure 8. $C_{m1/4}$ vs α, Extended Range

Figure 7 shows the lift coefficient versus angle of attack for the extended angle of attack sweeps, for the model clean and with LEGR at 1 million Reynolds Number. Increases in lift coefficient occurred when the model was in its post stall region for both positive and negative angles of attack; the maximum lift coefficient occurred just before positive stall and is 1.51. Correspondingly, for the LEGR data, the maximum lift coefficient prior to stall is 1.12 and occurs at a slightly lower angle of attack in comparison with the clean case. The overall maximum lift of the LEGR case does not occur before stall but beyond it near 45° angle of attack. This can be observed in figure 7. Similar magnitudes of C_l= 1.35 also are apparent in the large angle of attack clean cases.

The quarter chord pitching moment results are shown in figure 8 for the Reynolds number of 1 million. The pitching moment is most negative when the airfoil is at high angles of attack, near 110°. This observation is consistent for both clean and LEGR cases. The pressure drag is shown in figure 9. The highest pressure drag occurs when the model is near 90° angle of attack. There is some scatter in the data at such conditions, caused by the severely detached, unstable flow on the leeward side of the model.

A number of test runs were made for nominal angles of attack from -20° to +40°. For some of the cases, there is no data shown for the highest angles of attack; the data was discounted as unreliable because the model was buffeting. Figure 10 and 11 show lift coefficient for all the test Reynolds numbers, for the model clean and with LEGR. The maximum positive lift coefficient for the clean cases is about 1.63 and the LEGR data have a C_{lmax} about 1.2. For the clean cases, the airfoil stalls more abruptly with higher

Reynolds numbers. Also note that for the 1 million Reynolds number case, the model with LEGR seems to stall more abruptly than the clean airfoil. The average lift curve slope for these data is about 0.1.

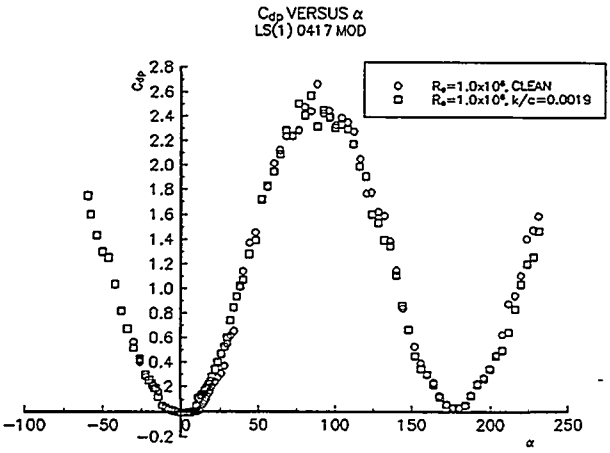

Figure 9. C_{dp} vs α, Extended Range

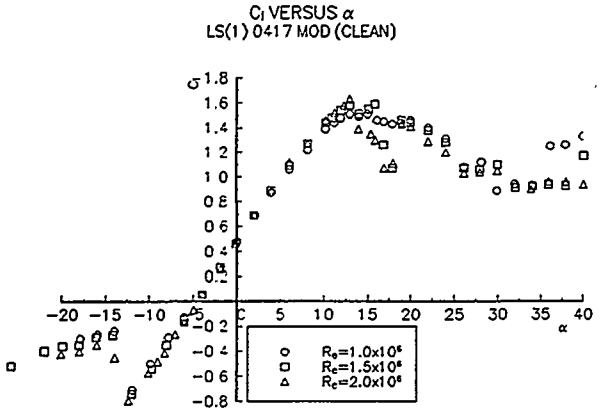

Figure 10. C_l vs α, Clean

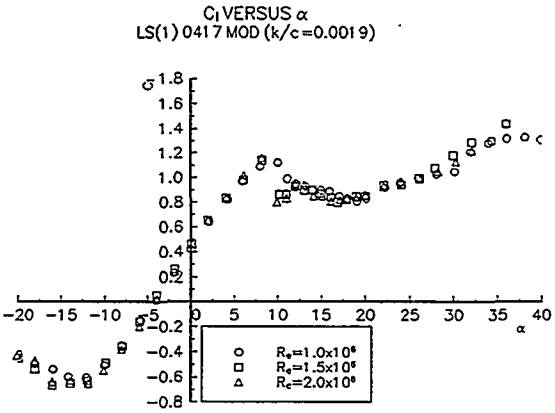

Figure 11. C_l vs α, LEGR, k/c=0.0019

Figure 12 shows the pitching moment about the quarter chord for the clean cases; figure 13 shows the LEGR cases. The LEGR data show a more positive pitching moment near 0° angle of attack. However, beyond stall, the pitching moment magnitude increases faster for the model with LEGR than for the clean model. The C_{mo} about the quarter chord for the clean case is -0.080 and -0.067 for the LEGR case.

VGs were fitted to the model at the 30% chord location, upper surface (suction side) only. The results from these cases are shown in figure 14 for lift coefficient, and in figure 15, for pitching moment coefficient. The maximum lift coefficient for the clean case with VGs is near 1.88 and near 1.41 for the LEGR case. This is a 25% reduction in maximum lift when the airfoil has leading edge roughness. The stall of this airfoil is more abrupt when the VGs are applied, and occurs at a slightly higher angle of attack than without VGs. The pitching moment shows slightly different characteristics with the VGs than without. Pre-stall pitching moment magnitude slightly increases with increased angle of attack with VGs applied, but slightly decreases without VGs. The pitching moment is affected more near stall without VGs than when the VGs are applied. Pressure drag for the VGs cases but is included only for completeness sake in figure 16. This form of drag coefficient is inherently inaccurate because it does not include

friction drag and should only be used for comparisons within the present data sets.

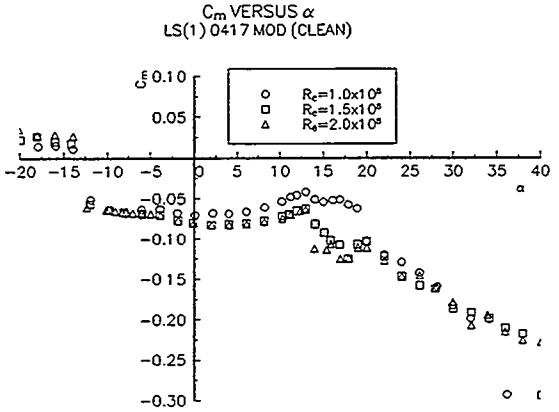

Figure 12. $C_{m¼}$ vs α, Clean

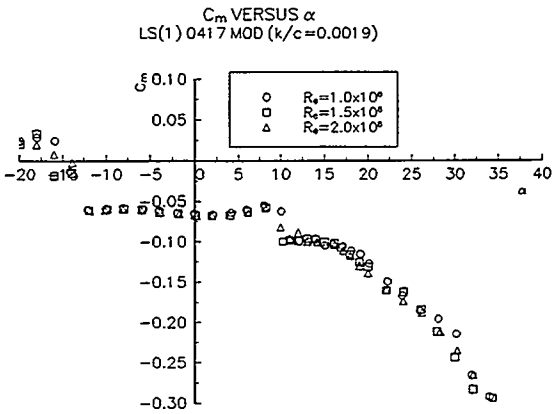

Figure 13. $C_{m¼}$ vs α, LEGR, k/c=0.0019

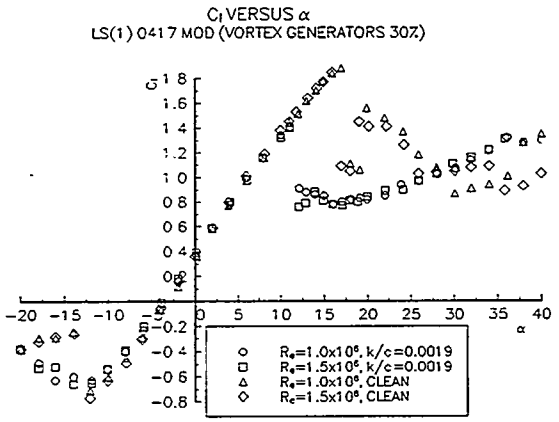

Figure 14. C_l vs α, Vortex Generators

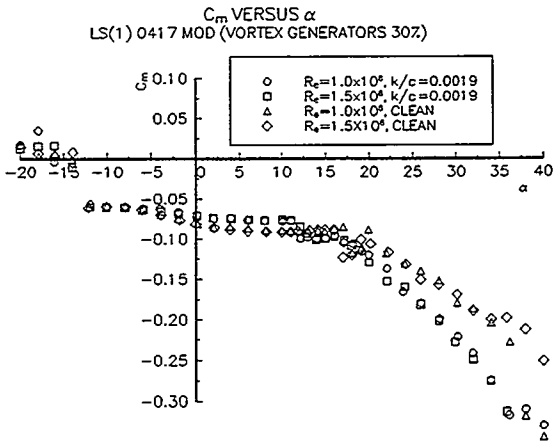

Figure 15. $C_{m¼}$ vs α, Vortex Generators

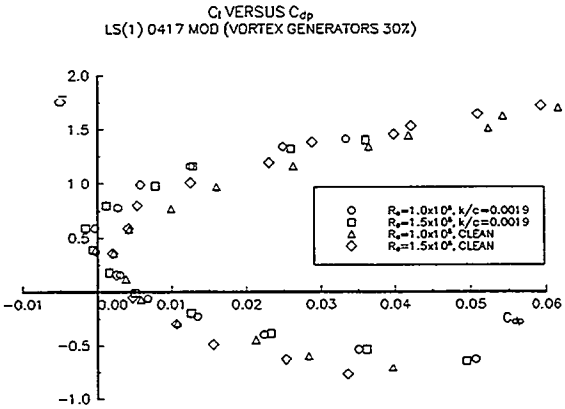

Figure 16. Drag Polar, Vortex Generators, C_l vs C_{dp}

All the pressure distributions shown are for a Reynolds number of 1 million and show cases of clean,

LEGR, and VGs with and without LEGR. Figure 17 shows the pressure distributions for 0° angle of attack. A trend toward reduced pressure magnitudes with LEGR can be observed. At angles of attack near stall, the trending is more apparent. For example, figure 18 shows pressure distributions for a 15° angle of attack. The data show the model has upper surface flow separation near the 20% chord station for the LEGR case. It further shows that the VGs increase the pressure magnitudes for both the clean and LEGR cases. Also, the VGs cause the separation point to move aft.

Figure 19 shows pressure data from the model at an angle of attack of 184° including clean and LEGR pressure distributions. The distributions are almost identical over the airfoil. This shows the roughness does not affect the airflow since it is located, for this unusual case, downstream of the trailing edge.

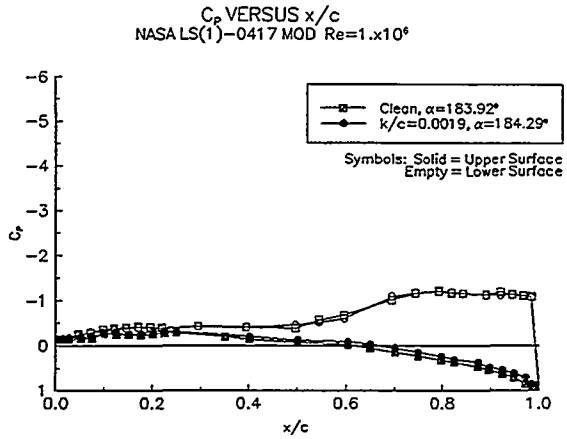

Figure 19. C_p vs x/c, α=184°

The final tests conducted on this wind tunnel model in the 7x10 were to repeat clean conditions at Reynolds numbers of 1 million and 1.5 million for a smaller angle of attack calibration range. In this case, the potentiometer measuring angle of attack was calibrated over a smaller range of -30° to 30° which made the angle of attack reading more sensitive than those for the other tests. The aerodynamic coefficients for this data are tabulated in Appendix B.

The pressure distributions and coefficient data for other test conditions are in Appendix B.

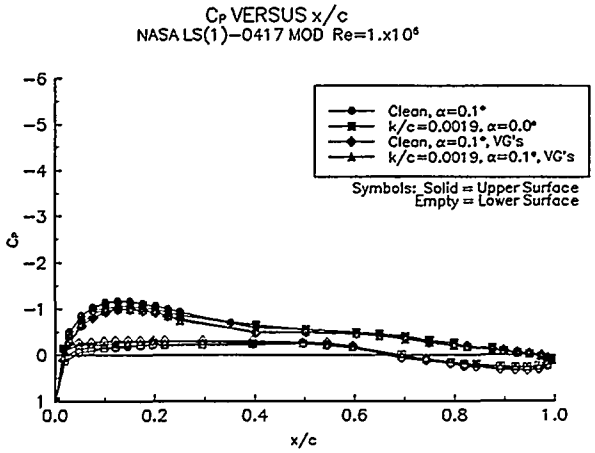

Figure 17. C_p vs x/c, α=0°

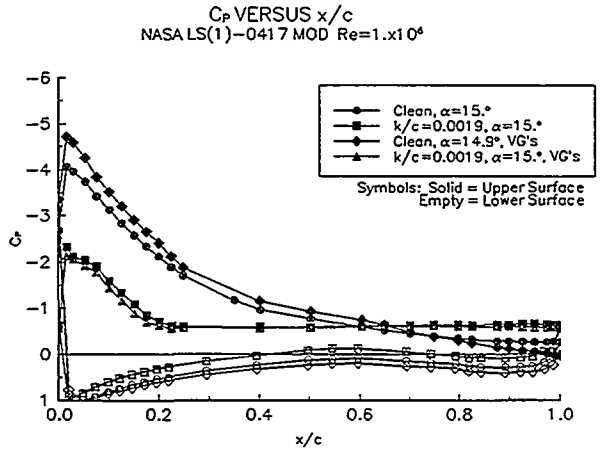

Figure 18. C_p vs x/c, α=15°

Summary

A LS(1)-0417MOD model was installed in the OSU/AARL 7x10 subsonic wind tunnel and tested at three Reynolds numbers and with model clean, roughened, and with VGs. Table 1 is a summary of the aerodynamic coefficient data for the LS(1)-0417MOD.

Table 1. LS(1)-0417MOD Aerodynamic Parameters Summary

CASE	Re num	C_{lmax}	$dC_l/d\alpha$	C_{mo}
Clean	$1.0x10^6$	1.51	0.099	-0.071
Clean	$1.5x10^6$	1.58	0.103	-0.080
Clean	$2.0x10^6$	1.63	0.107	-0.080
k/c=0.0019	$1.0x10^6$	1.12	0.099	-0.065
k/c=0.0019	$1.5x10^6$	1.14	0.098	-0.067
k/c=0.0019	$2.0x10^6$	1.16	0.102	-0.068
Clean VG's	$1.0x10^6$	1.88	0.105	-0.082
Clean VG's	$1.5x10^6$	1.85	0.107	-0.082
k/c=0.0019 VG's	$1.0x10^6$	1.41	0.105	-0.070
k/c=0.0019 VG's	$1.5x10^6$	1.40	0.099	-0.072

For the clean LS(1)-0417MOD model, Reynolds number changes from 1 to 2 million did not a significant affect the maximum positive lift or the pitching moment at zero degrees angle of attack. However, the addition of leading edge grit roughness to the model reduced the maximum lift coefficient by 28% and caused a 16% change in the pitching moment at zero degrees angle of attack. Also, the lift curve slope showed slight increases with Reynolds number. Adding VGs on the model's upper surface at the 30% chord station caused the maximum lift coefficient to increase by 25% in the clean cases and by about 26% for the roughened cases. The VGs apparently energized the boundary layer sufficiently to increase the lift curve slope and to delay stall to a higher angle of attack and, consequently, a higher maximum lift coefficient. However, the positive stall with VG's was more abrupt than the stall without VG's.

Appendix A: Model and Surface Pressure Tap Coordinates

Table A1. LS(1)-0417MOD Measured Model Coordinates 18 inch desired chord				
Chord Station (in)	Lower Ordinate (in)		Chord Station (in)	Upper Ordinate (in)
0.000	-0.003		0.000	-0.003
0.004	-0.027		0.001	0.146
0.013	-0.069		0.003	0.165
0.034	-0.145		0.005	0.175
0.058	-0.195		0.010	0.200
0.118	-0.277		0.022	0.245
0.190	-0.344		0.052	0.330
0.288	-0.407		0.081	0.389
0.359	-0.445		0.147	0.496
0.445	-0.485		0.227	0.602
0.580	-0.539		0.330	0.718
0.710	-0.585		0.407	0.795
0.864	-0.632		0.498	0.876
1.092	-0.700		0.636	0.986
1.316	-0.746		0.770	1.078
1.527	-0.788		0.925	1.172
1.690	-0.818		1.077	1.253
1.855	-0.846		1.195	1.311
2.364	-0.922		1.389	1.397
2.917	-0.989		1.601	1.479
3.297	-1.027		1.768	1.536
3.754	-1.064		1.933	1.587
4.834	-1.122		2.067	1.625
5.782	-1.146		2.447	1.715
6.668	-1.148		3.381	1.863
7.448	-1.132		3.840	1.901
8.461	-1.092		4.245	1.920

Table A1. LS(1)-0417MOD Measured Model Coordinates
18 inch desired chord

Chord Station (in)	Lower Ordinate (in)		Chord Station (in)	Upper Ordinate (in)
9.318	-1.037		4.924	1.927
10.250	-0.943		5.869	1.905
11.131	-0.819		6.756	1.861
12.905	-0.504		7.534	1.814
13.820	-0.330		8.546	1.743
14.514	-0.207		9.398	1.673
14.980	-0.137		10.327	1.579
15.487	-0.070		11.202	1.466
15.854	-0.027		12.958	1.174
16.293	0.007		13.860	0.999
16.829	0.032		14.543	0.859
17.177	0.029		15.006	0.762
17.389	0.018		15.509	0.655
17.457	0.013		15.869	0.577
17.551	0.004		16.338	0.473
17.618	-0.003		16.829	0.362
17.703	-0.013		17.171	0.280
17.781	-0.023		17.293	0.250
17.802	-0.025		17.381	0.227
17.833	-0.029		17.448	0.209
17.953	-0.037		17.541	0.183
			17.605	0.164
			17.686	0.138
			17.953	0.058

End of Table A1

Table A2. LS(1)-0417MOD Surface Pressure Taps		
Tap Number	Chord Station	Ordinate
1	1.0000	-0.0035
2	0.9847	-0.0009
3	0.9681	0.0006
4	0.9448	0.0016
5	0.9209	0.0013
6	0.8915	-0.0003
7	0.8694	-0.0025
8	0.8435	-0.0058
9	0.8188	-0.0093
10	0.7919	-0.0138
11	0.7432	-0.0227
12	0.6941	-0.0320
13	0.6444	-0.0408
14	0.5955	-0.0487
15	0.5448	-0.0550
16	0.4967	-0.0590
17	0.3951	-0.0632
18	0.2951	-0.0631
19	0.2462	-0.0614
20	0.2196	-0.0598
21	0.1963	-0.0581
22	0.1714	-0.0559
23	0.1461	-0.0531
24	0.1207	-0.0497
25	0.0977	-0.0461
26	0.0721	-0.0410
27	0.0467	-0.0344
28	0.0187	-0.0238

Table A2. LS(1)-0417MOD Surface Pressure Taps		
Tap Number	Chord Station	Ordinate
29	0.0000	0.0006
30	0.0152	0.0365
31	0.0284	0.0492
32	0.0517	0.0651
33	0.0751	0.0767
34	0.1012	0.0863
35	0.1263	0.0934
36	0.1508	0.0985
37	0.1761	0.1024
38	0.2009	0.1050
39	0.2264	0.1066
40	0.2503	0.1073
41	0.3009	0.1068
42	0.3513	0.1046
43	0.4018	0.1017
44	0.4517	0.0984
45	0.5016	0.0947
46	0.5491	0.0905
47	0.6043	0.0842
48	0.6500	0.0776
49	0.7009	0.0689
50	0.7494	0.0596
51	0.7980	0.0497
52	0.8246	0.0442
53	0.8533	0.0381
54	0.8751	0.0333
55	0.8979	0.0284
56	0.9250	0.0223

Table A2. LS(1)-0417MOD Surface Pressure Taps		
Tap Number	Chord Station	Ordinate
57	0.9494	0.0167
58	0.9726	0.0112
59	0.9857	0.0069
End of Table A2		

Appendix B: Integrated Coefficients and Pressure Distributions

List of Tables

Page

B1. LS(1)-0417MOD, Clean, Re = 1 million B-8
B2. LS(1)-0417MOD, Clean, Re = 1.5 million B-12
B3. LS(1)-0417MOD, Clean, Re = 2 million B-14
B4. LS(1)-0417MOD, LEGR k/c=0.0019, Re = 1 million B-16
B5. LS(1)-0417MOD, LEGR k/c=0.0019, Re = 1.5 million B-20
B6. LS(1)-0417MOD, LEGR k/c=0.0019, Re = 2 million B-22
B7. LS(1)-0417MOD, LEGR k/c=0.0019, VGs, Re = 1 million B-24
B8. LS(1)-0417MOD, LEGR k/c=0.0019, VGs, Re = 1.5 million B-26
B9. LS(1)-0417MOD, Clean, VGs, Re = 1 million B-28
B10. LS(1)-0417MOD, Clean, VGs, Re = 1.5 million B-30
B11. LS(1)-0417MOD, Clean, Re = 1 million, Small α Cal Range B-32
B12. LS(1)-0417MOD, Clean, Re = 1.5 million, Small α Cal Range B-34

List of Figures

Page

Steady State Pressure Distributions Re = 1.0 million B-36
1. $\alpha = -60^\circ$ B-37
2. $\alpha = -58^\circ$ B-37
3. $\alpha = -54^\circ$ B-37
4. $\alpha = -50^\circ$ B-37
5. $\alpha = -46^\circ$ B-38
6. $\alpha = -42^\circ$ B-38
7. $\alpha = -38^\circ$ B-38
8. $\alpha = -34^\circ$ B-38
9. $\alpha = -30^\circ$ B-39
10. $\alpha = -26^\circ$ B-39
11. $\alpha = -22^\circ$ B-39
12. $\alpha = -20^\circ$ B-39
13. $\alpha = -18^\circ$ B-40
14. $\alpha = -16^\circ$ B-40
15. $\alpha = -14^\circ$ B-40
16. $\alpha = -12^\circ$ B-40
17. $\alpha = -10^\circ$ B-41
18. $\alpha = -8^\circ$ B-41
19. $\alpha = -6^\circ$ B-41
20. $\alpha = -4^\circ$ B-41
21. $\alpha = -2^\circ$ B-42
22. $\alpha = 0^\circ$ B-42
23. $\alpha = 2^\circ$ B-42
24. $\alpha = 4^\circ$ B-42
25. $\alpha = 6^\circ$ B-43
26. $\alpha = 8^\circ$ B-43
27. $\alpha = 10^\circ$ B-43
28. $\alpha = 11^\circ$ B-43
29. $\alpha = 12^\circ$ B-44
30. $\alpha = 13^\circ$ B-44
31. $\alpha = 14^\circ$ B-44
32. $\alpha = 15^\circ$ B-44
33. $\alpha = 16^\circ$ B-45
34. $\alpha = 17^\circ$ B-45
35. $\alpha = 18^\circ$ B-45
36. $\alpha = 19^\circ$ B-45
37. $\alpha = 20^\circ$ B-46
38. $\alpha = 22^\circ$ B-46
39. $\alpha = 24^\circ$ B-46
40. $\alpha = 26^\circ$ B-46
41. $\alpha = 28^\circ$ B-47
42. $\alpha = 30^\circ$ B-47
43. $\alpha = 32^\circ$ B-47
44. $\alpha = 34^\circ$ B-47

45. $\alpha = 36^\circ$ B-48
46. $\alpha = 38^\circ$ B-48
47. $\alpha = 40^\circ$ B-48
48. $\alpha = 44^\circ$ B-48
49. $\alpha = 48^\circ$ B-49
50. $\alpha = 52^\circ$ B-49
51. $\alpha = 56^\circ$ B-49
52. $\alpha = 60^\circ$ B-49
53. $\alpha = 64^\circ$ B-50
54. $\alpha = 68^\circ$ B-50
55. $\alpha = 72^\circ$ B-50
56. $\alpha = 76^\circ$ B-50
57. $\alpha = 80^\circ$ B-51
58. $\alpha = 84^\circ$ B-51
59. $\alpha = 88^\circ$ B-51
60. $\alpha = 92^\circ$ B-51
61. $\alpha = 96^\circ$ B-52
62. $\alpha = 100^\circ$ B-52
63. $\alpha = 104^\circ$ B-52
64. $\alpha = 108^\circ$ B-52
65. $\alpha = 112^\circ$ B-53
66. $\alpha = 116^\circ$ B-53
67. $\alpha = 120^\circ$ B-53
68. $\alpha = 124^\circ$ B-53
69. $\alpha = 128^\circ$ B-54
70. $\alpha = 132^\circ$ B-54
71. $\alpha = 136^\circ$ B-54
72. $\alpha = 140^\circ$ B-54
73. $\alpha = 144^\circ$ B-55
74. $\alpha = 148^\circ$ B-55
75. $\alpha = 152^\circ$ B-55
76. $\alpha = 156^\circ$ B-55
77. $\alpha = 160^\circ$ B-56
78. $\alpha = 164^\circ$ B-56
79. $\alpha = 168^\circ$ B-56
80. $\alpha = 172^\circ$ B-56
81. $\alpha = 176^\circ$ B-57
82. $\alpha = 180^\circ$ B-57
83. $\alpha = 184^\circ$ B-57
84. $\alpha = 188^\circ$ B-57
85. $\alpha = 192^\circ$ B-58
86. $\alpha = 196^\circ$ B-58
87. $\alpha = 200^\circ$ B-58
88. $\alpha = 204^\circ$ B-58
89. $\alpha = 208^\circ$ B-59
90. $\alpha = 212^\circ$ B-59
91. $\alpha = 216^\circ$ B-59
92. $\alpha = 220^\circ$ B-59

93. $\alpha = 224^\circ$ B-60
94. $\alpha = 228^\circ$ B-60
95. $\alpha = 231^\circ$ B-60
Steady State Pressure Distributions, VGs, Re = 1.0 million B-61
96. $\alpha = -20^\circ$ B-62
97. $\alpha = -18^\circ$ B-62
98. $\alpha = -16^\circ$ B-62
99. $\alpha = -14^\circ$ B-62
100. $\alpha = -12^\circ$ B-63
101. $\alpha = -10^\circ$ B-63
102. $\alpha = -8^\circ$ B-63
103. $\alpha = -6^\circ$ B-63
104. $\alpha = -4^\circ$ B-64
105. $\alpha = -2^\circ$ B-64
106. $\alpha = 0^\circ$ B-64
107. $\alpha = 2^\circ$ B-64
108. $\alpha = 4^\circ$ B-65
109. $\alpha = 6^\circ$ B-65
110. $\alpha = 8^\circ$ B-65
111. $\alpha = 10^\circ$ B-65
112. $\alpha = 11^\circ$ B-66
113. $\alpha = 12^\circ$ B-66
114. $\alpha = 13^\circ$ B-66
115. $\alpha = 14^\circ$ B-66
116. $\alpha = 15^\circ$ B-67
117. $\alpha = 16^\circ$ B-67
118. $\alpha = 17^\circ$ B-67
119. $\alpha = 18^\circ$ B-67
120. $\alpha = 19^\circ$ B-68
121. $\alpha = 20^\circ$ B-68
122. $\alpha = 22^\circ$ B-68
123. $\alpha = 24^\circ$ B-68
Steady State Pressure Distributions, Re = 1.5 million B-69
124. $\alpha = -30^\circ$ B-70
125. $\alpha = -26^\circ$ B-70
126. $\alpha = -22^\circ$ B-70
127. $\alpha = -20^\circ$ B-70
128. $\alpha = -18^\circ$ B-71
129. $\alpha = -16^\circ$ B-71
130. $\alpha = -14^\circ$ B-71
131. $\alpha = -12^\circ$ B-71
132. $\alpha = -10^\circ$ B-72
133. $\alpha = -8^\circ$ B-72
134. $\alpha = -6^\circ$ B-72
135. $\alpha = -4^\circ$ B-72
136. $\alpha = -2^\circ$ B-73
137. $\alpha = 0^\circ$ B-73
138. $\alpha = 2^\circ$ B-73

139. $\alpha = 4^\circ$ B-73
140. $\alpha = 6^\circ$ B-74
141. $\alpha = 8^\circ$ B-74
142. $\alpha = 10^\circ$ B-74
143. $\alpha = 11^\circ$ B-74
144. $\alpha = 12^\circ$ B-75
145. $\alpha = 13^\circ$ B-75
146. $\alpha = 14^\circ$ B-75
147. $\alpha = 15^\circ$ B-75
148. $\alpha = 16^\circ$ B-76
149. $\alpha = 17^\circ$ B-76
150. $\alpha = 18^\circ$ B-76
151. $\alpha = 20^\circ$ B-76
152. $\alpha = 22^\circ$ B-77
153. $\alpha = 24^\circ$ B-77
154. $\alpha = 26^\circ$ B-77
155. $\alpha = 28^\circ$ B-77
156. $\alpha = 30^\circ$ B-78
157. $\alpha = 32^\circ$ B-78
158. $\alpha = 34^\circ$ B-78
159. $\alpha = 36^\circ$ B-78
160. $\alpha = 38^\circ$ B-79
161. $\alpha = 40^\circ$ B-79
Steady State Pressure Distributions Re = 2.0 million B-80
162. $\alpha = -20^\circ$ B-81
163. $\alpha = -18^\circ$ B-81
164. $\alpha = -16^\circ$ B-81
165. $\alpha = -14^\circ$ B-81
166. $\alpha = -12^\circ$ B-82
167. $\alpha = -10^\circ$ B-82
168. $\alpha = -8^\circ$ B-82
169. $\alpha = -6^\circ$ B-82
170. $\alpha = -4^\circ$ B-83
171. $\alpha = -2^\circ$ B-83
172. $\alpha = 0^\circ$ B-83
173. $\alpha = 2^\circ$ B-83
174. $\alpha = 4^\circ$ B-84
175. $\alpha = 6^\circ$ B-84
176. $\alpha = 8^\circ$ B-84
177. $\alpha = 10^\circ$ B-84
178. $\alpha = 11^\circ$ B-85
179. $\alpha = 12^\circ$ B-85
180. $\alpha = 13^\circ$ B-85
181. $\alpha = 14^\circ$ B-85
182. $\alpha = 15^\circ$ B-86
183. $\alpha = 16^\circ$ B-86
184. $\alpha = 17^\circ$ B-86
185. $\alpha = 18^\circ$ B-86

186. $\alpha = 19^\circ$ B-87
187. $\alpha = 20^\circ$ B-87
188. $\alpha = 22^\circ$ B-87
189. $\alpha = 24^\circ$ B-87
190. $\alpha = 26^\circ$ B-88
191. $\alpha = 28^\circ$ B-88
192. $\alpha = 30^\circ$ B-88
193. $\alpha = 32^\circ$ B-88
194. $\alpha = 34^\circ$ B-89
195. $\alpha = 36^\circ$ B-89
196. $\alpha = 38^\circ$ B-89
197. $\alpha = 40^\circ$ B-89

Table B1. LS(1)-0417MOD, Clean, Re = 1 million					
RUN	AOA	C_l	C_{dp}	$C_{m¼}$	Re x10^{-6}
112	-29.9	-0.79	0.5651	0.1097	1.00
113	-25.8	-0.61	0.4151	0.0688	1.00
114	-25.9	-0.58	0.3992	0.0590	1.00
115	-21.9	-0.40	0.2765	0.0273	1.00
116	-17.9	-0.30	0.2069	0.0142	0.99
117	-15.9	-0.27	0.1836	0.0149	1.01
118	-13.9	-0.24	0.1581	0.0111	1.00
119	-11.9	-0.71	0.0444	-0.0514	1.00
120	-9.8	-0.50	0.0299	-0.0640	1.00
121	-7.8	-0.29	0.0177	-0.0691	1.00
122	-6.0	-0.13	0.0099	-0.0637	0.99
123	-3.9	0.05	0.0019	-0.0627	1.00
124	-1.9	0.27	-.0033	-0.0678	1.00
125	0.1	0.48	-.0072	-0.0706	1.00
126	2.2	0.69	-.0070	-0.0684	1.00
127	4.0	0.87	-.0056	-0.0692	1.00
128	6.1	1.06	-.0038	-0.0664	1.00
129	8.2	1.22	0.0028	-0.0612	1.00
130	10.2	1.39	0.0046	-0.0536	1.00
131	11.2	1.44	0.0105	-0.0483	1.00
132	11.9	1.48	0.0137	-0.0460	1.00
133	13.0	1.51	0.0227	-0.0417	1.00
134	14.0	1.49	0.0593	-0.0511	0.99
135	15.0	1.51	0.0813	-0.0541	0.99
136	16.1	1.46	0.1054	-0.0523	0.98
137	16.9	1.45	0.1241	-0.0512	0.98
138	17.9	1.43	0.1411	-0.0577	1.00

Table B1. LS(1)-0417MOD, Clean, Re = 1 million					
RUN	AOA	C_l	C_{dp}	$C_{m¼}$	Re x10^{-6}
139	18.9	1.44	0.1638	-0.0621	1.00
140	20.0	1.46	0.1996	-0.1036	0.99
141	22.1	1.40	0.2357	-0.1190	1.00
142	24.0	1.31	0.2701	-0.1287	0.99
143	26.1	1.08	0.3038	-0.1423	1.00
144	28.2	1.12	0.3670	-0.1594	0.99
145	30.0	0.89	0.5474	-0.1825	1.00
146	32.0	0.94	0.6135	-0.1985	1.00
147	34.1	0.93	0.6520	-0.2001	1.00
148	36.2	1.25	0.9319	-0.2931	1.00
149	38.0	1.26	1.0082	-0.3127	1.00
150	40.0	1.33	1.1364	-0.3447	0.89
151	44.2	1.39	1.3667	-0.4016	0.86
152	48.0	1.31	1.4531	-0.4090	0.82
153	52.0	1.35	1.7181	-0.4772	0.81
154	56.0	1.25	1.8152	-0.4884	0.81
155	60.2	1.19	2.0100	-0.5310	0.80
156	64.0	1.08	2.1204	-0.5562	0.78
157	68.1	0.94	2.2310	-0.5849	0.77
158	72.0	0.80	2.2325	-0.5788	0.74
159	76.1	0.64	2.2805	-0.5936	0.73
160	79.9	0.53	2.4723	-0.6421	0.73
161	84.1	0.35	2.4377	-0.6523	0.71
162	87.9	0.22	2.6610	-0.7007	0.69
163	92.1	0.02	2.4182	-0.6662	0.70
164	95.7	-0.10	2.4400	-0.6757	0.69
165	100.1	-0.29	2.3237	-0.6765	0.70

Table B1. LS(1)-0417MOD, Clean, Re = 1 million					
RUN	AOA	C_l	C_{dp}	$C_{m¼}$	Re x10^{-6}
166	104.2	-0.44	2.3826	-0.6824	0.69
167	108.0	-0.60	2.3449	-0.7174	0.69
168	112.1	-0.76	2.2704	-0.7271	0.70
169	116.3	-0.85	2.0492	-0.7001	0.71
170	120.4	-0.88	1.7661	-0.6356	0.73
171	123.7	-0.99	1.7734	-0.6522	0.73
172	128.1	-1.06	1.6170	-0.6374	0.75
173	132.2	-1.26	1.5870	-0.6547	0.77
174	135.8	-1.19	1.3838	-0.6086	0.79
175	140.0	-1.15	1.1450	-0.5688	0.78
176	144.3	-0.97	0.8381	-0.4096	0.82
178	152.1	-0.80	0.5259	-0.3918	0.98
179	156.0	-0.68	0.3901	-0.3350	1.00
180	160.1	-0.62	0.2962	-0.2980	0.99
181	164.1	-0.78	0.2292	-0.3584	1.00
182	167.9	-0.91	0.1249	-0.4385	1.01
183	172.1	-0.60	0.0559	-0.2607	0.98
184	176.3	-0.08	0.0299	-0.0688	1.00
185	180.1	0.34	0.0304	0.1299	1.00
186	183.9	0.67	0.0472	0.3152	0.99
187	188.0	0.72	0.1270	0.3381	0.99
188	192.2	0.57	0.2199	0.2642	1.00
189	196.0	0.53	0.2718	0.2729	0.99
190	200.1	0.58	0.3471	0.3189	0.98
191	204.2	0.65	0.4600	0.3571	1.00
192	208.1	0.78	0.6256	0.4231	0.96
193	211.9	0.98	0.8752	0.5024	0.93

Table B1. LS(1)-0417MOD, Clean, Re = 1 million					
RUN	AOA	C_l	C_{dp}	$C_{m¼}$	Re x10^{-6}
194	216.0	0.94	0.9417	0.5156	0.89
195	219.8	0.99	1.1053	0.5599	0.82
196	223.8	1.05	1.4040	0.6100	0.79
197	227.9	0.99	1.4705	0.6286	0.77
198	231.0	0.96	1.5822	0.6286	0.71
End of Table B1					

Table B2. LS(1)-0417MOD, Clean, Re = 1.5 million					
RUN	AOA	C_l	C_{dp}	$C_{m¼}$	Re x10^{-6}
201	-25.8	-0.52	0.3684	0.0480	1.45
202	-22.0	-0.40	0.2735	0.0271	1.47
203	-19.9	-0.36	0.2441	0.0220	1.49
204	-18.0	-0.35	0.2228	0.0263	1.50
205	-16.0	-0.29	0.1922	0.0200	1.51
206	-14.1	-0.27	0.1672	0.0176	1.48
207	-12.0	-0.74	0.0387	-0.0569	1.49
208	-9.7	-0.54	0.0246	-0.0646	1.49
209	-8.0	-0.35	0.0182	-0.0667	1.49
210	-6.0	-0.15	0.0081	-0.0695	1.49
211	-3.9	0.05	0.0014	-0.0705	1.48
212	-1.8	0.27	-.0030	-0.0772	1.49
213	-0.1	0.46	-.0052	-0.0799	1.49
214	2.0	0.69	-.0064	-0.0833	1.49
215	4.0	0.89	-.0038	-0.0819	1.49
216	6.1	1.09	-.0013	-0.0808	1.48
217	8.2	1.27	0.0038	-0.0779	1.48
218	10.3	1.44	0.0073	-0.0720	1.48
219	10.9	1.48	0.0111	-0.0697	1.49
220	12.0	1.54	0.0144	-0.0653	1.49
221	13.0	1.58	0.0193	-0.0623	1.49
222	14.1	1.51	0.0760	-0.0817	1.49
223	15.1	1.55	0.1003	-0.0925	1.49
224	15.9	1.59	0.1209	-0.1026	1.49
225	16.9	1.26	0.1353	-0.1076	1.49
226	17.9	1.07	0.1614	-0.1250	1.49
227	19.0	1.46	0.1870	-0.1071	1.49

Table B2. LS(1)-0417MOD, Clean, Re = 1.5 million					
RUN	AOA	C_l	C_{dp}	$C_{m¼}$	Re x10^{-6}
228	20.0	1.44	0.2014	-0.1031	1.50
229	22.1	1.38	0.2380	-0.1217	1.49
230	24.1	1.28	0.2897	-0.1465	1.50
231	26.1	1.07	0.3358	-0.1578	1.49
232	27.9	1.06	0.3677	-0.1623	1.49
233	30.0	1.10	0.4473	-0.1865	1.50
234	32.1	0.91	0.5984	-0.1914	1.49
235	34.1	0.92	0.6488	-0.1985	1.48
236	36.0	0.94	0.7066	-0.2108	1.49
237	38.0	0.93	0.7503	-0.2176	1.48
238	40.1	1.17	1.0041	-0.2939	1.42
End of Table B2					

Table B3. LS(1)-0417MOD, Clean, Re = 2 million					
RUN	AOA	C_l	C_{dp}	$C_{m¼}$	Re x10^{-6}
250	-20.1	-0.42	0.2703	0.0353	2.16
251	-18.0	-0.40	0.2411	0.0277	2.16
252	-16.0	-0.35	0.2087	0.0290	1.98
253	-13.9	-0.45	0.1906	0.0271	1.99
254	-12.3	-0.79	0.0362	-0.0608	2.02
255	-10.1	-0.57	0.0265	-0.0639	2.02
256	-9.0	-0.48	0.0207	-0.0658	2.02
257	-8.2	-0.41	0.0164	-0.0667	2.02
258	-7.0	-0.26	0.0131	-0.0677	2.01
259	-6.0	-0.17	0.0088	-0.0674	2.01
260	-5.0	-0.07	0.0047	-0.0691	2.01
261	-3.9	0.05	0.0016	-0.0709	2.02
262	-1.9	0.26	-.0027	-0.0770	2.02
263	-0.1	0.46	-.0051	-0.0805	2.01
264	2.0	0.69	-.0058	-0.0830	2.01
265	4.1	0.89	-.0038	-0.0832	2.02
266	6.1	1.12	-.0063	-0.0818	2.01
267	8.2	1.27	0.0069	-0.0791	2.09
268	10.2	1.46	0.0080	-0.0746	2.09
269	11.2	1.52	0.0116	-0.0706	2.08
270	12.3	1.58	0.0162	-0.0658	2.06
271	13.0	1.63	0.0176	-0.0640	2.05
272	14.0	1.39	0.1034	-0.1124	2.04
273	15.4	1.35	0.1261	-0.1143	2.04
274	15.9	1.30	0.1252	-0.1063	2.04
275	16.9	1.07	0.1511	-0.1251	2.02
276	18.0	1.11	0.1670	-0.1241	2.01

Table B3. LS(1)-0417MOD, Clean, Re = 2 million					
RUN	AOA	C_l	C_{dp}	$C_{m¼}$	Re x10^{-6}
277	19.0	1.43	0.1938	-0.1110	1.99
278	20.0	1.41	0.2125	-0.1119	1.99
279	22.0	1.29	0.2428	-0.1273	1.96
280	24.1	1.20	0.2964	-0.1471	1.95
281	26.1	1.03	0.3240	-0.1455	1.93
282	28.0	1.04	0.3788	-0.1614	1.92
283	30.0	1.05	0.4441	-0.1790	1.90
284	32.1	0.94	0.6192	-0.2073	1.87
285	33.9	0.90	0.6328	-0.1947	1.85
286	36.0	0.96	0.7159	-0.2154	1.83
287	38.0	0.96	0.7720	-0.2254	1.80
288	40.1	0.94	0.8094	-0.2278	1.77
End of Table B3					

Table B4. LS(1)-0417MOD, LEGR k/c=0.0019, Re = 1 million					
RUN	AOA	C_l	C_{dp}	$C_{m¼}$	Re x10^{-6}
290	-59.6	-1.05	1.7466	0.4086	0.75
291	-57.9	-1.02	1.5992	0.3634	0.76
292	-53.8	-1.05	1.4305	0.3142	0.77
293	-49.9	-1.08	1.2987	0.2823	0.79
294	-46.1	-1.16	1.2496	0.2833	0.81
295	-41.9	-1.08	1.0347	0.2302	0.83
296	-37.8	-0.96	0.8190	0.1649	0.89
297	-33.9	-0.86	0.6740	0.1325	0.92
298	-30.1	-0.71	0.5178	0.0910	1.01
299	-26.0	-0.65	0.4270	0.0752	0.99
300	-22.1	-0.47	0.2986	0.0416	1.00
301	-20.0	-0.42	0.2516	0.0239	1.00
302	-18.0	-0.50	0.2290	0.0284	1.01
303	-15.9	-0.54	0.1888	0.0242	1.02
304	-14.1	-0.60	0.1185	-0.0128	1.00
305	-12.1	-0.61	0.0496	-0.0601	1.00
306	-10.0	-0.51	0.0330	-0.0593	1.00
307	-8.0	-0.35	0.0209	-0.0583	1.00
308	-5.8	-0.15	0.0107	-0.0596	1.00
309	-4.0	0.01	0.0032	-0.0614	0.99
310	-2.0	0.23	-.0030	-0.0647	0.99
311	0.0	0.42	-.0066	-0.0652	0.99
312	2.1	0.64	-.0079	-0.0669	1.00
313	4.2	0.82	-.0062	-0.0642	0.99
314	5.9	0.97	-.0061	-0.0604	1.00
315	8.0	1.09	0.0027	-0.0550	0.99
316	10.0	1.12	0.0423	-0.0627	0.99

Table B4. LS(1)-0417MOD, LEGR k/c=0.0019, Re = 1 million					
RUN	AOA	C_l	C_{dp}	$C_{m¼}$	Re x10^{-6}
317	11.1	0.99	0.1001	-0.0990	1.00
318	12.1	0.95	0.1135	-0.0992	0.99
319	13.1	0.93	0.1282	-0.1000	0.99
320	14.0	0.90	0.1387	-0.0966	0.99
321	15.0	0.90	0.1595	-0.1052	0.99
322	16.0	0.89	0.1735	-0.1038	0.99
323	17.1	0.85	0.1932	-0.1064	1.00
324	18.1	0.83	0.2130	-0.1120	1.00
325	19.1	0.81	0.2372	-0.1158	0.99
326	20.1	0.83	0.2714	-0.1276	0.99
327	22.2	0.92	0.3374	-0.1495	0.98
328	24.0	0.96	0.3949	-0.1674	1.00
329	26.0	1.00	0.4647	-0.1860	0.99
330	28.1	1.03	0.5225	-0.1960	1.00
331	30.1	1.05	0.5983	-0.2144	0.98
332	32.0	1.21	0.7398	-0.2656	1.00
333	34.0	1.28	0.8424	-0.2928	0.98
334	36.1	1.32	0.9321	-0.3105	0.99
335	38.1	1.33	1.0180	-0.3287	1.00
336	39.9	1.31	1.0671	-0.3301	0.99
337	44.0	1.36	1.2757	-0.3761	0.95
338	48.2	1.28	1.3897	-0.3945	0.91
339	52.0	1.37	1.7165	-0.4839	0.88
340	55.9	1.29	1.8241	-0.4970	0.85
341	60.0	1.18	1.9439	-0.5176	0.82
342	64.2	1.07	2.0845	-0.5487	0.81
343	68.0	0.98	2.2775	-0.6065	0.78

Table B4. LS(1)-0417MOD, LEGR k/c=0.0019, Re = 1 million					
RUN	AOA	C_l	C_{dp}	$C_{m¼}$	Re x10^{-6}
344	72.2	0.80	2.2386	-0.5867	0.75
345	76.0	0.72	2.4993	-0.6482	0.75
346	80.2	0.53	2.4017	-0.6347	0.72
347	84.0	0.38	2.5666	-0.6890	0.71
348	88.2	0.18	2.3121	-0.6356	0.69
349	92.0	0.05	2.4472	-0.6727	0.70
350	96.1	-0.11	2.3864	-0.6828	0.70
351	100.0	-0.25	2.2996	-0.6745	0.70
352	104.0	-0.43	2.3265	-0.7078	0.68
353	108.2	-0.58	2.2918	-0.7203	0.67
354	111.8	-0.67	2.1689	-0.6975	0.68
355	115.9	-0.76	1.9872	-0.6744	0.69
356	120.1	-0.89	1.9050	-0.6818	0.69
357	124.2	-0.89	1.5996	-0.6267	0.71
358	128.1	-0.97	1.5307	-0.6196	0.73
359	132.1	-1.04	1.3922	-0.6122	0.75
360	136.0	-1.14	1.3455	-0.6187	0.76
361	140.1	-1.06	1.1082	-0.5455	0.79
362	144.1	-0.93	0.8575	-0.5040	0.80
363	148.1	-0.85	0.6661	-0.4560	0.91
364	152.2	-0.65	0.4492	-0.3695	0.95
365	156.2	-0.55	0.3453	-0.3227	1.00
366	160.1	-0.59	0.2956	-0.3127	0.98
367	164.1	-0.70	0.2149	-0.3424	1.00
368	168.2	-0.85	0.1130	-0.4109	1.00
369	172.0	-0.57	0.0577	-0.2502	1.01
370	176.1	-0.19	0.0223	-0.0864	1.01

Table B4. LS(1)-0417MOD, LEGR k/c=0.0019, Re = 1 million					
RUN	AOA	C_l	C_{dp}	$C_{m¼}$	Re x10^{-6}
371	180.0	0.28	0.0305	0.1104	1.01
372	184.3	0.65	0.0523	0.3159	1.01
373	187.9	0.70	0.1229	0.3298	1.00
374	192.1	0.56	0.2121	0.2679	1.00
375	196.1	0.49	0.2611	0.2668	0.98
376	200.1	0.55	0.3391	0.3071	1.00
377	203.9	0.62	0.4492	0.3554	0.99
378	208.0	0.50	0.4972	0.3897	1.00
379	212.1	0.59	0.6449	0.4511	0.97
380	216.1	0.70	0.8337	0.5105	0.93
381	219.9	0.80	1.0344	0.5592	0.90
382	224.0	0.81	1.1933	0.5951	0.88
383	228.1	0.73	1.2522	0.5950	0.85
384	231.2	0.79	1.4616	0.6397	0.83
End of Table B4					

Table B5. LS(1)-0417MOD, LEGR k/c=0.0019, Re = 1.5 million					
RUN	AOA	C_l	C_{dp}	$C_{m¼}$	Re x10^{-6}
400	-29.9	-0.75	0.5281	0.0967	1.37
401	-25.8	-0.58	0.3890	0.0575	1.41
402	-22.0	-0.43	0.2840	0.0252	1.49
403	-19.9	-0.45	0.2499	0.0207	1.50
404	-18.0	-0.54	0.2345	0.0333	1.50
405	-16.0	-0.67	0.1417	-0.0181	1.49
406	-13.9	-0.65	0.1118	-0.0150	1.48
407	-11.9	-0.63	0.0476	-0.0613	1.49
408	-9.9	-0.49	0.0326	-0.0601	1.50
409	-8.0	-0.36	0.0208	-0.0598	1.50
410	-6.0	-0.16	0.0116	-0.0602	1.50
411	-4.0	0.05	0.0033	-0.0638	1.50
412	-1.9	0.26	-.0025	-0.0654	1.50
413	0.1	0.46	-.0068	-0.0675	1.50
414	2.0	0.65	-.0086	-0.0682	1.50
415	4.0	0.83	-.0048	-0.0673	1.49
416	6.1	0.98	0.0003	-0.0627	1.49
417	8.2	1.14	0.0044	-0.0575	1.49
418	10.2	0.86	0.0857	-0.1003	1.50
419	11.0	0.86	0.0974	-0.0987	1.48
420	12.0	0.93	0.1148	-0.0992	1.48
421	13.1	0.90	0.1286	-0.0967	1.49
422	14.0	0.90	0.1411	-0.0977	1.50
423	15.0	0.87	0.1579	-0.1011	1.49
424	16.1	0.84	0.1760	-0.1022	1.49
425	16.9	0.80	0.1937	-0.1077	1.49
426	17.9	0.82	0.2193	-0.1160	1.48

Table B5. LS(1)-0417MOD, LEGR k/c=0.0019, Re = 1.5 million					
RUN	AOA	C_l	C_{dp}	$C_{m¼}$	Re x10^{-6}
427	19.0	0.85	0.2502	-0.1262	1.50
428	20.0	0.85	0.2754	-0.1316	1.50
429	22.1	0.94	0.3521	-0.1606	1.48
430	24.1	0.94	0.3891	-0.1624	1.52
431	26.1	1.00	0.4640	-0.1847	1.50
432	28.0	1.08	0.5477	-0.2118	1.50
433	30.0	1.18	0.6526	-0.2439	1.49
434	32.1	1.29	0.7849	-0.2838	1.48
435	34.3	1.30	0.8587	-0.2945	1.45
436	36.0	1.44	1.0090	-0.3466	1.38
End of Table B5					

Table B6. LS(1)-0417MOD, LEGR k/c=0.0019, Re = 2 million					
RUN	AOA	C_l	C_{dp}	$C_{m¼}$	Re x10^{-6}
440	-20.1	-0.43	0.2607	0.0240	1.88
441	-18.0	-0.47	0.2254	0.0196	1.87
442	-16.0	-0.64	0.1760	0.0080	1.88
443	-13.9	-0.63	0.1309	-0.0023	1.91
444	-11.9	-0.65	0.0481	-0.0616	1.99
445	-10.1	-0.55	0.0361	-0.0612	1.99
446	-8.0	-0.38	0.0239	-0.0600	1.99
447	-6.0	-0.20	0.0123	-0.0611	1.99
448	-3.9	0.02	0.0036	-0.0631	1.99
449	-1.8	0.24	-.0020	-0.0655	1.99
450	0.2	0.46	-.0063	-0.0681	1.99
451	2.0	0.65	-.0077	-0.0683	1.99
452	4.1	0.84	-.0065	-0.0674	1.98
453	6.1	1.02	-.0032	-0.0641	1.98
454	8.2	1.16	0.0028	-0.0588	1.97
455	9.9	0.80	0.0737	-0.0825	1.99
456	11.0	0.83	0.1001	-0.0969	1.98
457	12.0	0.94	0.1082	-0.0895	1.97
458	13.0	0.94	0.1307	-0.1010	1.99
459	14.1	0.85	0.1464	-0.1005	1.98
460	15.1	0.85	0.1643	-0.1035	2.00
461	16.1	0.81	0.1809	-0.1047	1.99
462	17.2	0.82	0.2038	-0.1121	1.98
463	18.0	0.83	0.2252	-0.1180	1.97
464	19.0	0.84	0.2593	-0.1303	1.99
465	20.0	0.86	0.2902	-0.1390	1.98
466	22.1	0.93	0.3530	-0.1602	1.99

Table B6. LS(1)-0417MOD, LEGR k/c=0.0019, Re = 2 million					
RUN	AOA	C_l	C_{dp}	$C_{m¼}$	Re x10^{-6}
467	24.1	0.97	0.4140	-0.1740	1.99
468	26.2	0.99	0.4766	-0.1879	1.97
469	28.3	1.05	0.5642	-0.2122	1.93
470	30.3	1.13	0.6518	-0.2352	1.87
471	32.1	1.22	0.7512	-0.2657	1.82
End of Table B6					

Table B7. LS(1)-0417MOD, LEGR k/c=0.0019, VGs, Re = 1 million					
RUN	AOA	C_l	C_{dp}	$C_{m¼}$	Re x10^{-6}
480	-20.0	-0.38	0.2492	0.0170	0.98
481	-17.9	-0.49	0.2522	0.0351	0.98
482	-16.1	-0.63	0.1822	-0.0041	1.00
483	-14.0	-0.60	0.1392	-0.0046	1.00
484	-11.9	-0.63	0.0506	-0.0567	1.01
485	-10.1	-0.54	0.0350	-0.0606	1.01
486	-8.0	-0.40	0.0223	-0.0604	1.01
487	-5.9	-0.23	0.0134	-0.0618	1.01
488	-4.1	-0.06	0.0068	-0.0630	0.99
489	-2.0	0.16	0.0031	-0.0670	1.00
490	0.1	0.37	-.0002	-0.0704	1.00
491	2.0	0.59	-.0003	-0.0746	1.00
492	4.0	0.78	0.0028	-0.0739	1.00
493	5.9	0.99	0.0058	-0.0767	1.00
494	7.9	1.16	0.0125	-0.0776	1.00
495	10.0	1.34	0.0249	-0.0788	0.99
496	11.1	1.41	0.0333	-0.0776	0.99
497	12.1	0.91	0.1124	-0.0997	1.00
498	12.9	0.88	0.1198	-0.0939	1.00
499	13.9	0.86	0.1415	-0.0999	0.99
500	15.0	0.85	0.1550	-0.0996	0.99
501	16.0	0.78	0.1661	-0.0966	0.99
502	17.1	0.80	0.1905	-0.1050	0.99
503	18.1	0.82	0.2090	-0.1065	0.99
504	19.1	0.83	0.2349	-0.1158	0.99
505	19.9	0.82	0.2548	-0.1200	1.00
506	22.0	0.85	0.3132	-0.1373	0.99

Table B7. LS(1)-0417MOD, LEGR k/c=0.0019, VGs, Re = 1 million					
RUN	AOA	C_l	C_{dp}	$C_{m¼}$	Re x10^{-6}
507	23.9	0.94	0.3928	-0.1660	1.00
508	26.0	0.97	0.4515	-0.1797	0.99
509	28.0	1.02	0.5314	-0.1992	0.99
510	30.1	1.07	0.6155	-0.2214	1.00
511	31.9	1.14	0.7001	-0.2419	1.00
512	34.0	1.22	0.8117	-0.2745	0.98
513	36.1	1.32	0.9493	-0.3180	0.99
514	38.0	1.28	0.9780	-0.3110	0.98
515	40.0	1.30	1.0665	-0.3307	1.00
End of Table B7					

Table B8. LS(1)-0417MOD, LEGR k/c=0.0019, VGs, Re = 1.5 million					
RUN	AOA	C_l	C_{dp}	$C_{m¼}$	Re x10^{-6}
520	-20.0	-0.38	0.2466	0.0129	1.49
521	-17.9	-0.53	0.2294	0.0160	1.50
522	-16.1	-0.52	0.2043	0.0165	1.51
523	-14.0	-0.66	0.1285	-0.0108	1.48
524	-11.9	-0.65	0.0494	-0.0606	1.50
525	-10.1	-0.54	0.0361	-0.0608	1.50
526	-8.0	-0.39	0.0232	-0.0610	1.50
527	-5.9	-0.20	0.0126	-0.0635	1.49
528	-3.8	-0.01	0.0051	-0.0658	1.50
529	-2.0	0.18	0.0016	-0.0690	1.50
530	0.1	0.39	-.0006	-0.0716	1.50
531	2.0	0.59	-.0016	-0.0740	1.49
532	4.0	0.80	0.0012	-0.0749	1.49
533	6.1	0.98	0.0078	-0.0759	1.49
534	7.9	1.16	0.0128	-0.0772	1.49
535	10.0	1.32	0.0260	-0.0761	1.49
536	11.1	1.40	0.0360	-0.0768	1.49
537	12.1	0.76	0.1051	-0.0849	1.47
538	12.9	0.79	0.1236	-0.0970	1.48
539	13.9	0.88	0.1452	-0.1015	1.50
540	14.9	0.81	0.1595	-0.0996	1.49
541	16.0	0.78	0.1718	-0.0977	1.48
542	17.1	0.77	0.1929	-0.1028	1.48
543	17.9	0.81	0.2120	-0.1082	1.50
544	18.9	0.80	0.2337	-0.1137	1.50
545	19.9	0.84	0.2713	-0.1295	1.49
546	22.0	0.89	0.3405	-0.1527	1.49

Table B8. LS(1)-0417MOD, LEGR k/c=0.0019, VGs, Re = 1.5 million					
RUN	AOA	C_l	C_{dp}	$C_{m¼}$	Re x10^{-6}
547	24.1	0.90	0.3897	-0.1598	1.47
548	25.9	0.97	0.4613	-0.1817	1.50
549	28.0	1.03	0.5387	-0.2021	1.50
550	29.8	1.11	0.6272	-0.2281	1.50
551	32.0	1.16	0.7145	-0.2492	1.47
552	34.0	1.22	0.8159	-0.2764	1.50
553	35.9	1.31	0.9361	-0.3142	1.48
End of Table B8					

Table B9. LS(1)-0417MOD, Clean, VGs, Re = 1 million					
RUN	AOA	C_l	C_{dp}	$C_{m¼}$	Re x10^{-6}
560	-20.0	-0.38	0.2613	0.0179	1.00
561	-17.9	-0.29	0.2130	0.0032	1.00
562	-16.0	-0.29	0.2005	0.0076	1.00
563	-14.1	-0.24	0.1700	-0.0007	1.01
564	-12.1	-0.71	0.0396	-0.0603	1.00
565	-10.0	-0.60	0.0283	-0.0585	1.00
566	-7.9	-0.45	0.0212	-0.0590	1.00
567	-6.0	-0.29	0.0107	-0.0642	1.00
568	-4.0	-0.07	0.0059	-0.0696	1.01
569	-2.0	0.12	0.0038	-0.0755	1.00
570	0.1	0.36	0.0022	-0.0817	0.99
571	2.0	0.58	0.0043	-0.0852	1.00
572	3.9	0.77	0.0099	-0.0846	1.00
573	6.0	0.97	0.0160	-0.0869	0.99
574	8.1	1.16	0.0263	-0.0892	1.00
575	9.9	1.34	0.0364	-0.0895	0.99
576	10.9	1.44	0.0418	-0.0903	0.99
577	12.0	1.51	0.0523	-0.0903	0.99
578	13.0	1.62	0.0542	-0.0901	0.99
579	14.1	1.70	0.0616	-0.0900	0.99
580	14.9	1.78	0.0708	-0.0913	0.99
581	15.9	1.84	0.0766	-0.0876	0.99
582	17.0	1.88	0.0906	-0.0858	1.00
583	18.0	1.11	0.1460	-0.1180	0.99
584	19.1	1.06	0.1548	-0.1111	0.99
585	19.9	1.56	0.2020	-0.0887	0.99
586	22.0	1.48	0.2470	-0.1178	0.99

Table B9. LS(1)-0417MOD, Clean, VGs, Re = 1 million					
RUN	AOA	C_l	C_{dp}	$C_{m¼}$	Re x10^{-6}
587	24.1	1.37	0.2803	-0.1313	1.00
588	25.9	1.18	0.3032	-0.1403	1.00
589	28.0	1.08	0.3472	-0.1519	1.00
590	30.1	0.87	0.5399	-0.1798	1.00
591	32.0	0.91	0.5896	-0.1867	1.00
592	34.0	0.94	0.6638	-0.2040	1.01
593	36.1	1.01	0.7595	-0.2280	0.99
594	37.9	1.28	1.0274	-0.3186	1.00
595	40.0	1.35	1.1498	-0.3446	1.00
End of Table B9					

Table B10. LS(1)-0417MOD, Clean, VGs, Re = 1.5 million					
RUN	AOA	C_l	C_{dp}	$C_{m¼}$	Re x10^{-6}
600	-20.0	-0.38	0.2518	0.0144	1.50
601	-17.9	-0.32	0.2169	0.0065	1.48
602	-16.0	-0.28	0.1921	0.0035	1.49
603	-13.9	-0.26	0.1740	0.0081	1.50
604	-12.1	-0.77	0.0335	-0.0612	1.50
605	-10.0	-0.63	0.0253	-0.0600	1.51
606	-7.9	-0.49	0.0155	-0.0601	1.49
607	-6.0	-0.30	0.0106	-0.0635	1.49
608	-3.9	-0.05	0.0048	-0.0705	1.50
609	-1.8	0.16	0.0026	-0.0768	1.50
610	-0.0	0.36	0.0021	-0.0818	1.50
611	2.0	0.59	0.0042	-0.0858	1.50
612	3.9	0.80	0.0054	-0.0884	1.50
613	6.0	1.01	0.0125	-0.0904	1.49
614	8.1	1.19	0.0230	-0.0914	1.50
615	9.9	1.38	0.0288	-0.0914	1.49
616	11.0	1.45	0.0398	-0.0916	1.49
617	11.8	1.53	0.0421	-0.0909	1.49
618	13.1	1.64	0.0509	-0.0899	1.49
619	14.1	1.72	0.0593	-0.0892	1.48
620	14.9	1.77	0.0684	-0.0890	1.50
621	15.9	1.85	0.0765	-0.0890	1.49
622	17.0	1.09	0.1409	-0.1230	1.48
623	18.0	1.05	0.1550	-0.1200	1.50
624	19.1	1.45	0.1923	-0.1009	1.49
625	20.1	1.41	0.2092	-0.1062	1.49
626	22.2	1.41	0.2511	-0.1170	1.50

Table B10. LS(1)-0417MOD, Clean, VGs, Re = 1.5 million					
RUN	AOA	C_l	C_{dp}	$C_{m¼}$	Re x10^{-6}
627	24.2	1.26	0.2798	-0.1315	1.49
628	25.9	1.03	0.3189	-0.1507	1.51
629	28.0	1.04	0.3637	-0.1573	1.50
630	30.1	1.05	0.4174	-0.1693	1.48
631	32.0	1.08	0.4848	-0.1893	1.50
632	34.0	1.09	0.5365	-0.1998	1.49
633	35.8	0.89	0.6706	-0.1982	1.50
634	37.9	0.93	0.7423	-0.2123	1.51
635	40.0	1.03	0.8851	-0.2511	1.49
End of Table B10					

Table B11. LS(1)-0417MOD, Clean, Re = 1 million, Small α Cal Range					
RUN	AOA	C_l	C_{dp}	$C_{m¼}$	Re x10^{-6}
640	-20.1	-0.37	0.2521	0.0272	1.00
641	-18.0	-0.39	0.2385	0.0344	1.00
642	-16.0	-0.27	0.1852	0.0136	1.01
643	-14.0	-0.29	0.1762	0.0281	1.00
644	-11.9	-0.74	0.0428	-0.0463	1.01
645	-10.0	-0.56	0.0299	-0.0608	1.00
646	-7.9	-0.38	0.0194	-0.0647	1.00
647	-6.0	-0.21	0.0105	-0.0703	1.00
648	-4.0	-0.03	0.0045	-0.0712	1.00
649	-2.1	0.19	0.0013	-0.0752	1.00
650	-0.0	0.40	-.0013	-0.0794	1.01
651	2.1	0.61	0.0016	-0.0801	1.01
652	4.0	0.80	0.0077	-0.0796	1.00
653	6.1	1.00	0.0108	-0.0784	1.00
654	8.0	1.17	0.0185	-0.0779	1.00
655	10.0	1.32	0.0277	-0.0724	0.99
656	11.1	1.39	0.0346	-0.0700	1.00
657	11.9	1.45	0.0390	-0.0677	1.00
658	13.0	1.52	0.0447	-0.0638	1.00
659	14.0	1.56	0.0484	-0.0586	0.99
660	15.1	1.55	0.0835	-0.0662	0.99
661	16.1	1.57	0.1018	-0.0671	0.99
662	17.2	1.06	0.1252	-0.1070	1.00
663	17.9	1.06	0.1357	-0.1080	1.00
664	19.0	1.51	0.1812	-0.0938	0.99
665	20.1	1.48	0.2048	-0.1003	1.00
666	21.9	1.42	0.2352	-0.1148	1.00

Table B11. LS(1)-0417MOD, Clean, Re = 1 million, Small α Cal Range					
RUN	AOA	C_l	C_{dp}	$C_{m¼}$	Re x10^{-6}
667	24.0	1.35	0.2731	-0.1273	1.00
668	26.1	1.13	0.3073	-0.1429	0.99
669	28.0	1.04	0.3392	-0.1471	0.99
670	30.0	1.15	0.4181	-0.1686	1.00
671	32.0	1.16	0.4784	-0.1882	0.99
672	34.0	1.19	0.8212	-0.2671	1.00
673	35.9	1.20	0.8904	-0.2793	0.99
674	38.0	1.31	1.0460	-0.3280	1.00
675	40.1	1.30	1.1211	-0.3425	0.99
End of Table B11					

Table B12. LS(1)-0417MOD, Clean, Re = 1.5 million, Small α Cal Range					
RUN	AOA	C_l	C_{dp}	$C_{m¼}$	Re x10^{-6}
680	-20.1	-0.37	0.2435	0.0220	1.50
681	-18.0	-0.37	0.2291	0.0255	1.50
682	-15.9	-0.31	0.1953	0.0206	1.49
683	-14.0	-0.29	0.1749	0.0203	1.49
684	-11.9	-0.76	0.0358	-0.0543	1.49
685	-10.0	-0.60	0.0237	-0.0639	1.49
686	-7.9	-0.40	0.0163	-0.0669	1.49
687	-6.1	-0.22	0.0092	-0.0690	1.49
688	-4.0	-0.01	0.0033	-0.0698	1.49
689	-1.9	0.20	0.0004	-0.0747	1.50
690	-0.0	0.40	-.0015	-0.0782	1.49
691	2.1	0.61	0.0019	-0.0814	1.49
692	4.0	0.79	0.0066	-0.0819	1.49
693	6.1	0.98	0.0121	-0.0785	1.49
694	7.9	1.17	0.0171	-0.0779	1.49
695	10.0	1.33	0.0259	-0.0740	1.49
696	11.2	1.42	0.0344	-0.0708	1.50
697	12.1	1.46	0.0439	-0.0690	1.50
698	13.1	1.52	0.0492	-0.0655	1.49
699	14.0	1.57	0.0530	-0.0612	1.49
700	15.0	1.60	0.0610	-0.0576	1.49
701	15.8	1.08	0.1154	-0.1118	1.50
702	17.1	1.05	0.1326	-0.1107	1.49
703	17.9	1.01	0.1468	-0.1128	1.50
704	19.0	1.09	0.1766	-0.1234	1.49
705	20.0	1.43	0.2137	-0.1127	1.49
706	22.1	1.39	0.2467	-0.1168	1.50

Table B12. LS(1)-0417MOD, Clean, Re = 1.5 million, Small α Cal Range					
RUN	AOA	C_l	C_{dp}	$C_{m¼}$	Re x10^{-6}
707	24.0	1.32	0.2779	-0.1265	1.49
708	26.1	1.17	0.3386	-0.1542	1.49
709	28.2	1.02	0.3585	-0.1499	1.50
710	30.0	1.06	0.4127	-0.1656	1.49
711	31.6	1.10	0.4793	-0.1855	1.50
712	34.1	0.88	0.6208	-0.1877	1.48
713	36.1	0.90	0.6814	-0.2000	1.50
714	38.0	0.97	0.7719	-0.2229	1.49
715	40.1	1.11	0.9667	-0.2812	1.50
End of Table B12					

Steady State Pressure Distributions

Re = 1.0 million

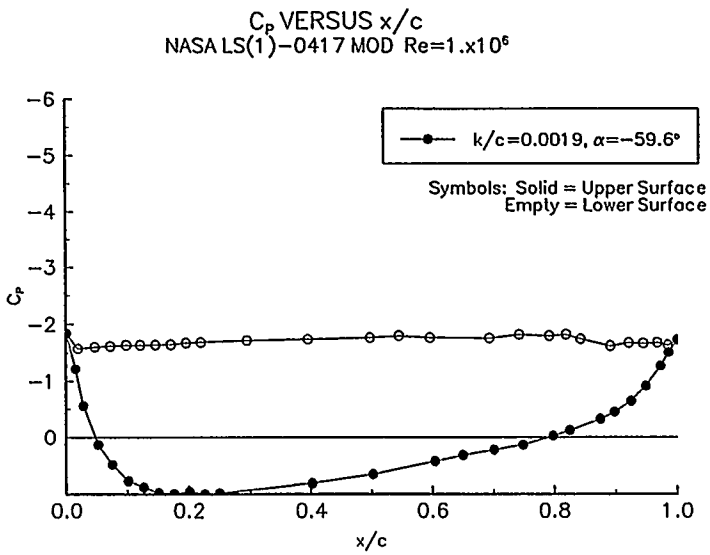

Figure 1. α = -60°

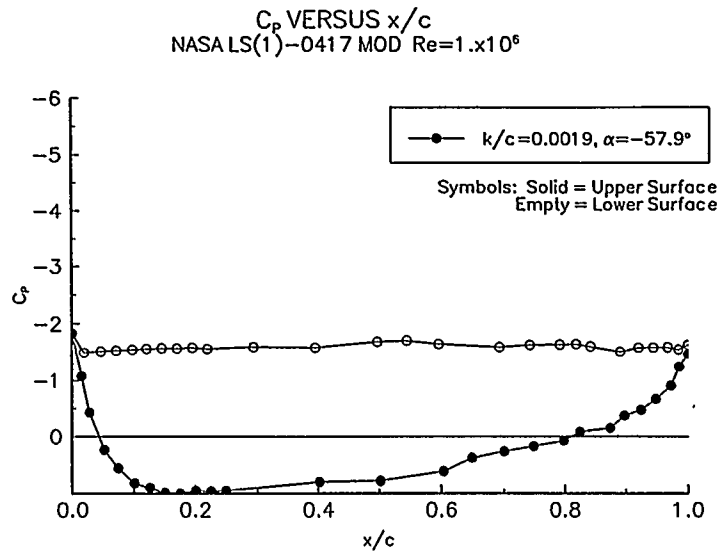

Figure 2. α = -58°

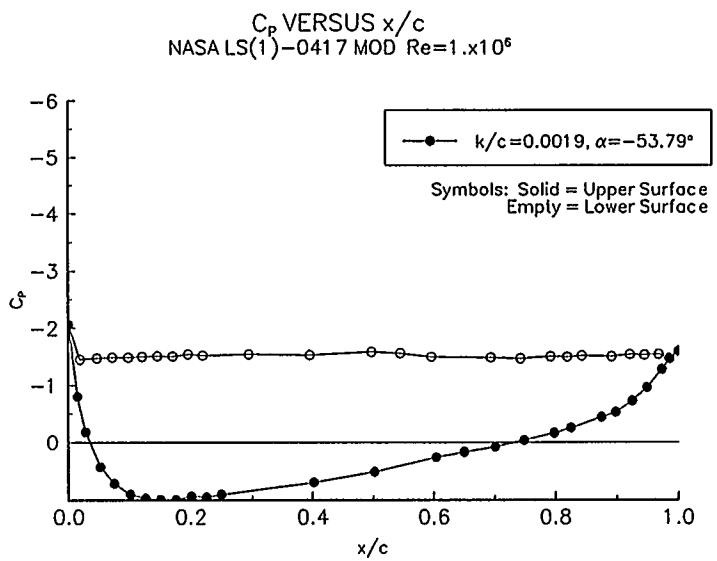

Figure 3. α = -54°

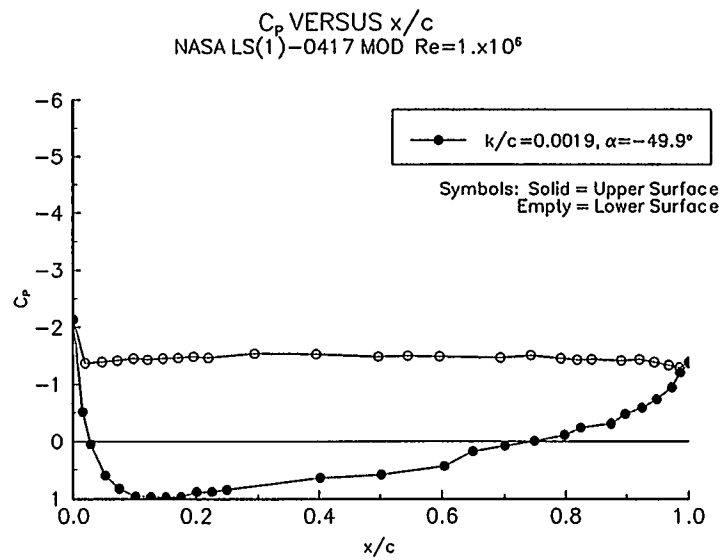

Figure 4. α = -50°

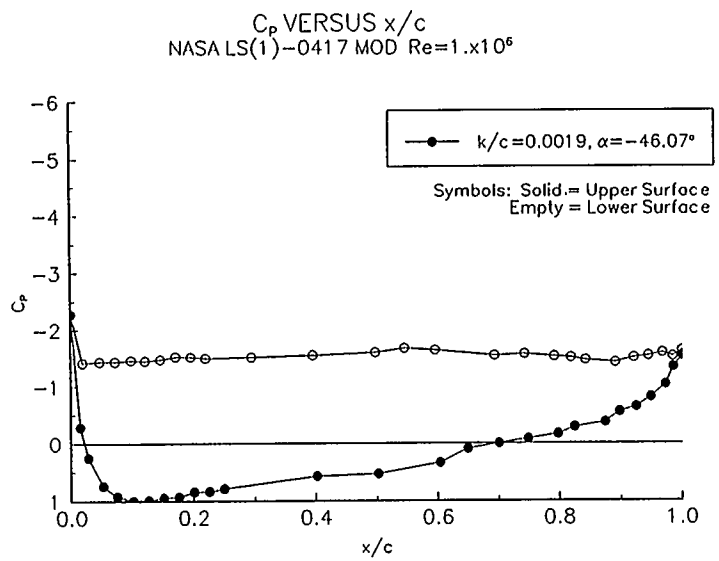

Figure 5. α = -46°

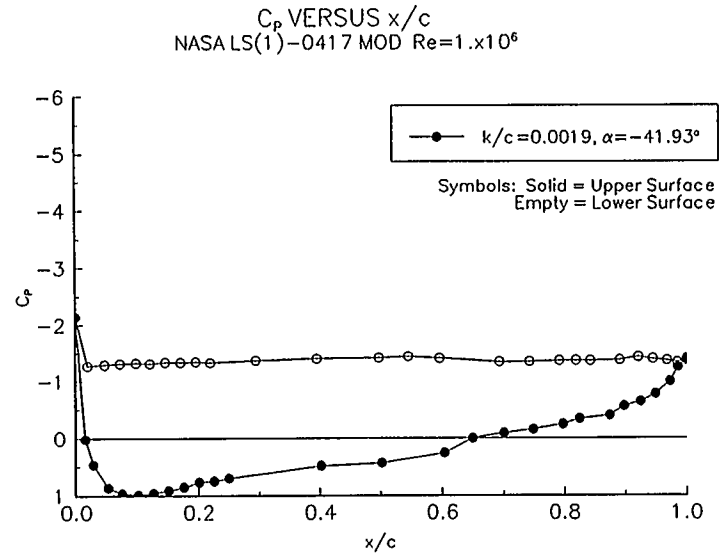

Figure 6. α = -42°

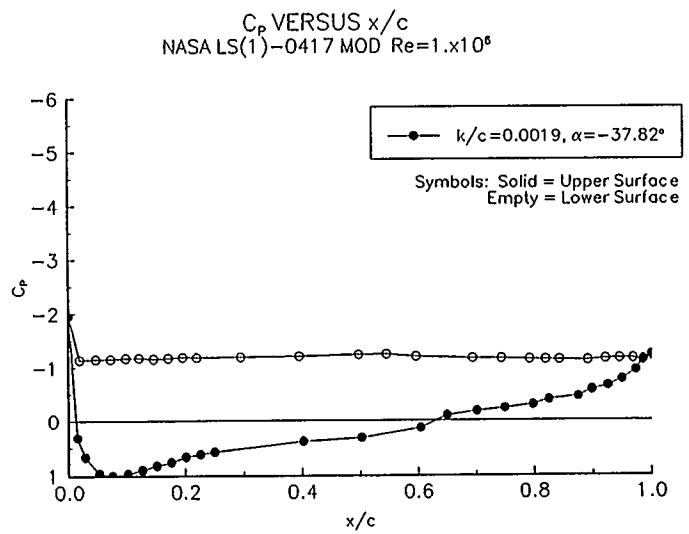

Figure 7. α = -38°

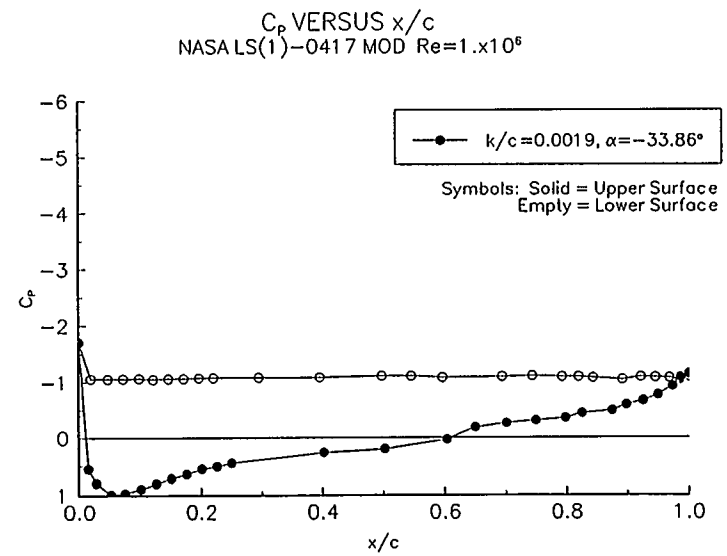

Figure 8. α = -34°

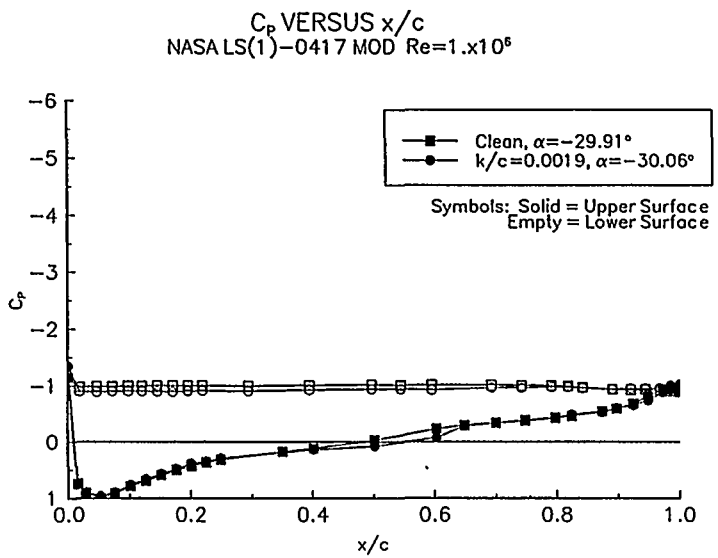

Figure 9. α = -30°

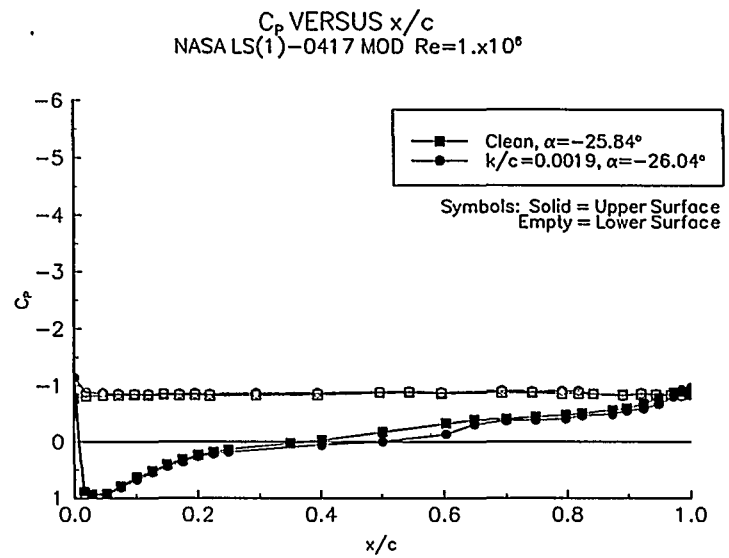

Figure 10. α = -26°

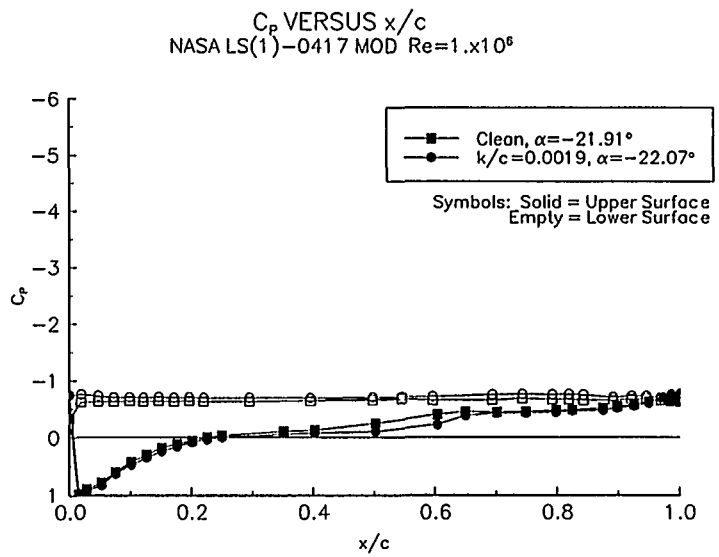

Figure 11. α = -22°

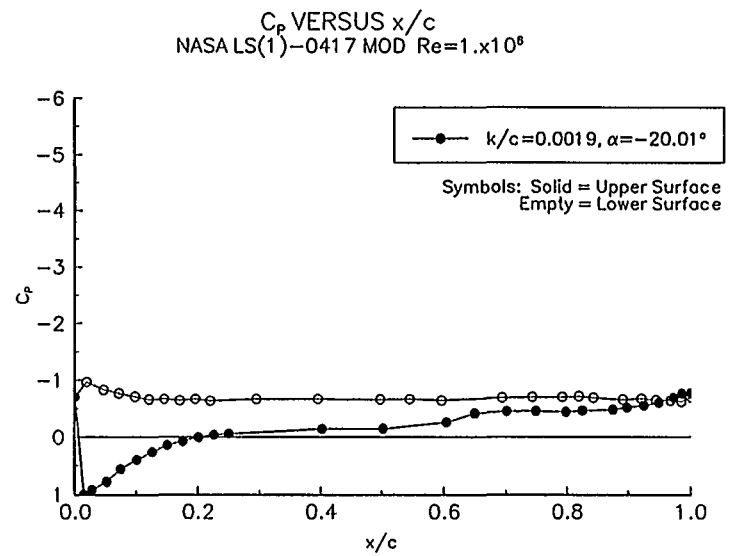

Figure 12. α = -20°

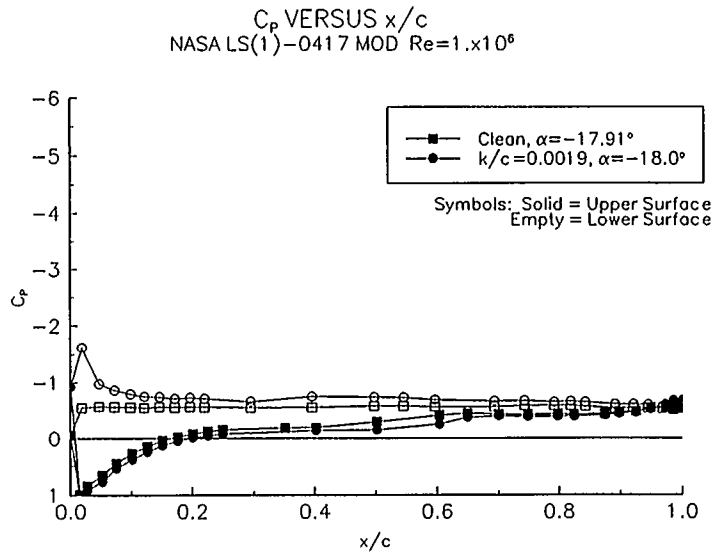

Figure 13. α = -18°

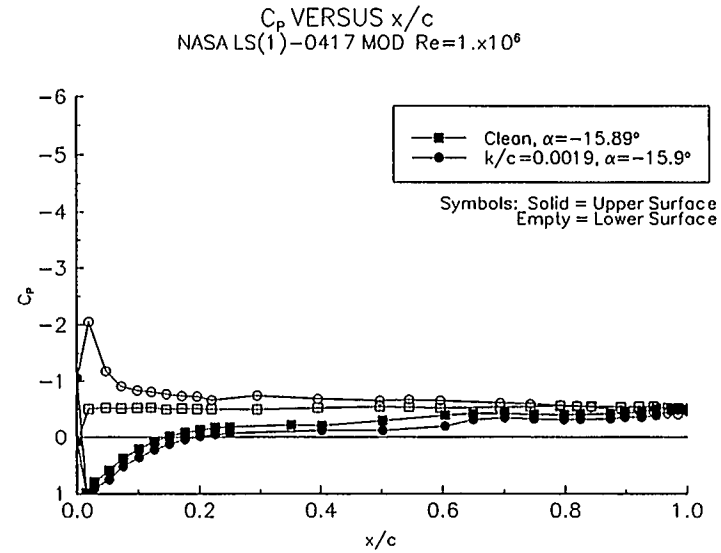

Figure 14. α = -16°

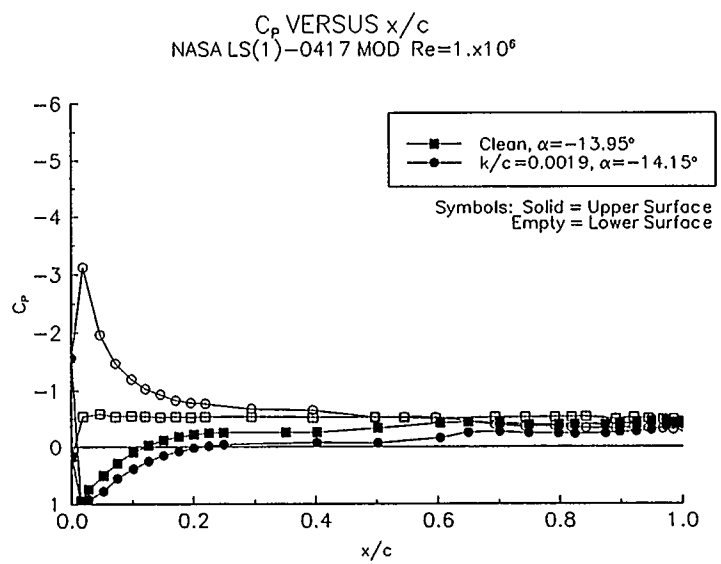

Figure 15. α = -14°

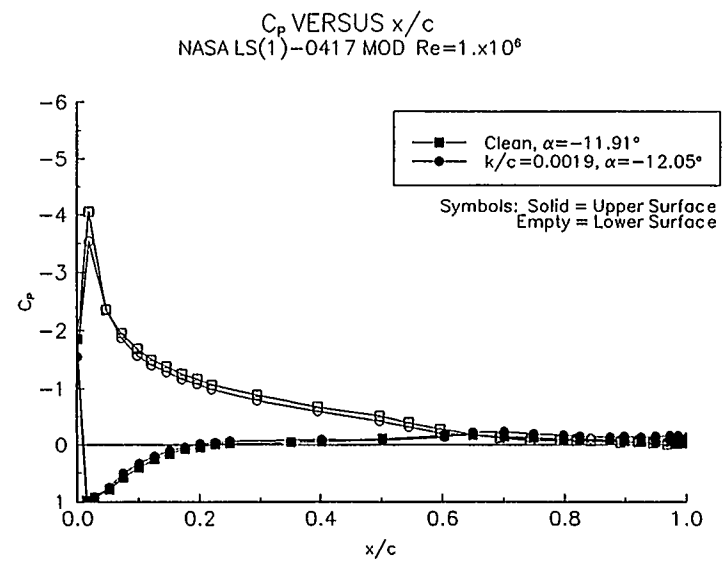

Figure 16. α = -12°

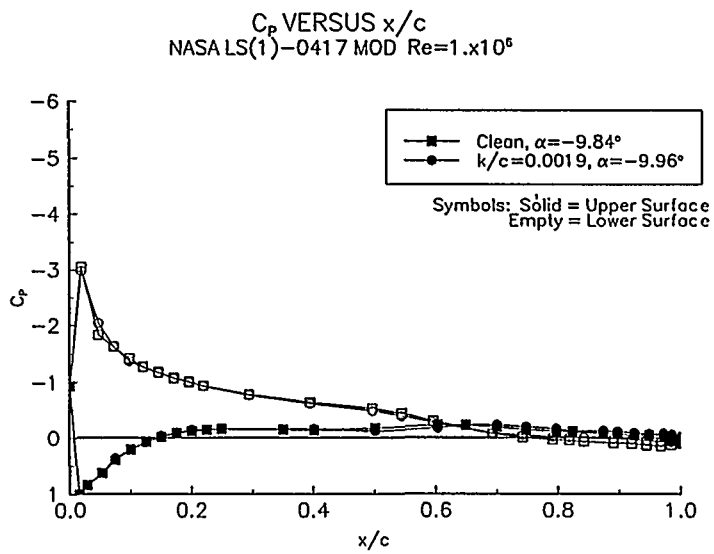

Figure 17. α = -10°

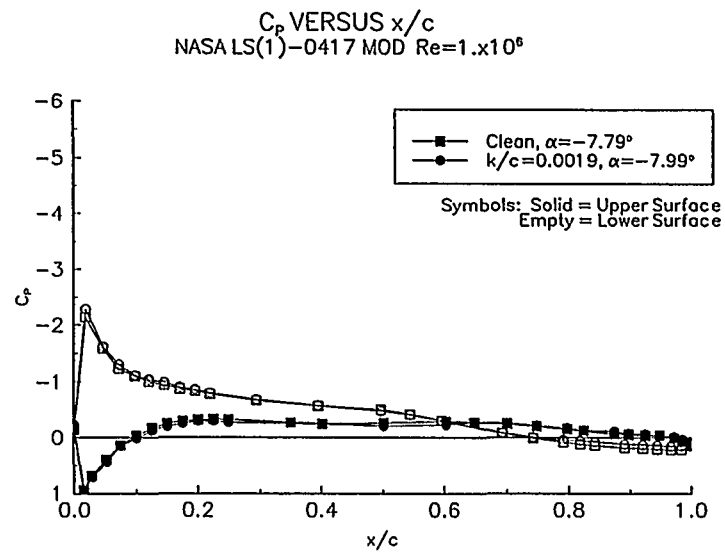

Figure 18. α = -8°

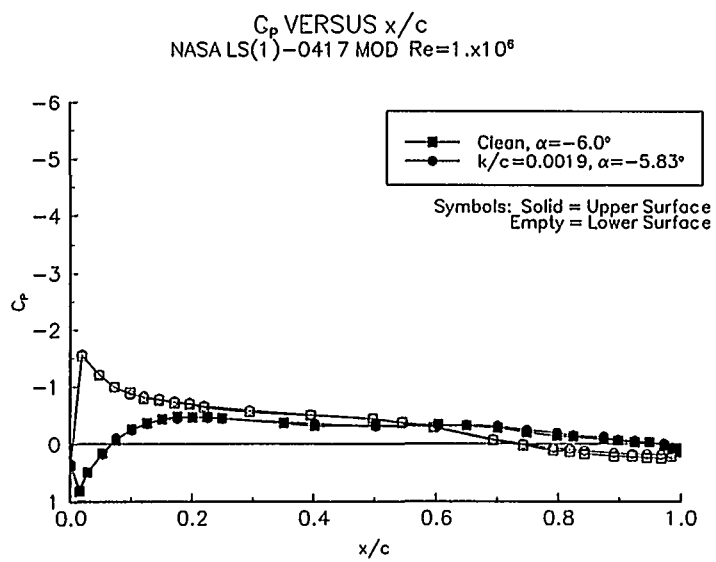

Figure 19. α = -6°

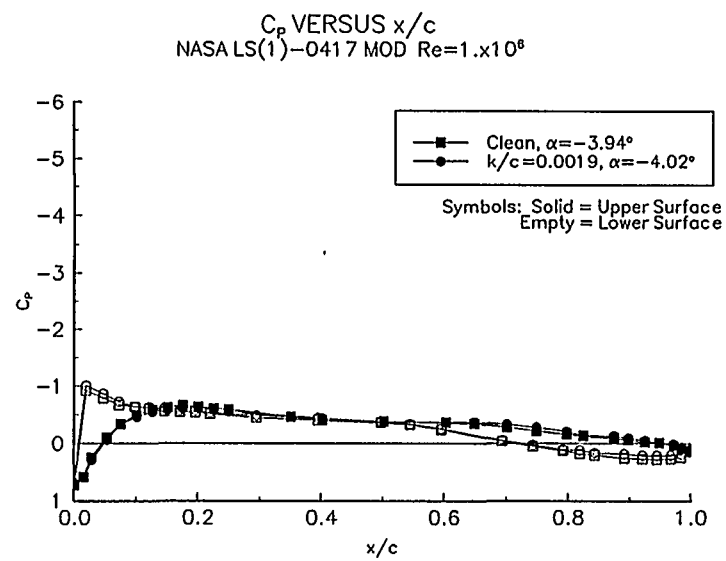

Figure 20. α = -4°

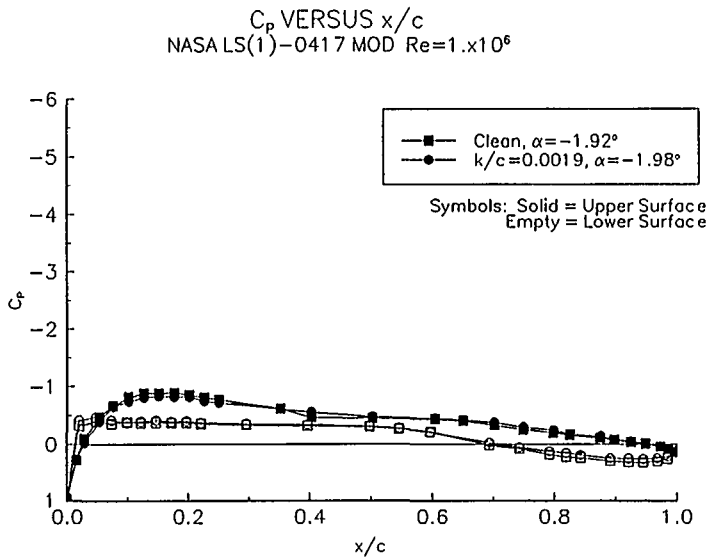

Figure 21. α = -2°

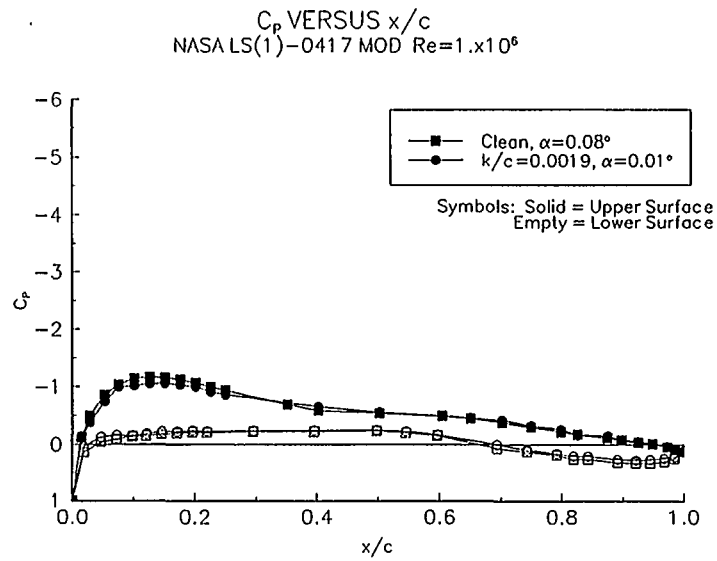

Figure 22. α = 0°

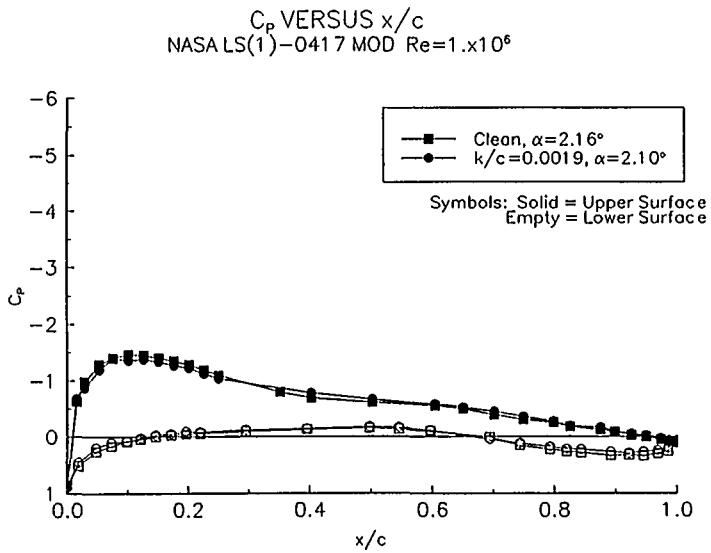

Figure 23. α = 2°

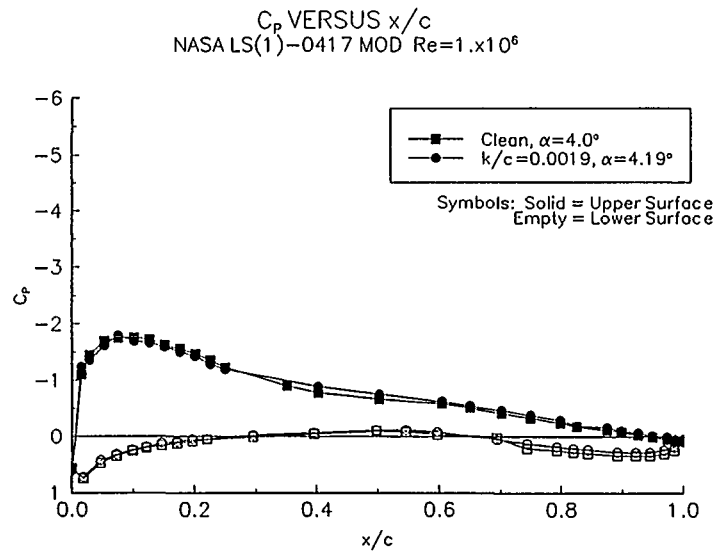

Figure 24. α = 4°

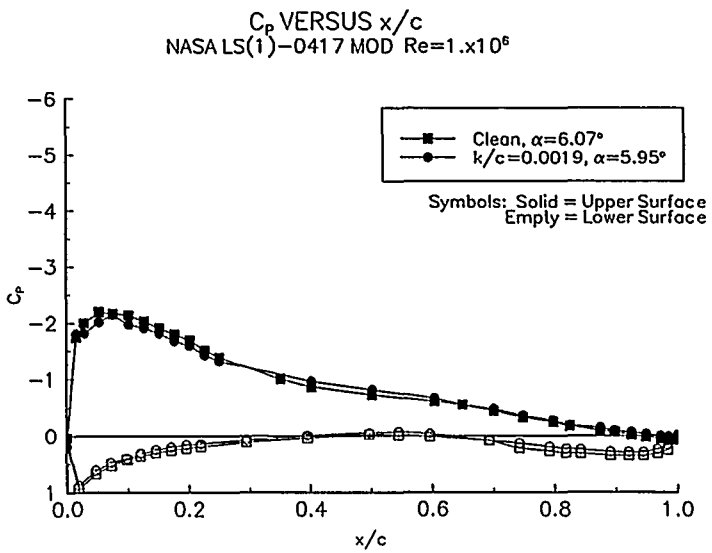

Figure 25. α = 6°

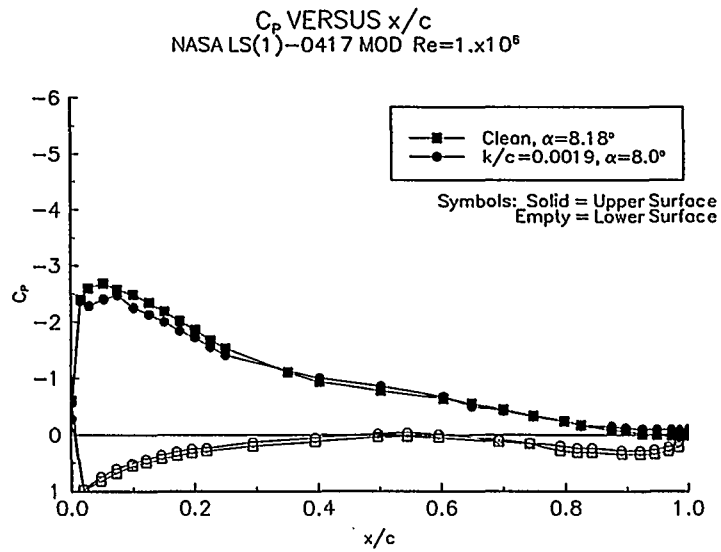

Figure 26. α = 8°

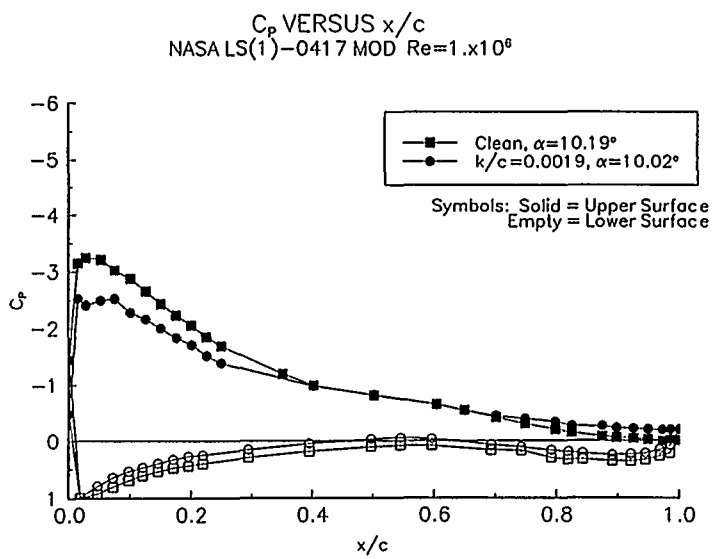

Figure 27. α = 10°

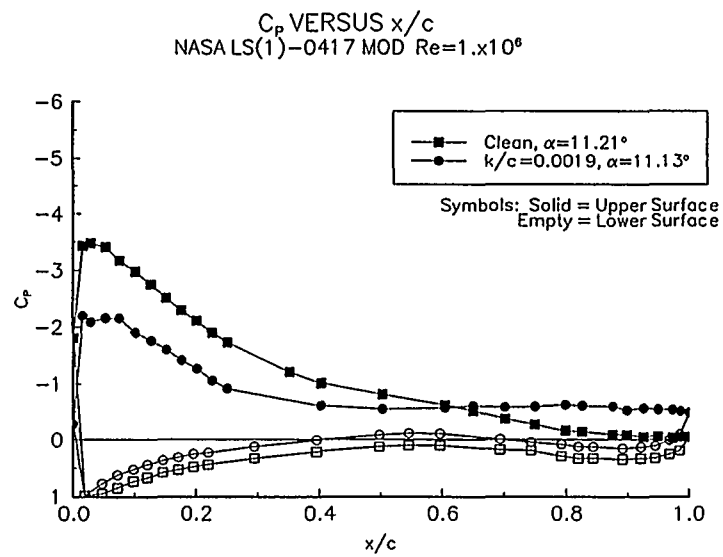

Figure 28. α = 11°

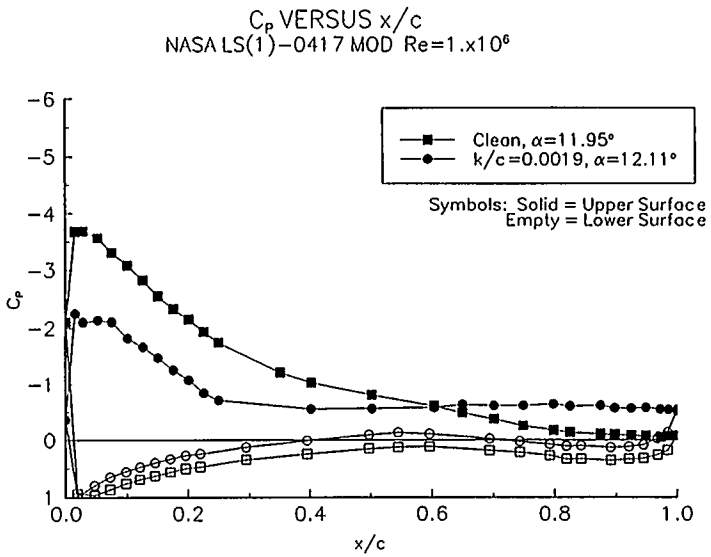

Figure 29. α = 12°

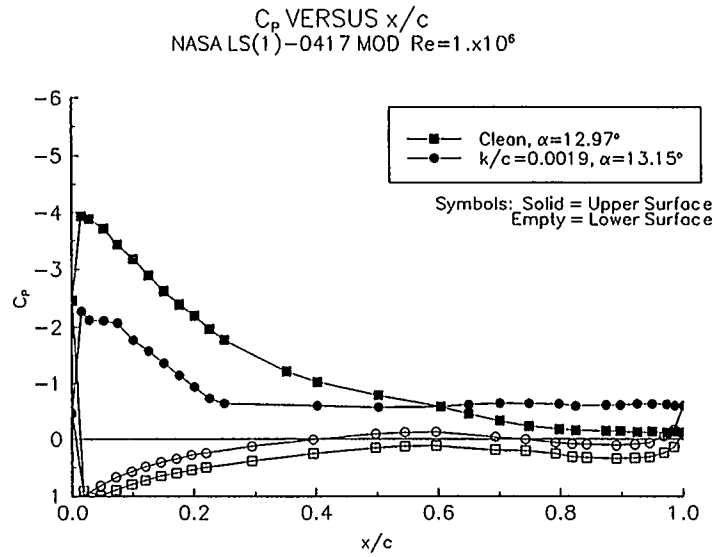

Figure 30. α = 13°

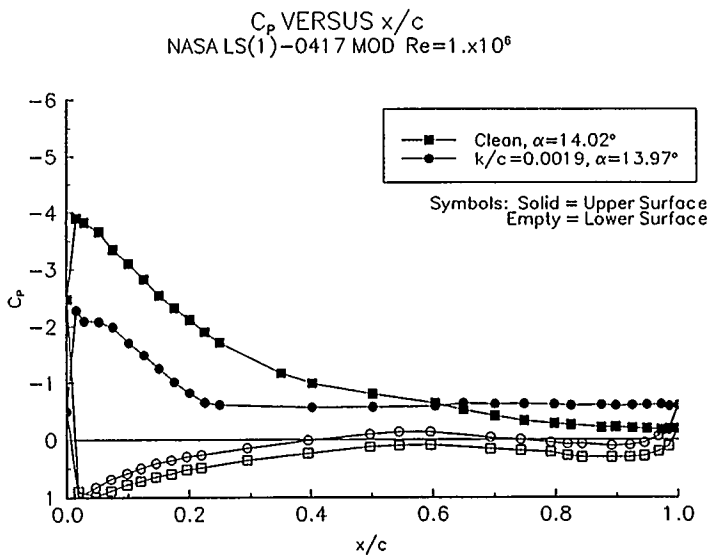

Figure 31. α = 14°

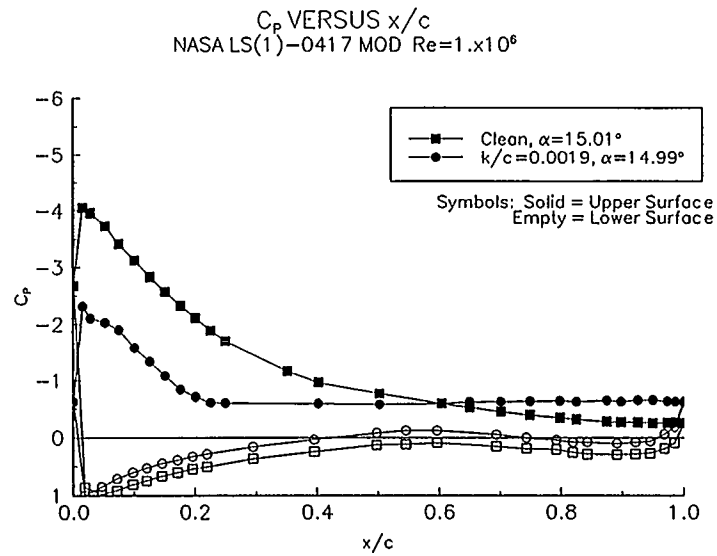

Figure 32. α = 15°

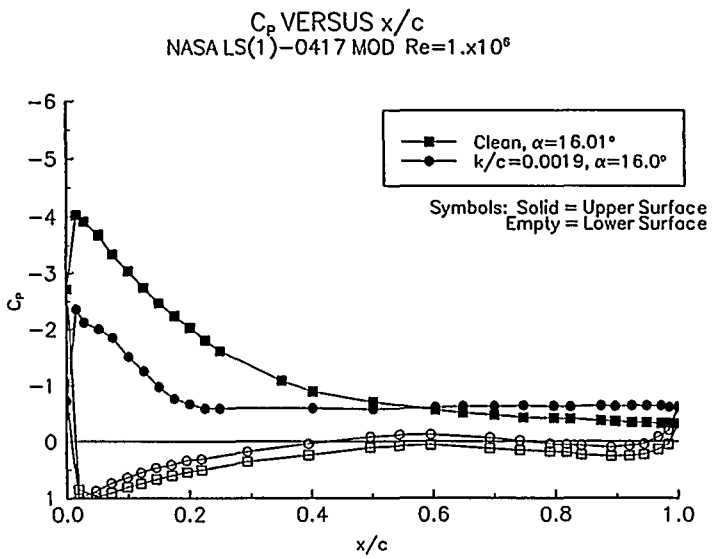

Figure 33. α = 16°

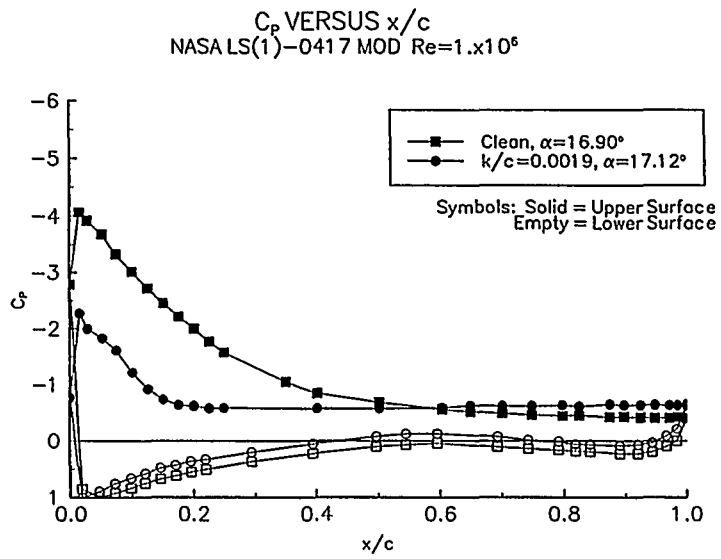

Figure 34. α = 17°

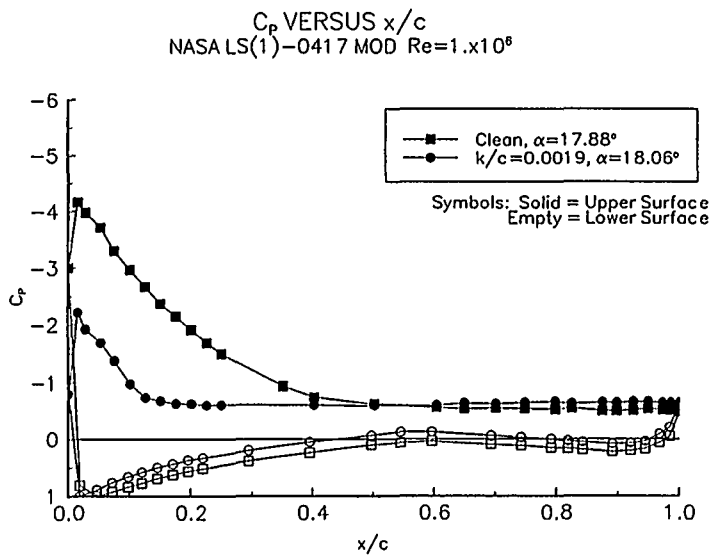

Figure 35. α = 18°

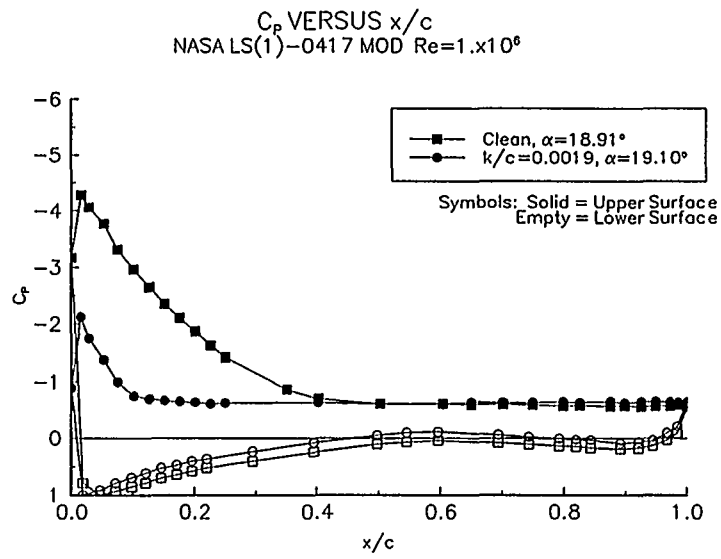

Figure 36. α = 19°

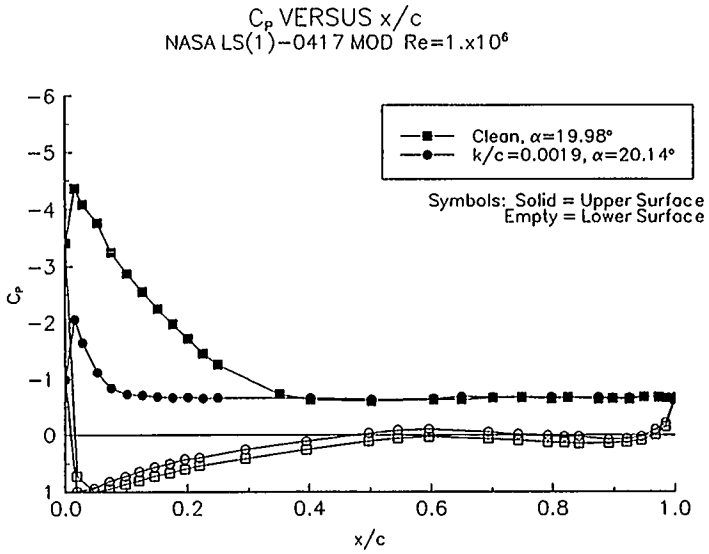

Figure 37. α = 20°

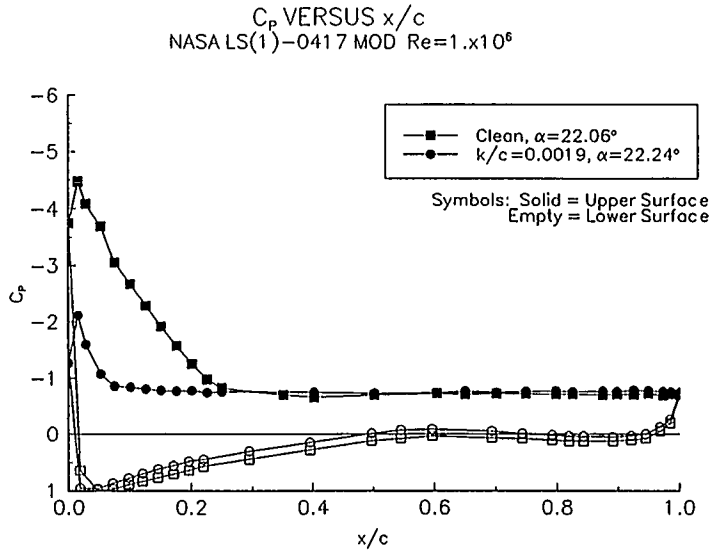

Figure 38. α = 22°

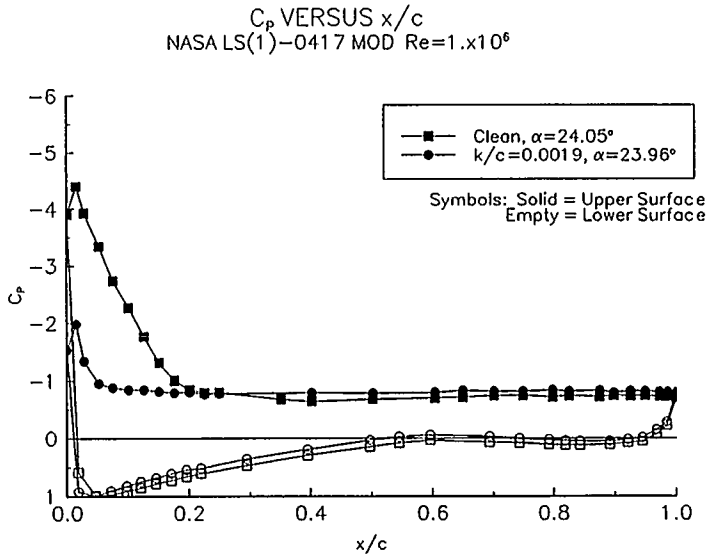

Figure 39. α = 24°

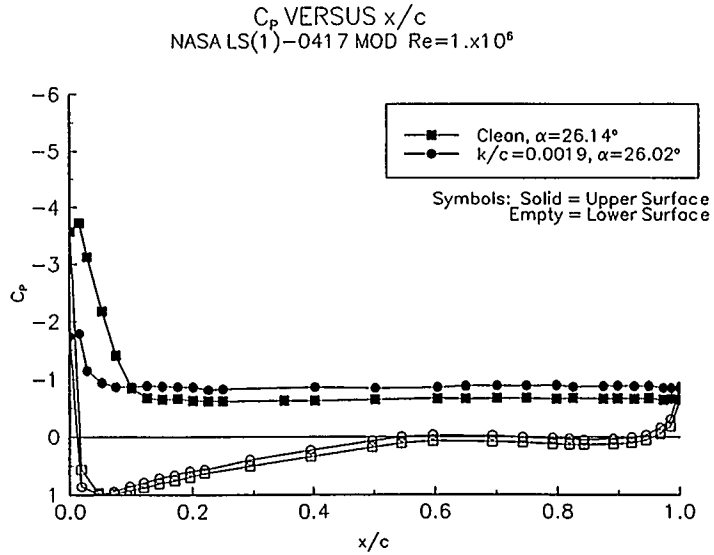

Figure 40. α = 26°

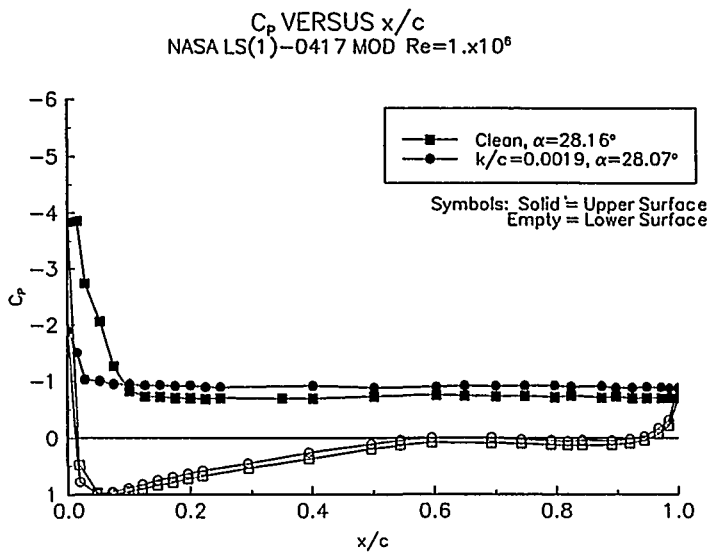

Figure 41. α = 28°

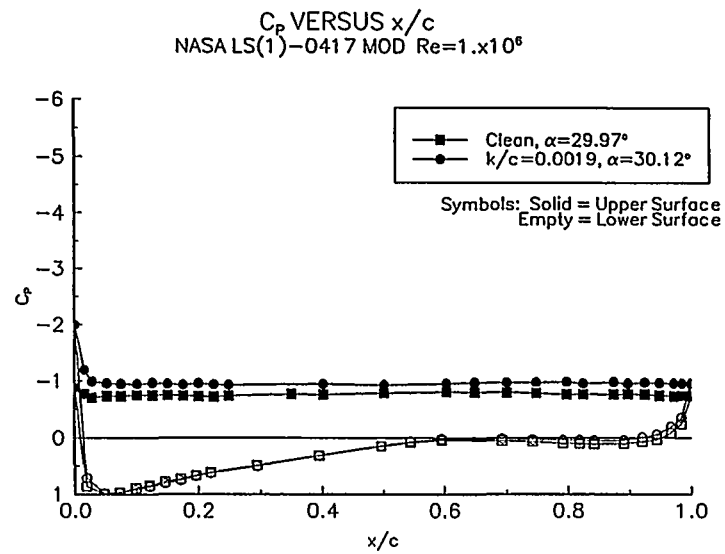

Figure 42. α = 30°

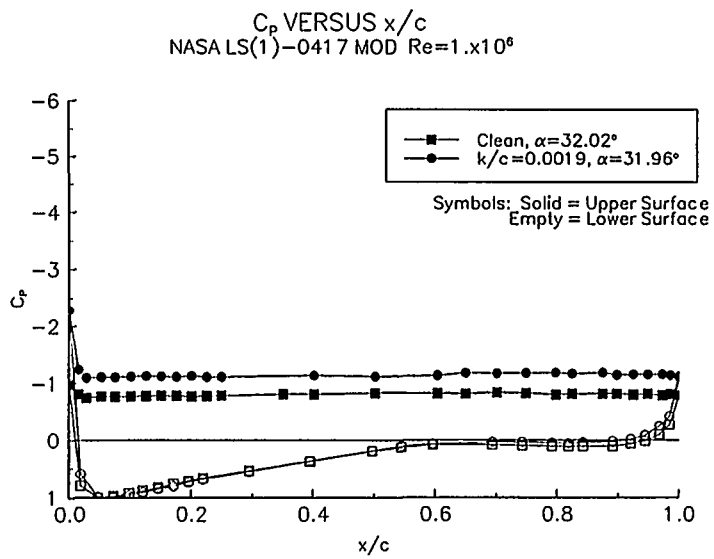

Figure 43. α = 32°

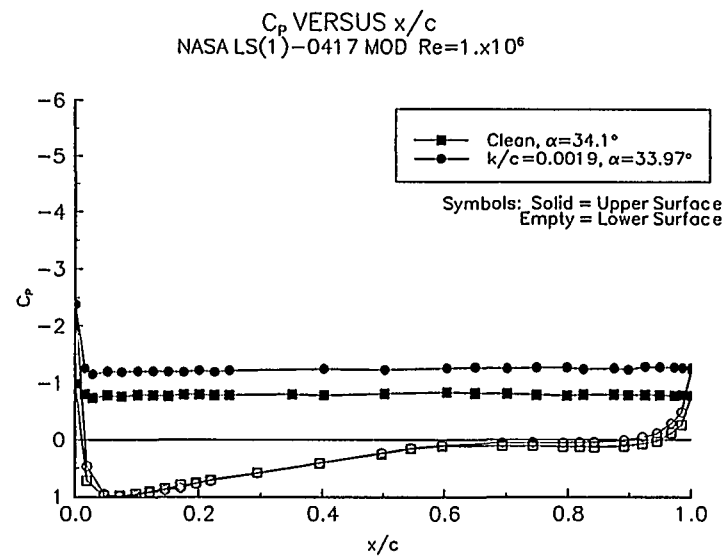

Figure 44. α = 34°

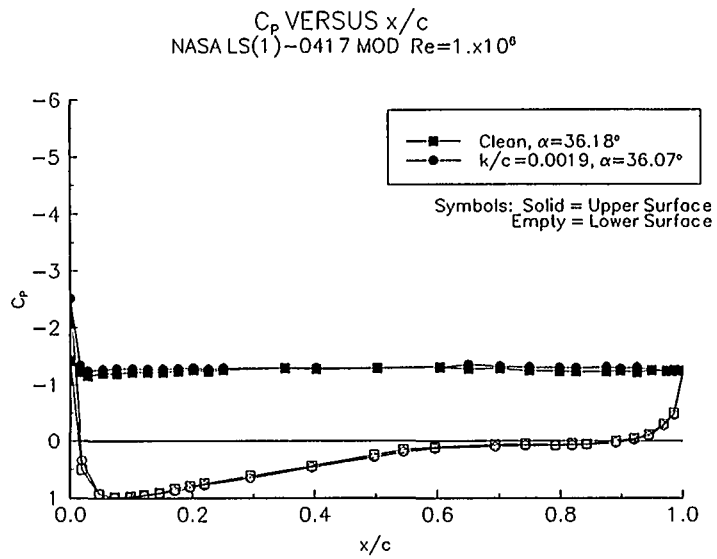

Figure 45. α = 36°

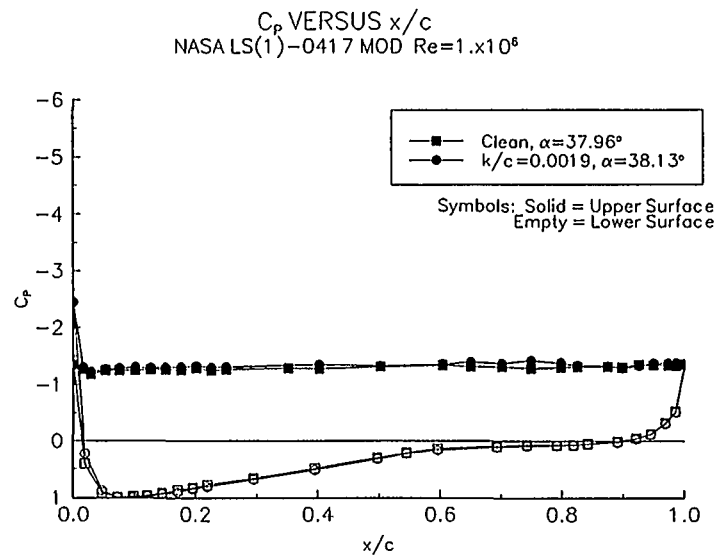

Figure 46. α = 38°

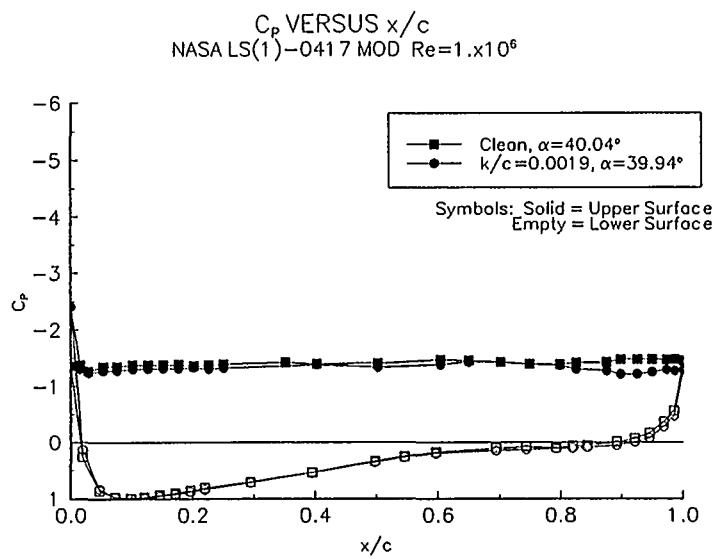

Figure 47. α = 40°

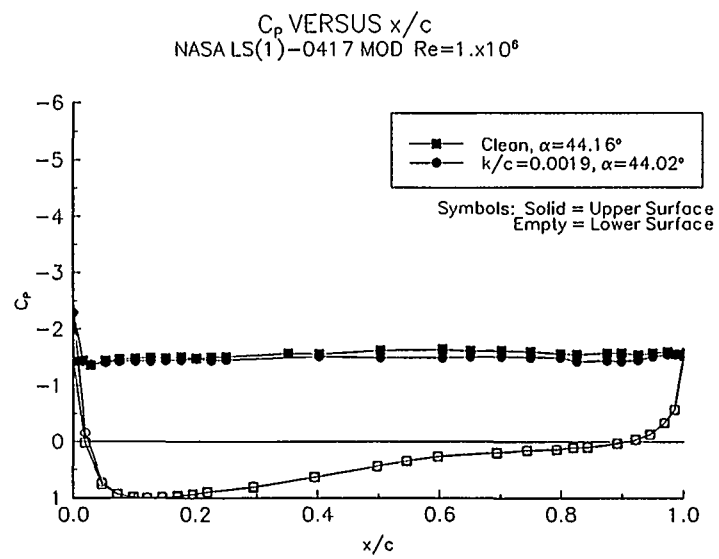

Figure 48. α = 44°

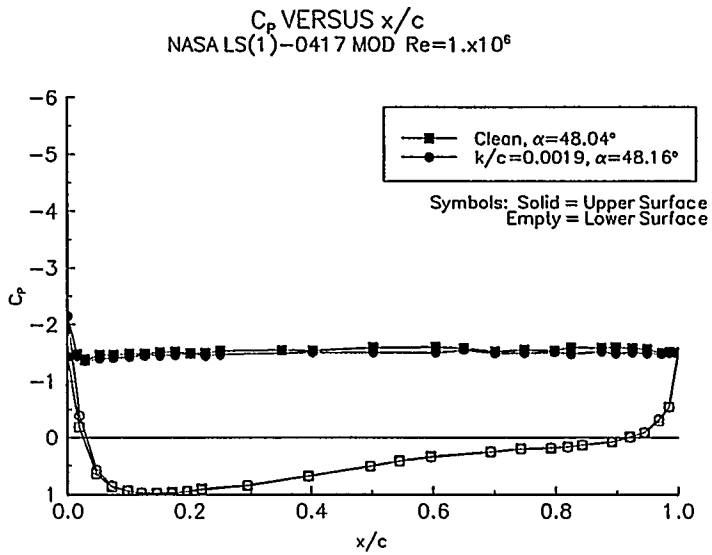

Figure 49. α = 48°

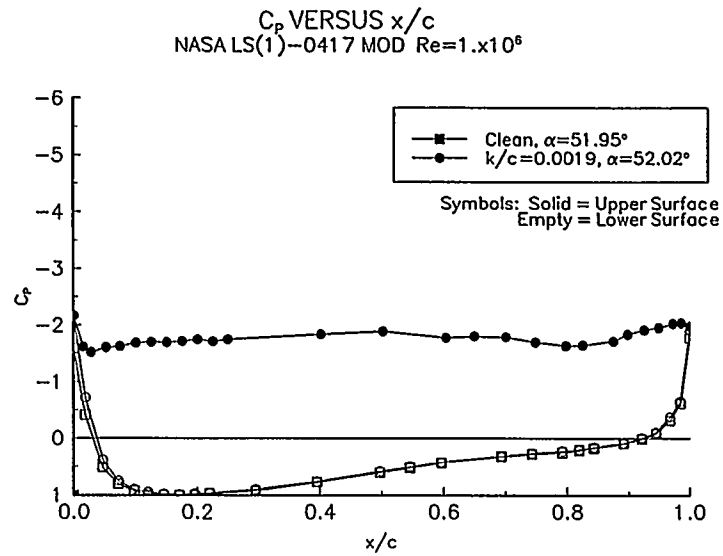

Figure 50. α = 52°

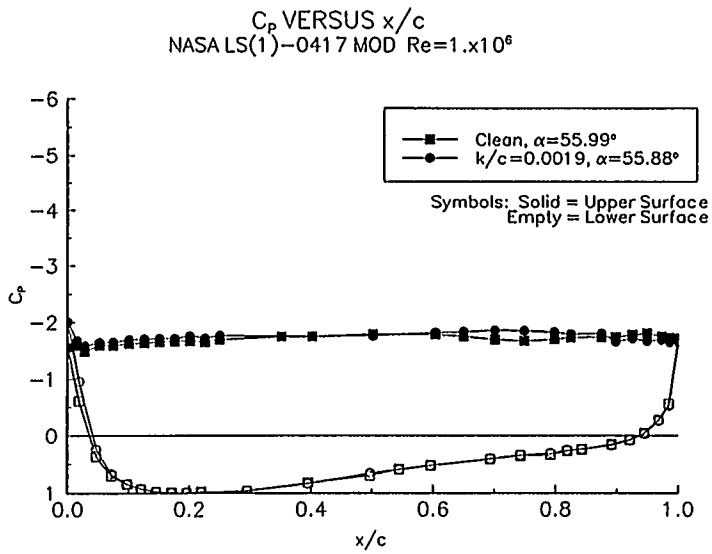

Figure 51. α = 56°

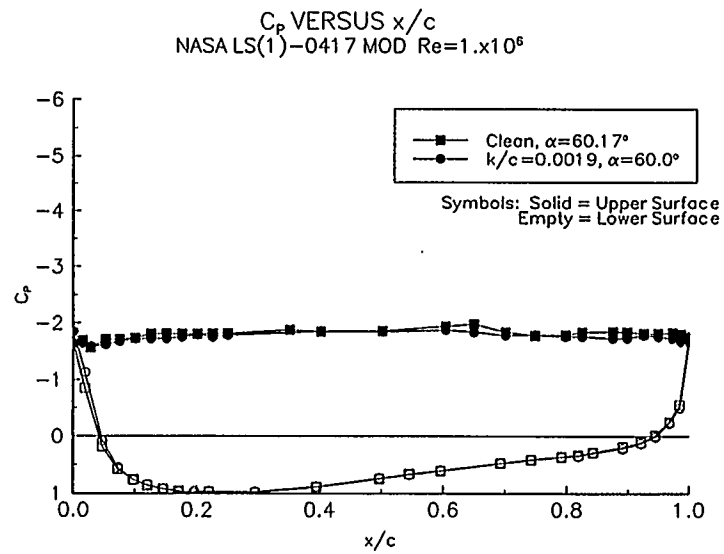

Figure 52. α = 60°

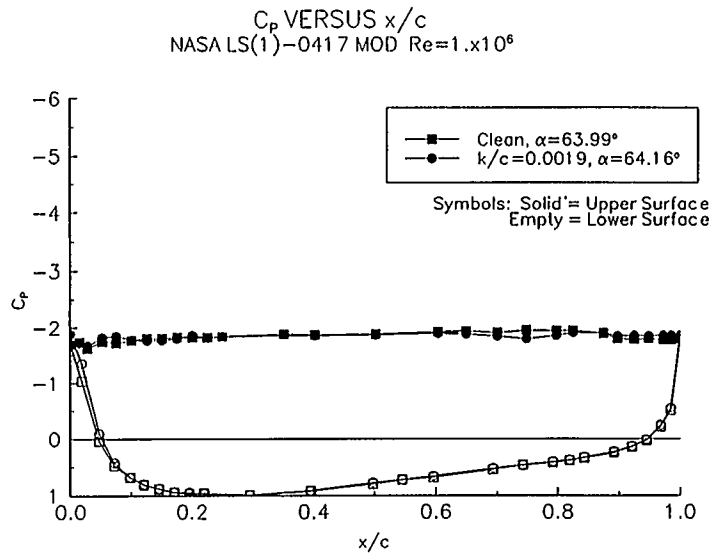

Figure 53. α = 64°

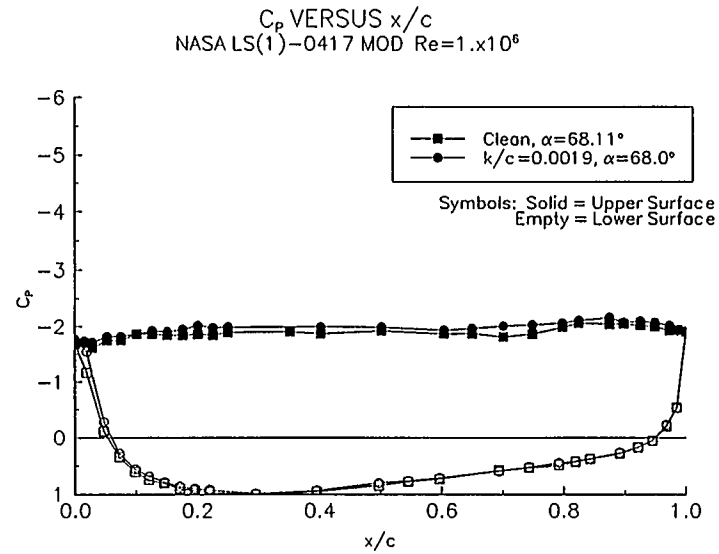

Figure 54. α = 68°

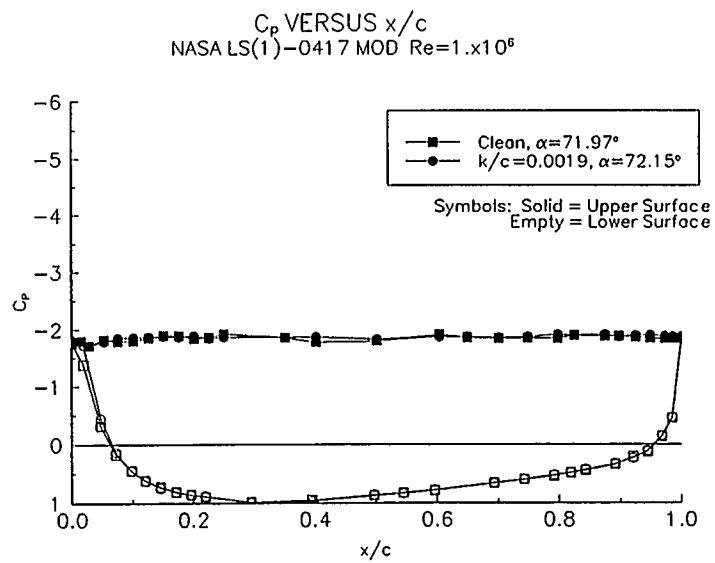

Figure 55. α = 72°

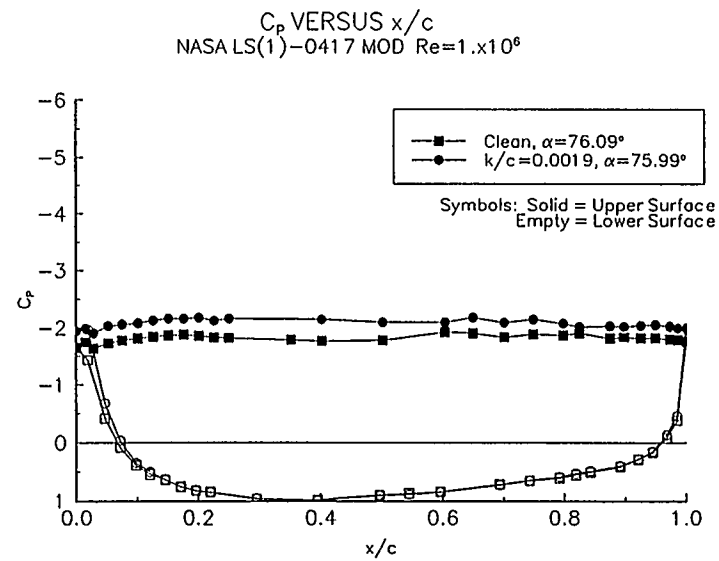

Figure 56. α = 76°

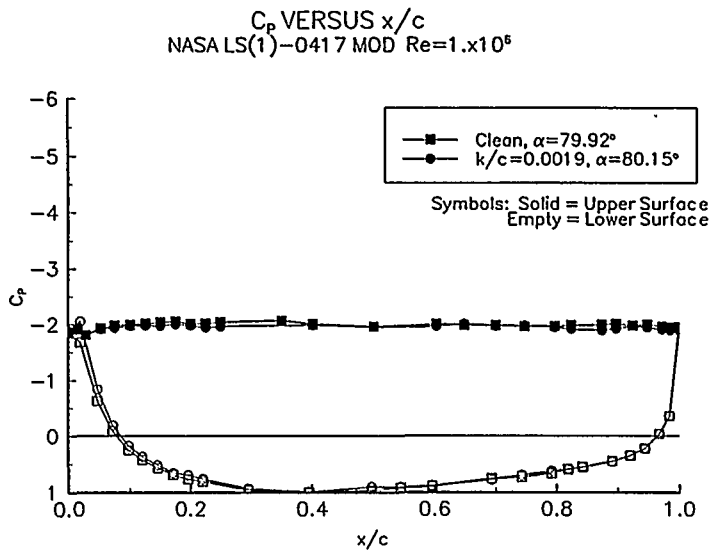

Figure 57. α = 80°

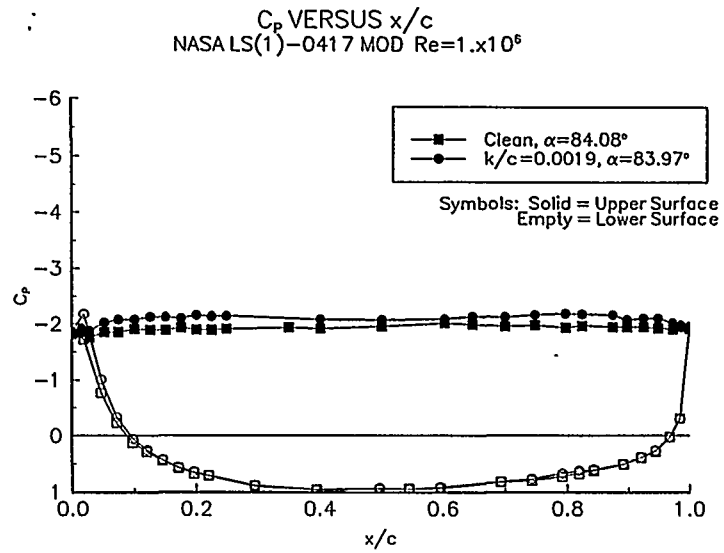

Figure 58. α = 84°

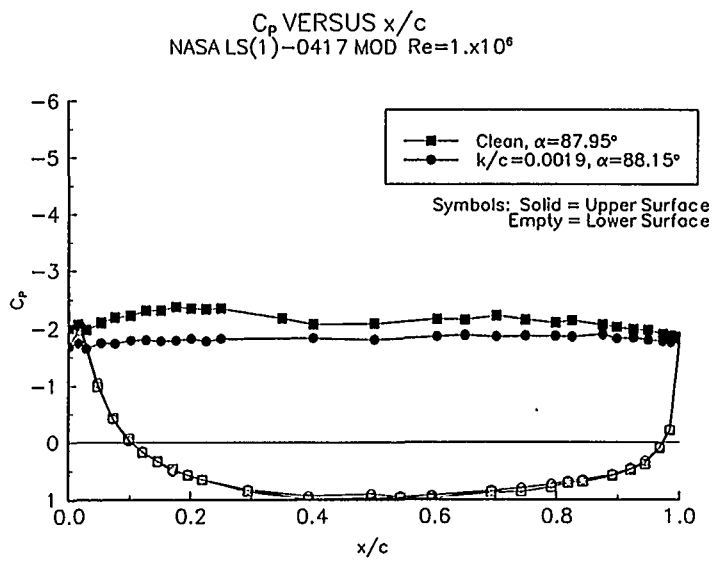

Figure 59. α = 88°

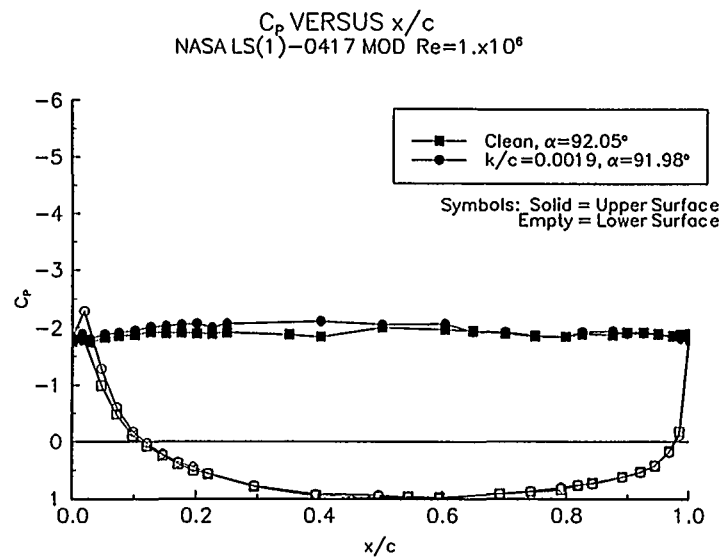

Figure 60. α = 92°

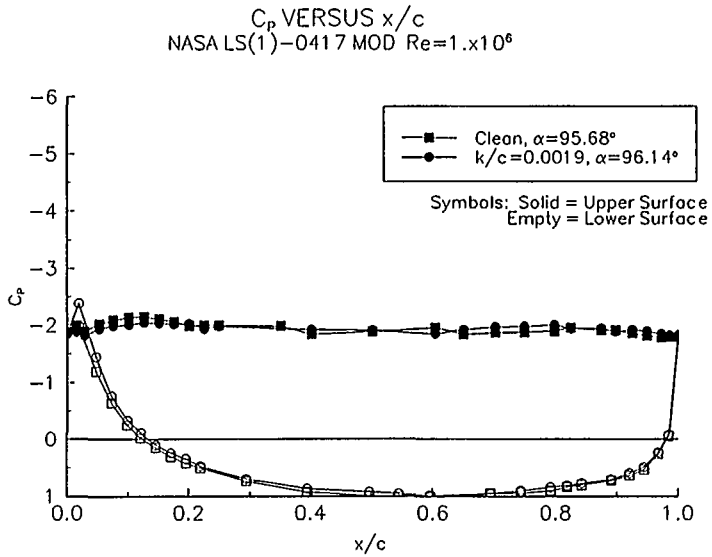

Figure 61. α = 96°

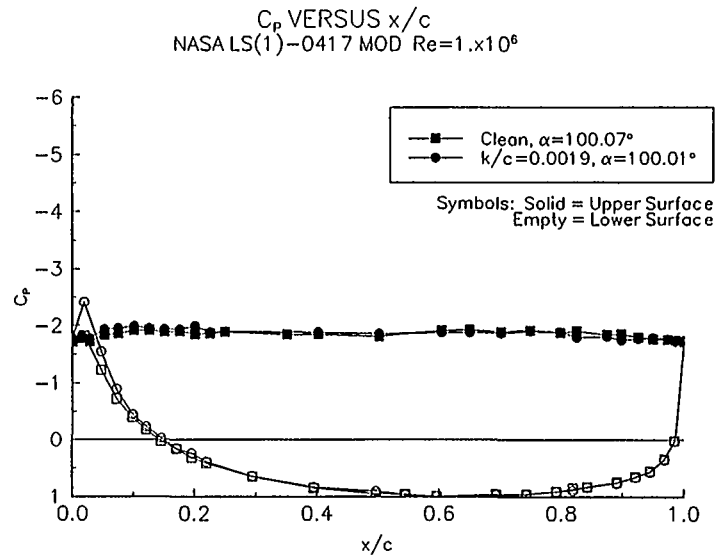

Figure 62. α = 100°

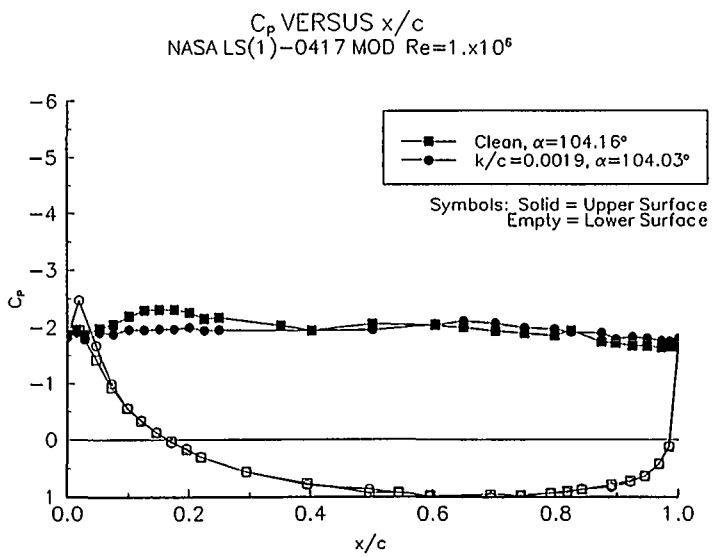

Figure 63. α = 104°

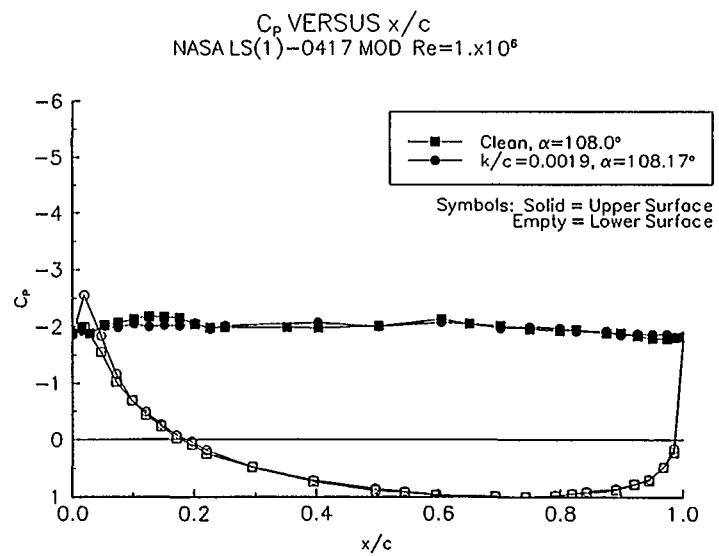

Figure 64. α = 108°

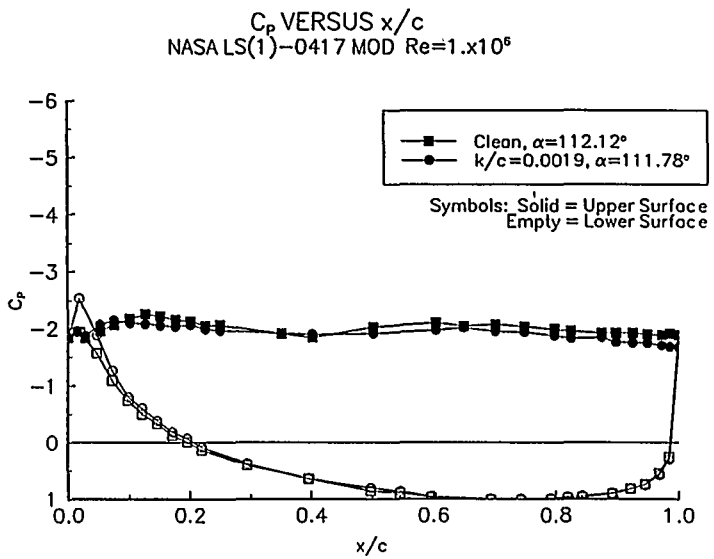

Figure 65. α = 112°

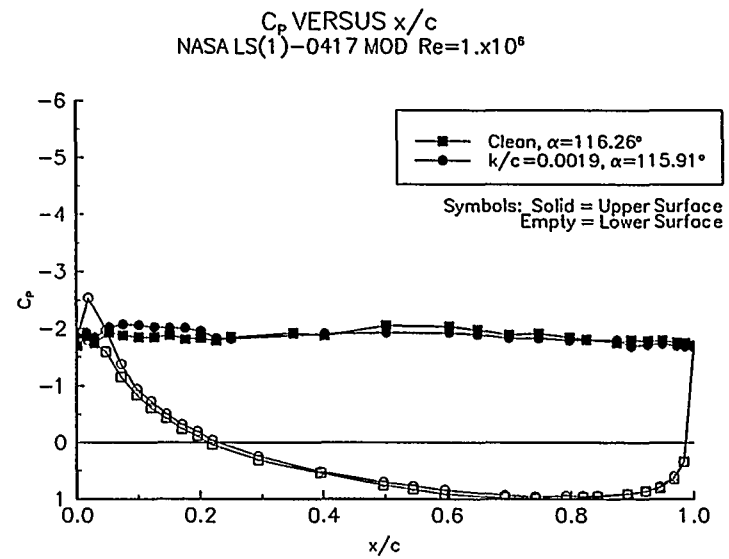

Figure 66. α = 116°

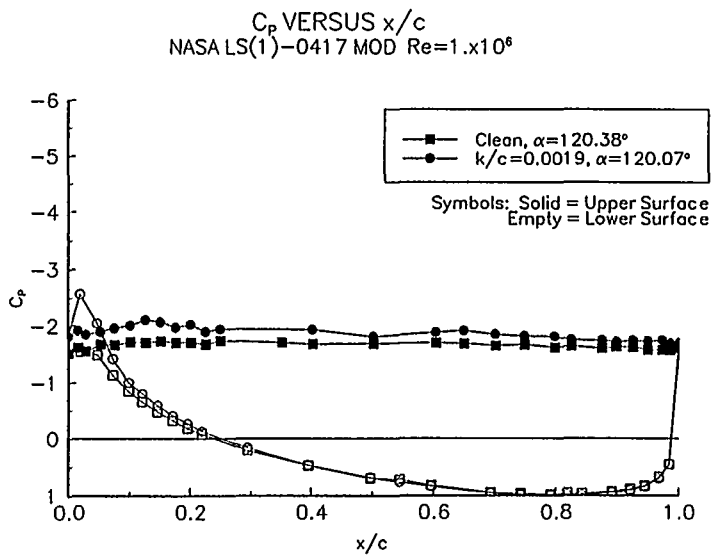

Figure 67. α = 120°

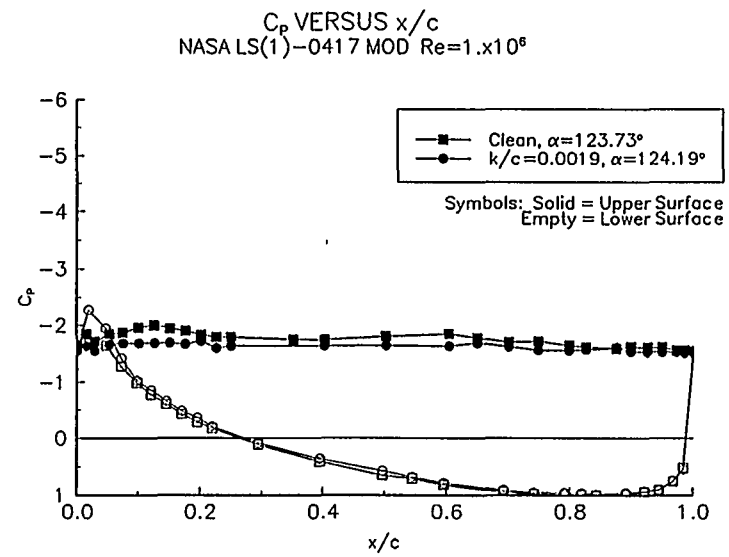

Figure 68. α = 124°

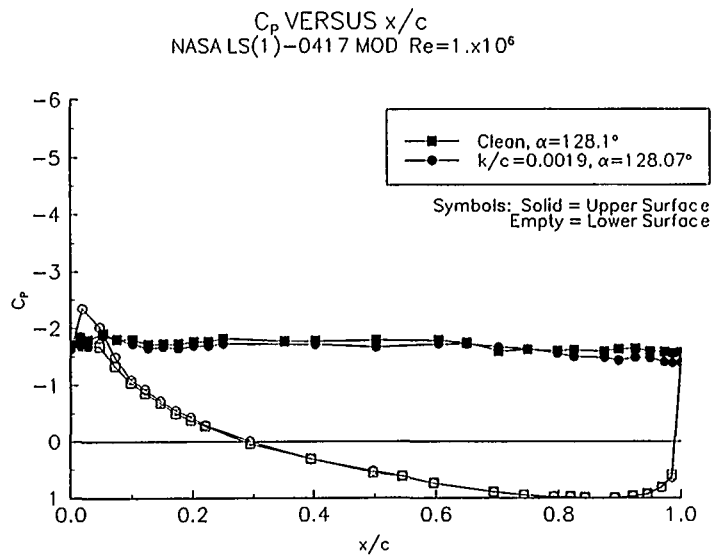

Figure 69. α = 128°

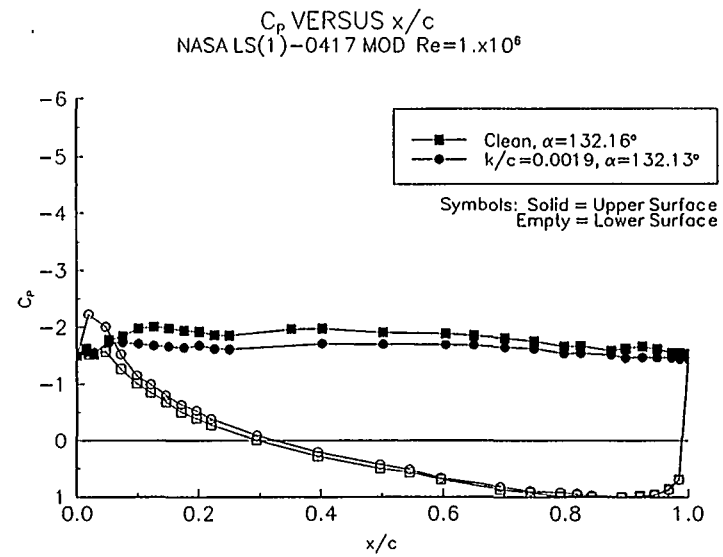

Figure 70. α = 132°

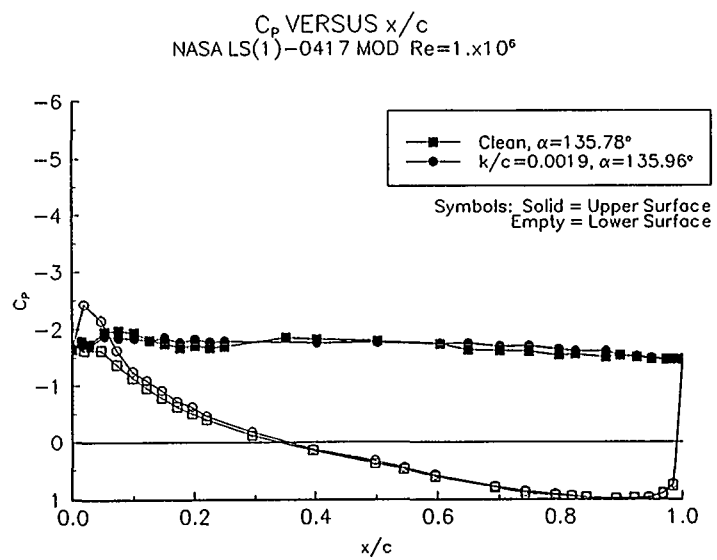

Figure 71. α = 136°

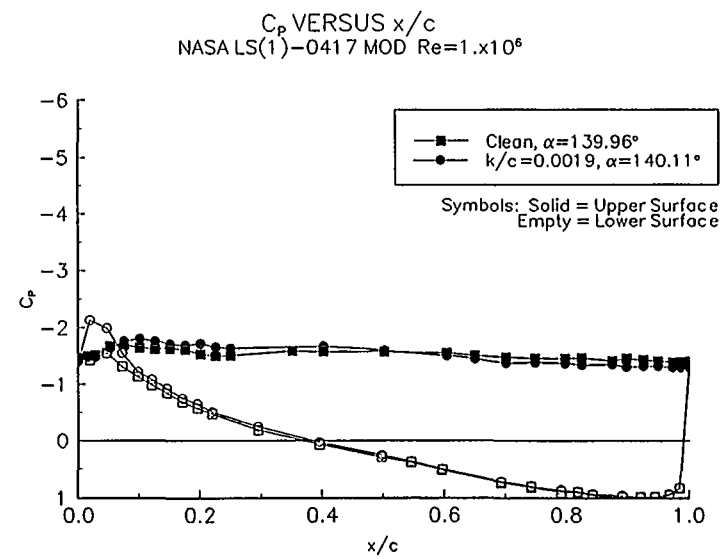

Figure 72. α = 140°

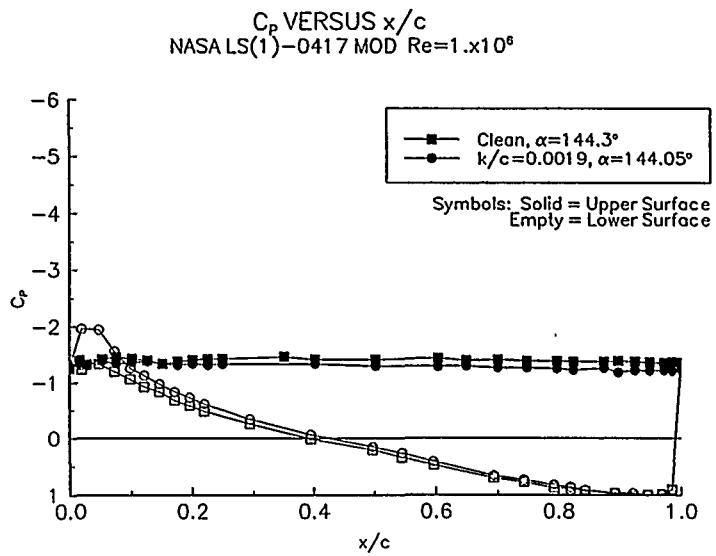

Figure 73. α = 144°

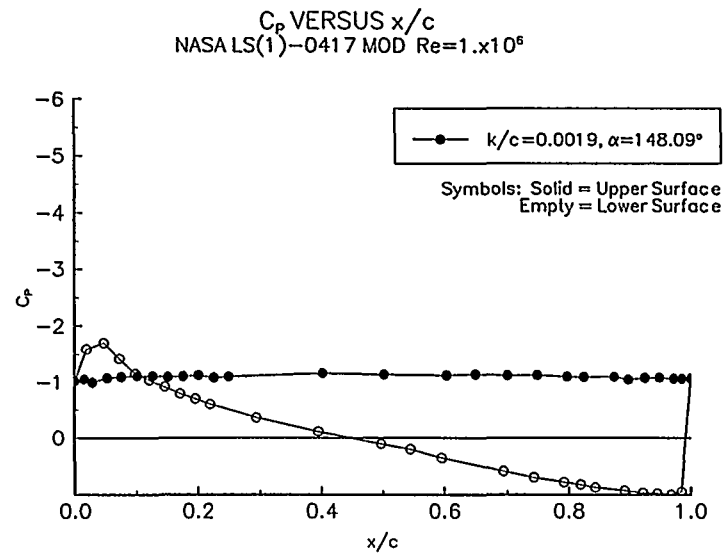

Figure 74. α = 148°

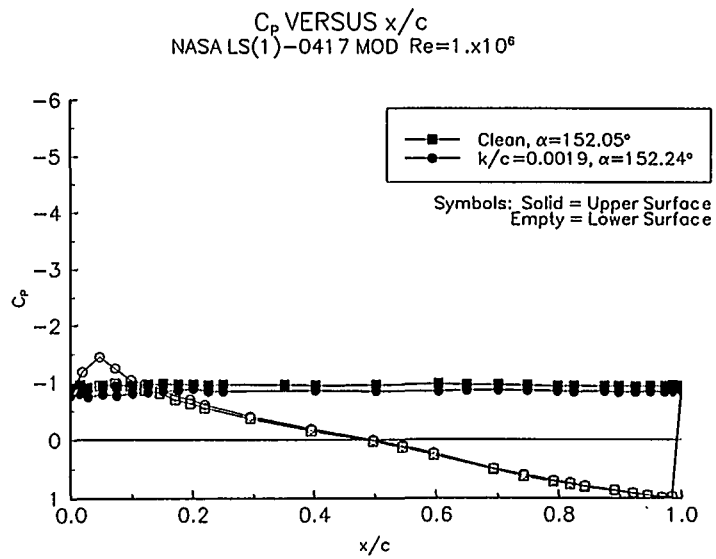

Figure 75. α = 152°

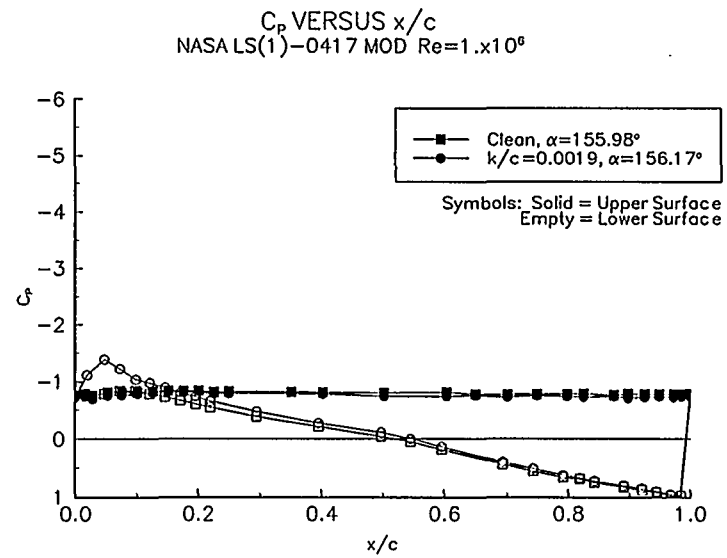

Figure 76. α = 156°

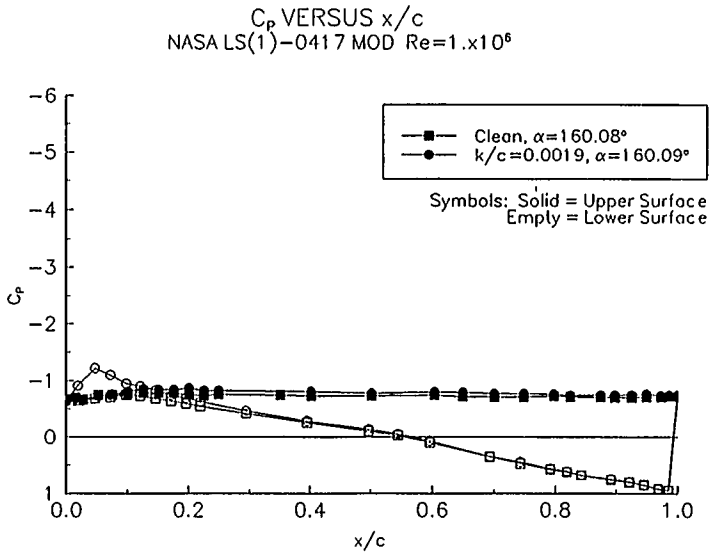

Figure 77. α = 160°

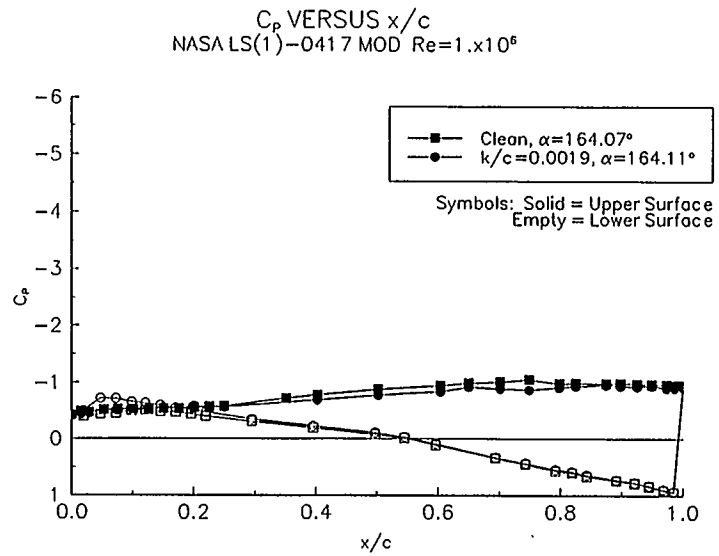

Figure 78. α = 164°

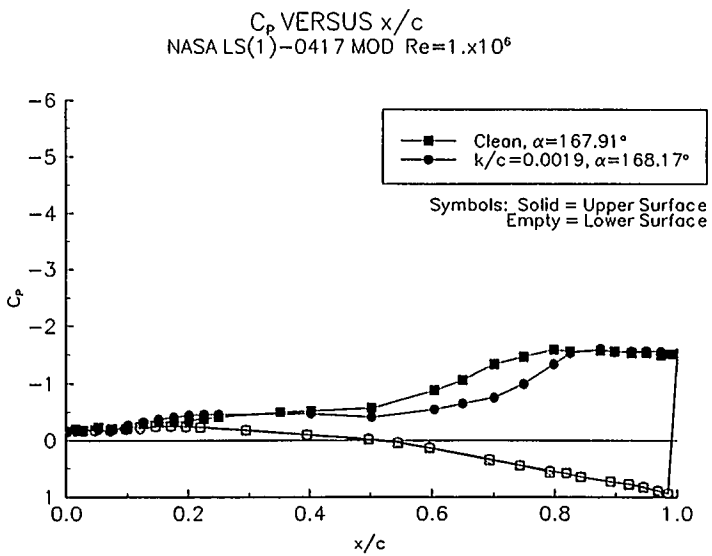

Figure 79. α = 168°

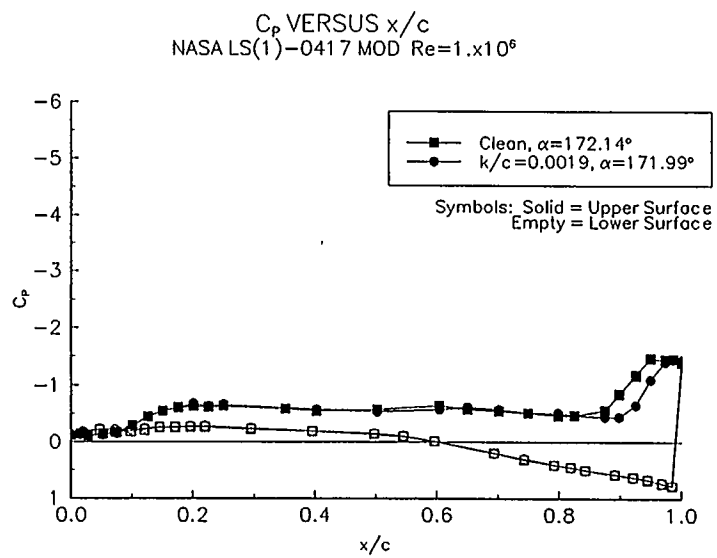

Figure 80. α = 172°

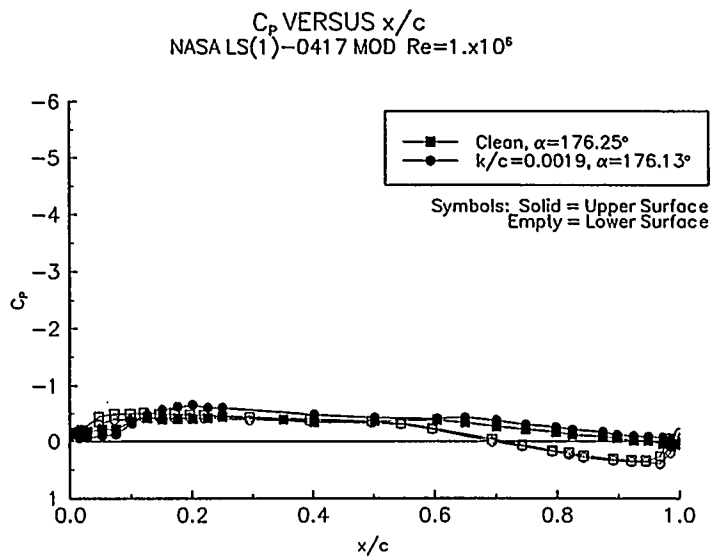

Figure 81. α = 176°

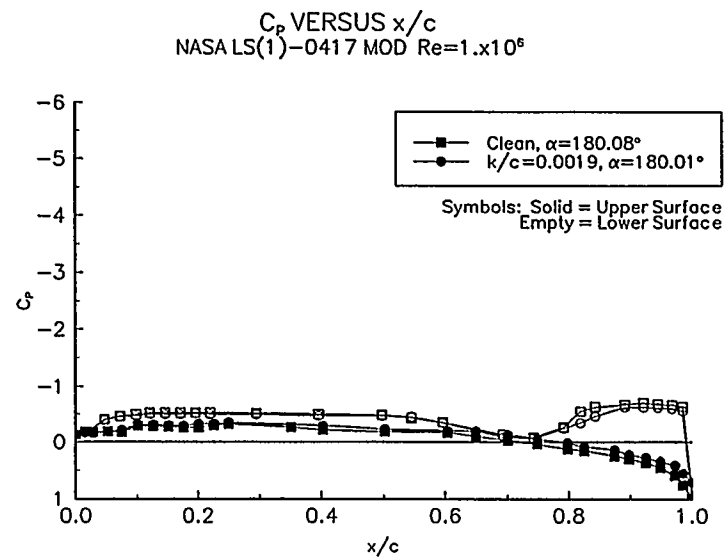

Figure 82. α = 180°

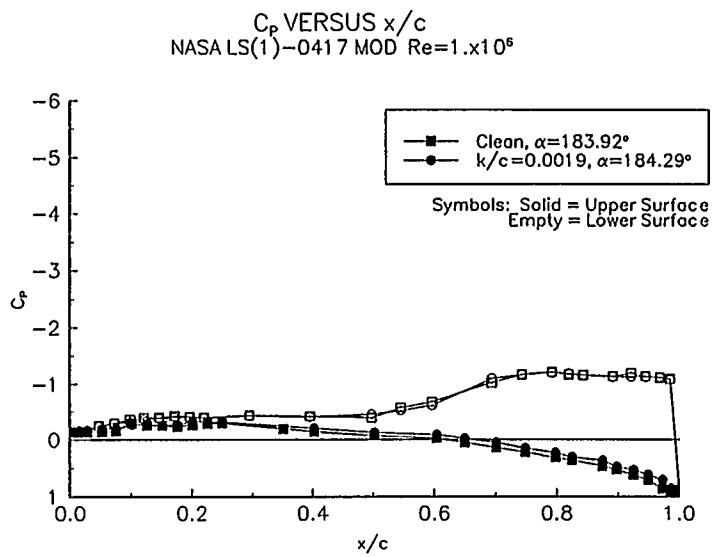

Figure 83. α = 184°

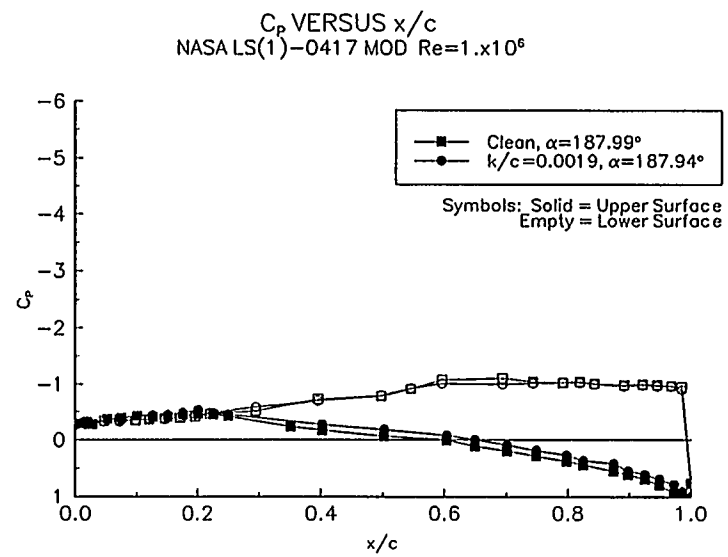

Figure 84. α = 188°

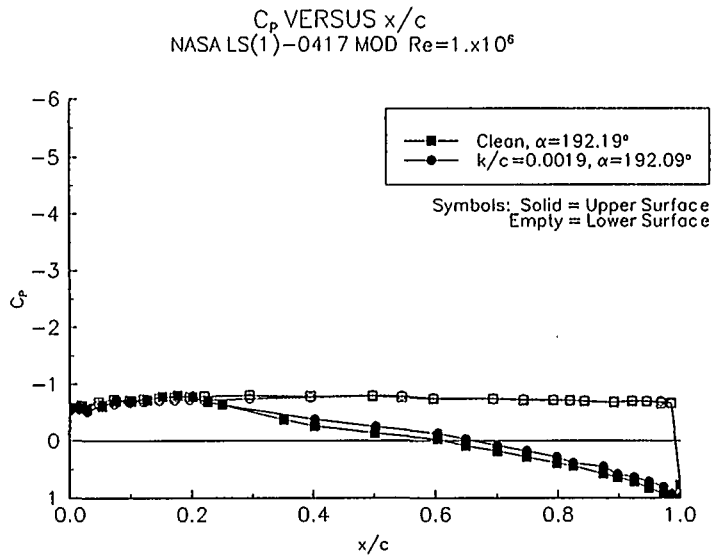

Figure 85. α = 192°

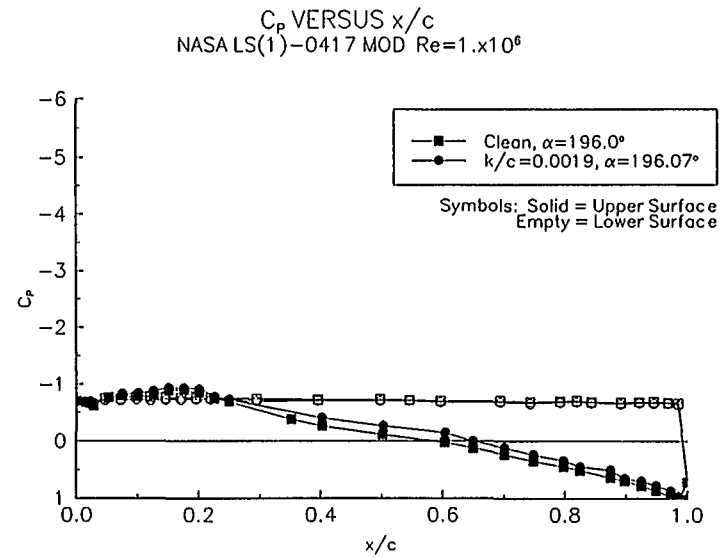

Figure 86. α = 196°

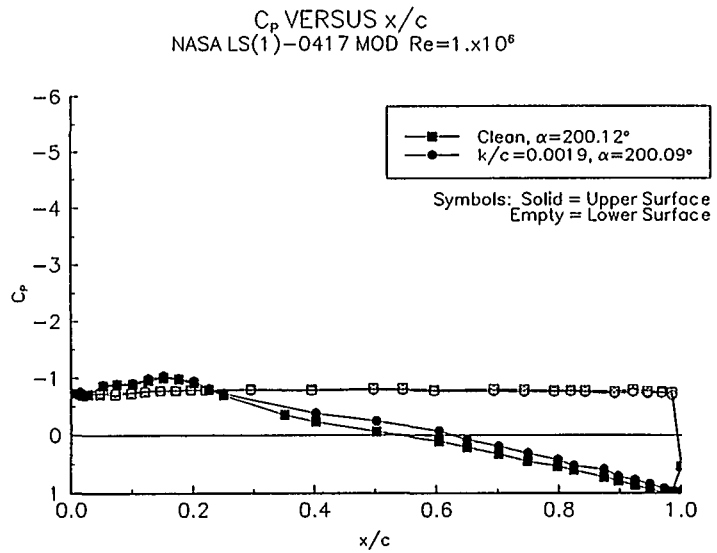

Figure 87. α = 200°

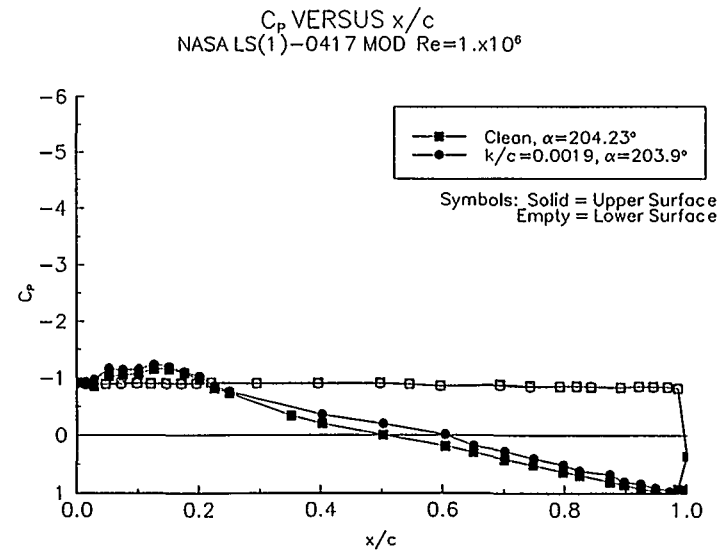

Figure 88. α = 204°

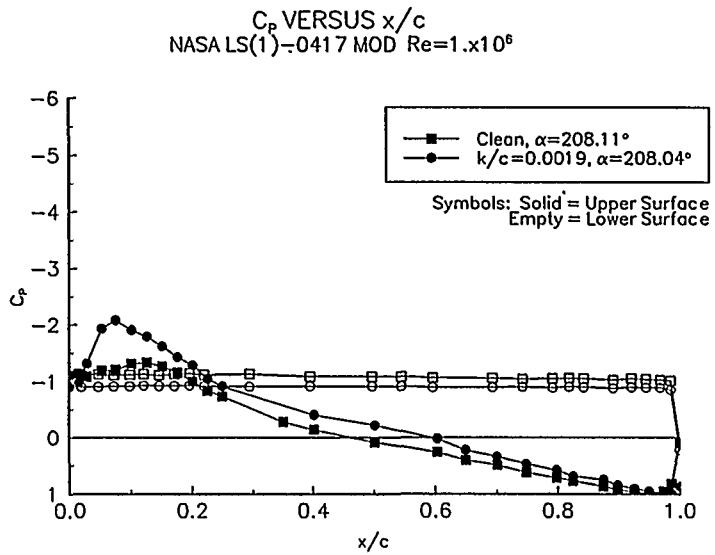

Figure 89. α = 208°

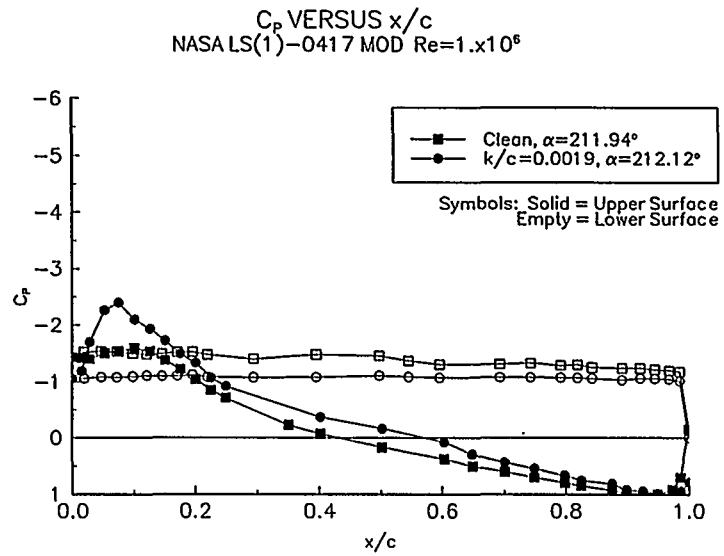

Figure 90. α = 212°

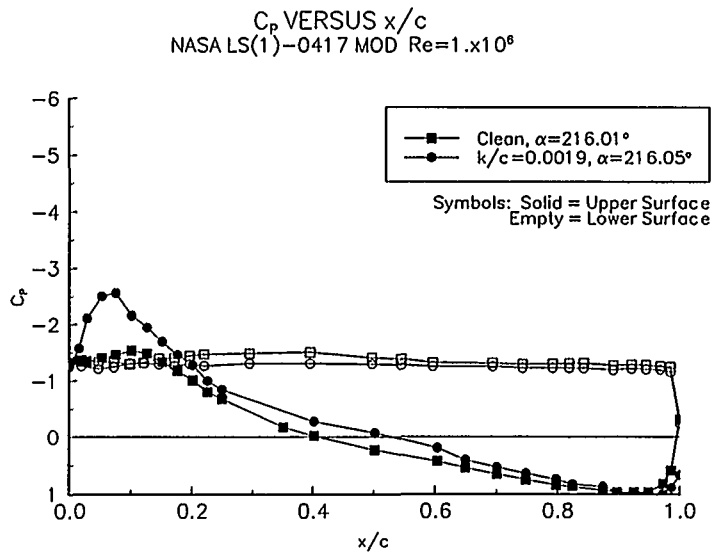

Figure 91. α = 216°

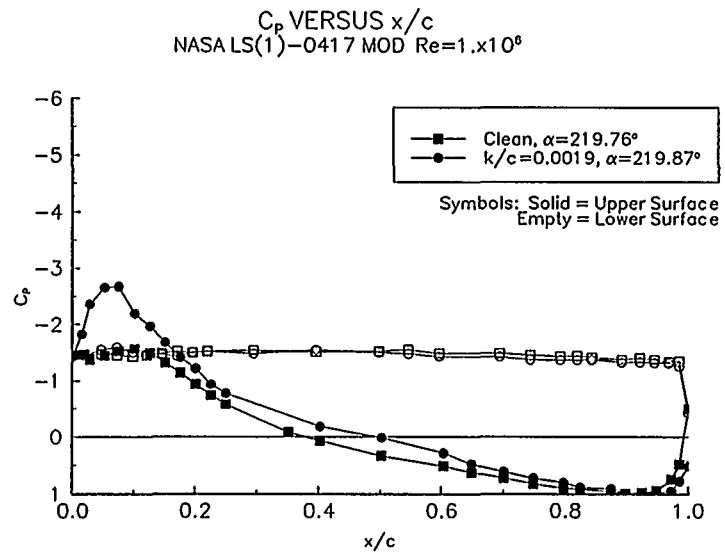

Figure 92. α = 220°

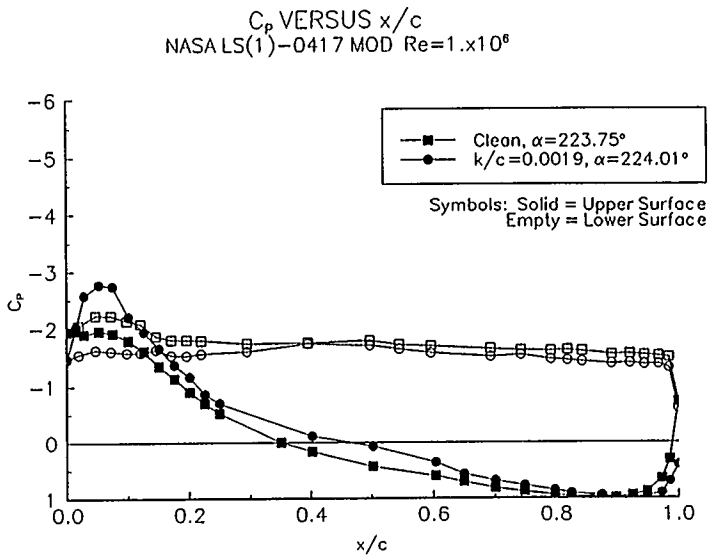

Figure 93. α = 224°

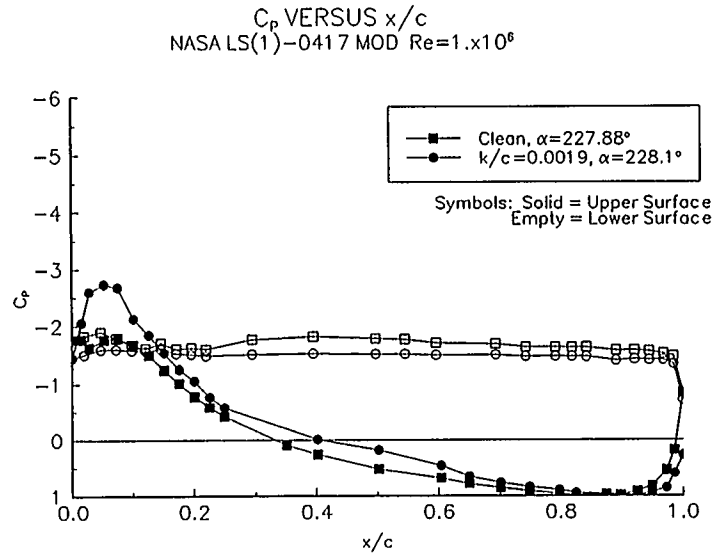

Figure 94. α = 228°

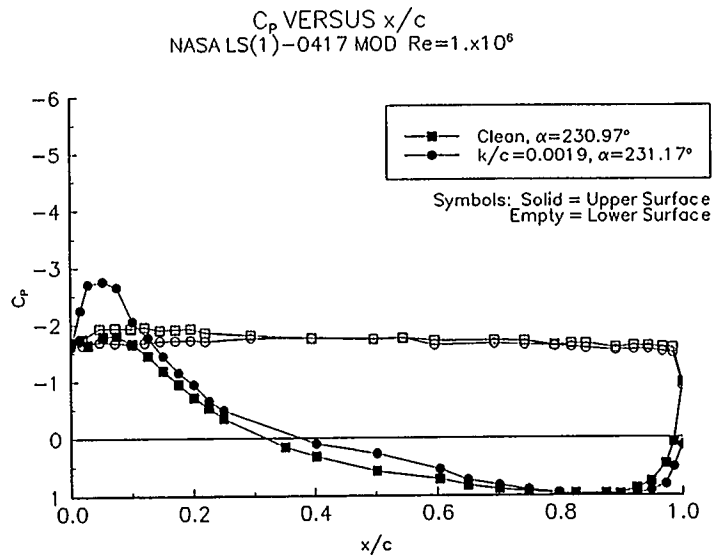

Figure 95. α = 231°

Steady State Pressure Distributions

VGs, Re = 1.0 million

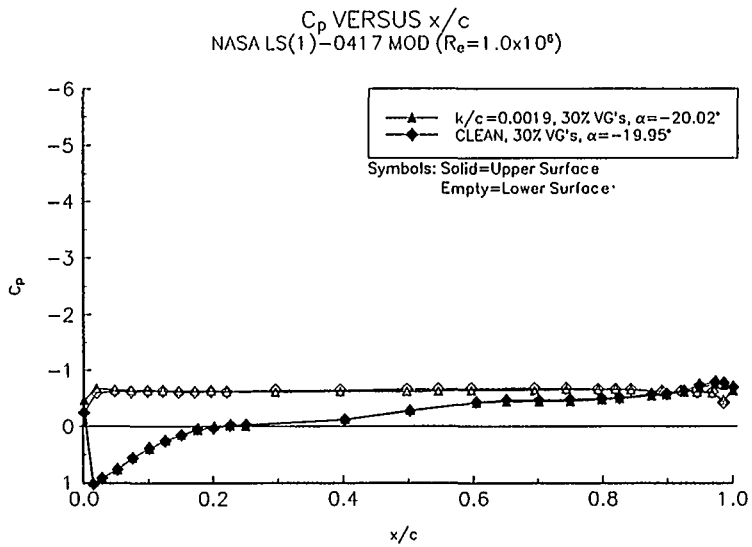

Figure 96. α = -20°

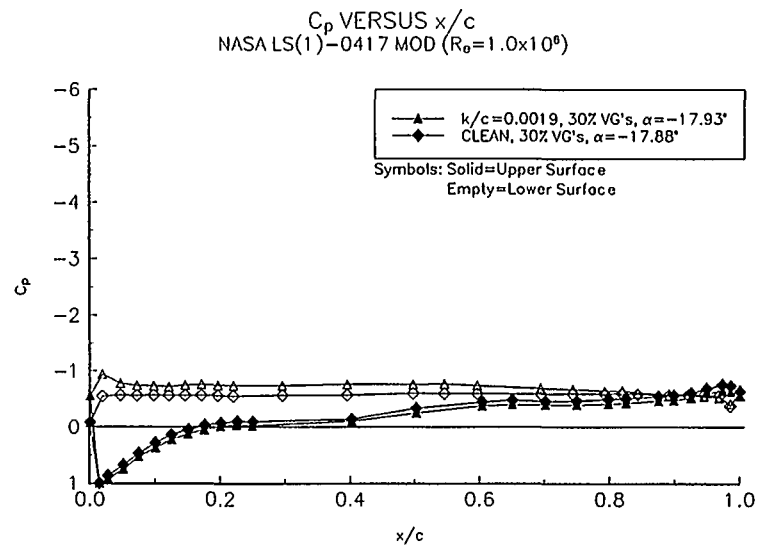

Figure 97. α = -18°

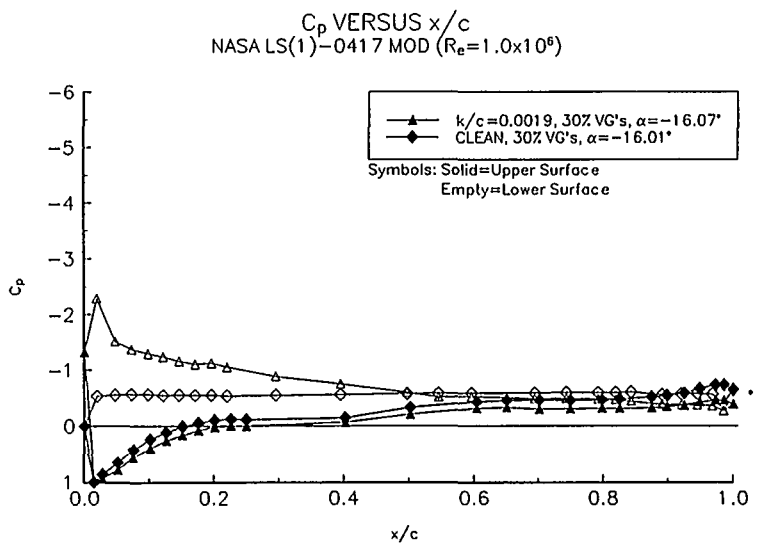

Figure 98. α = -16°

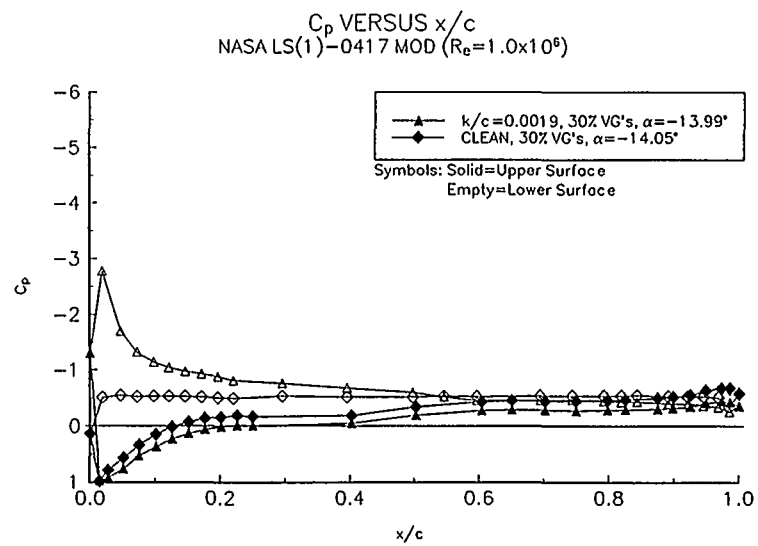

Figure 99. α = -14°

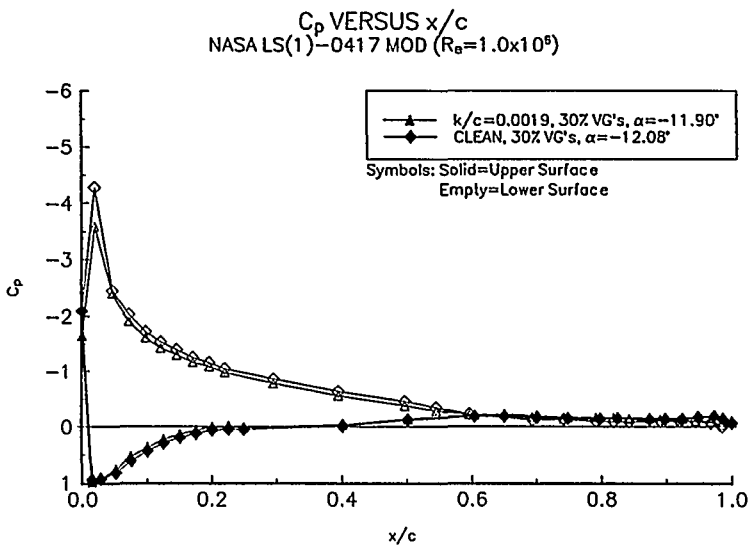

Figure 100. $\alpha = -12^\circ$

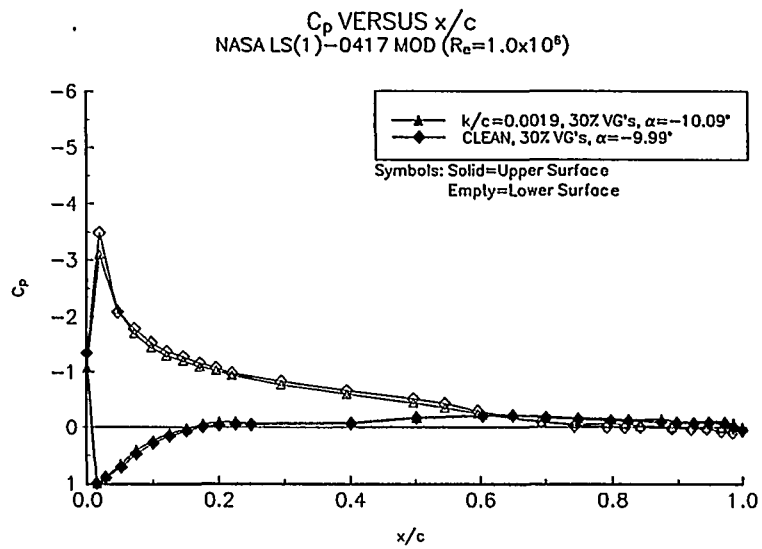

Figure 101. $\alpha = -10^\circ$

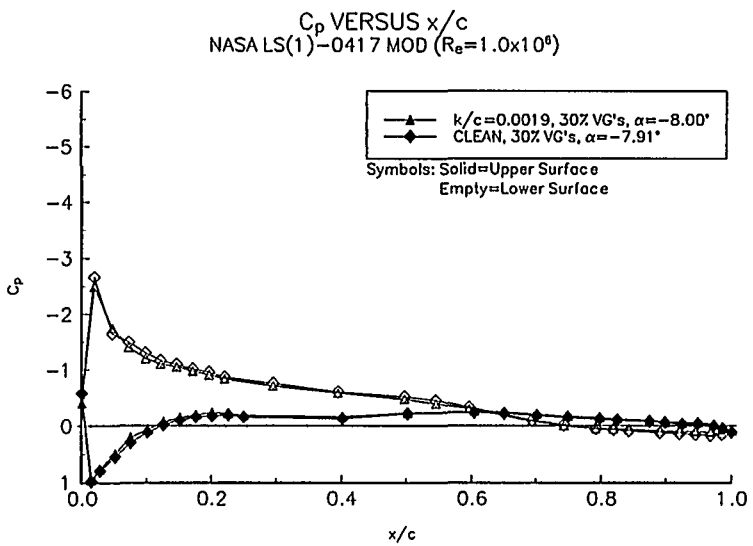

Figure 102. $\alpha = -8^\circ$

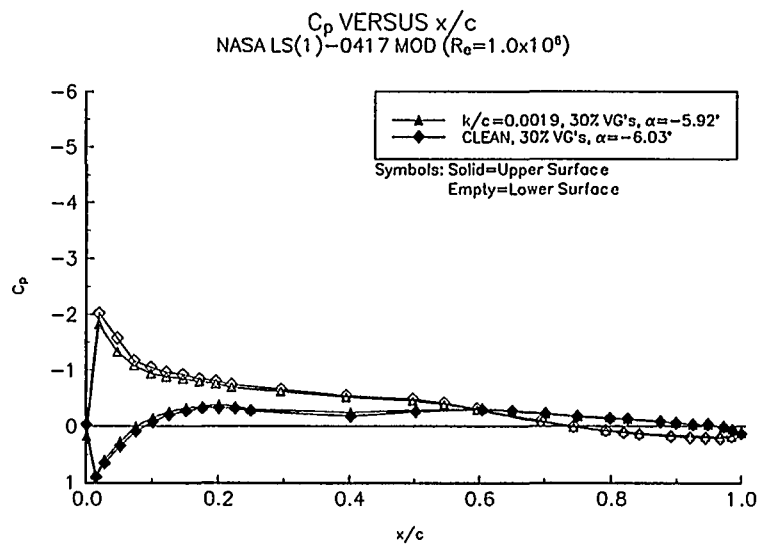

Figure 103. $\alpha = -6^\circ$

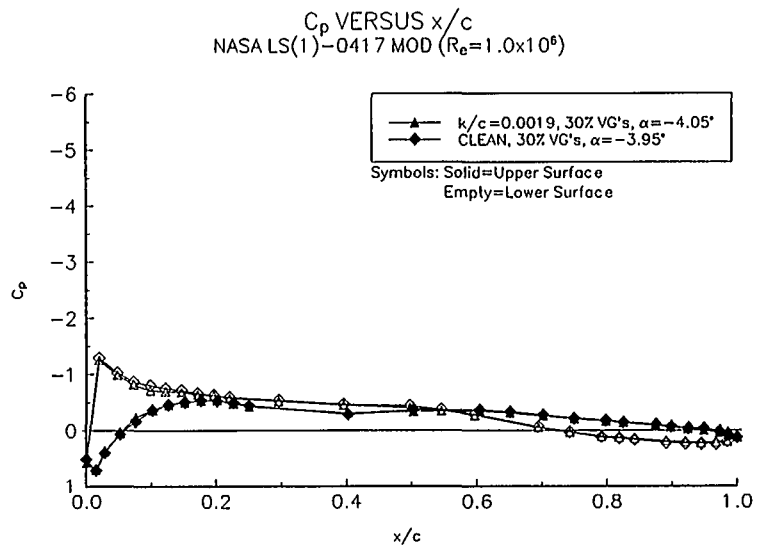

Figure **104.** $\alpha = -4^\circ$

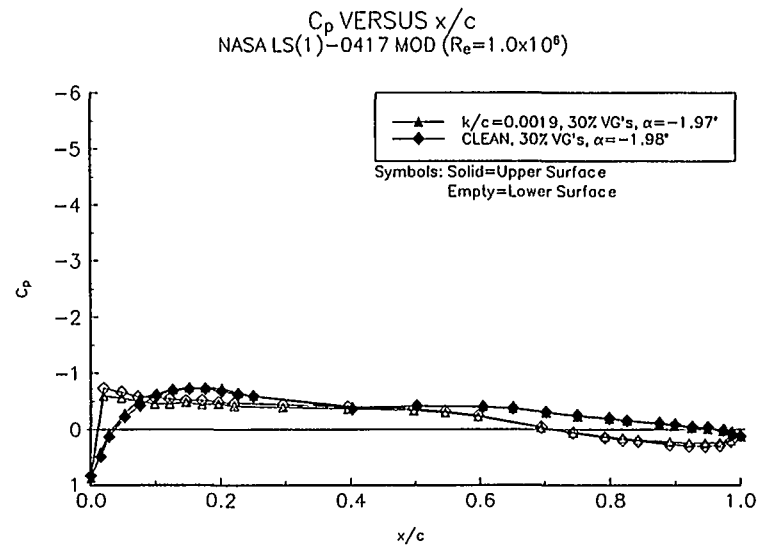

Figure **105.** $\alpha = -2^\circ$

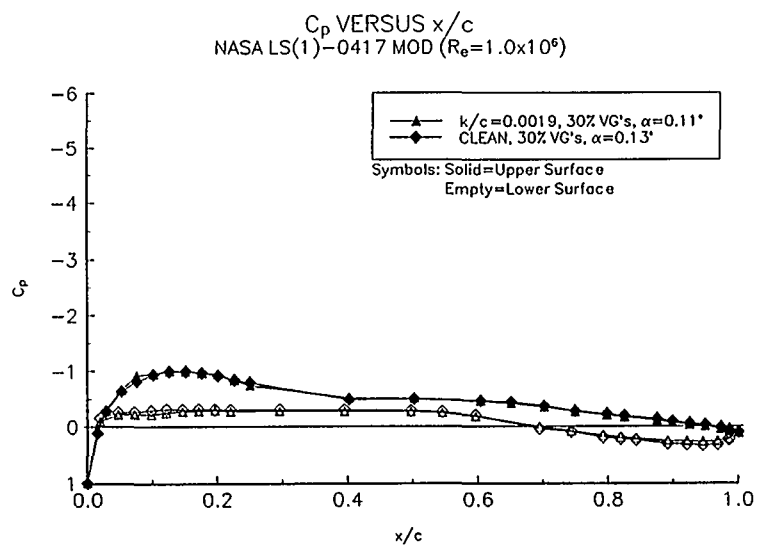

Figure **106.** $\alpha = 0^\circ$

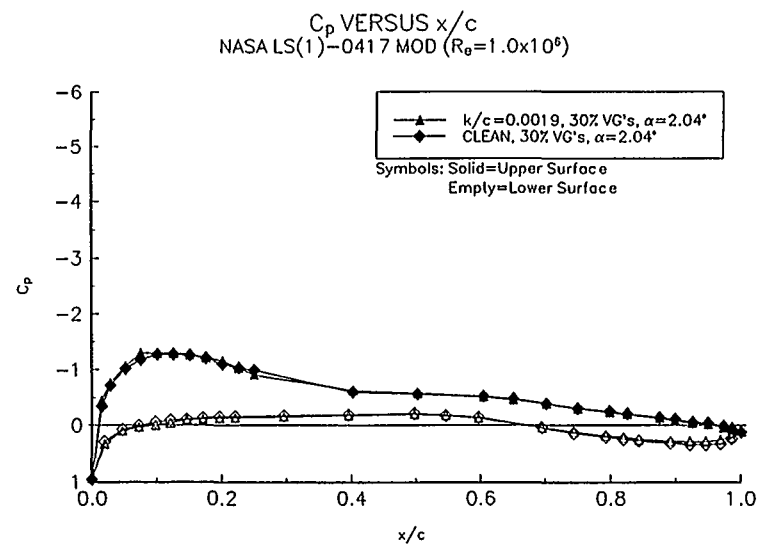

Figure **107.** $\alpha = 2^\circ$

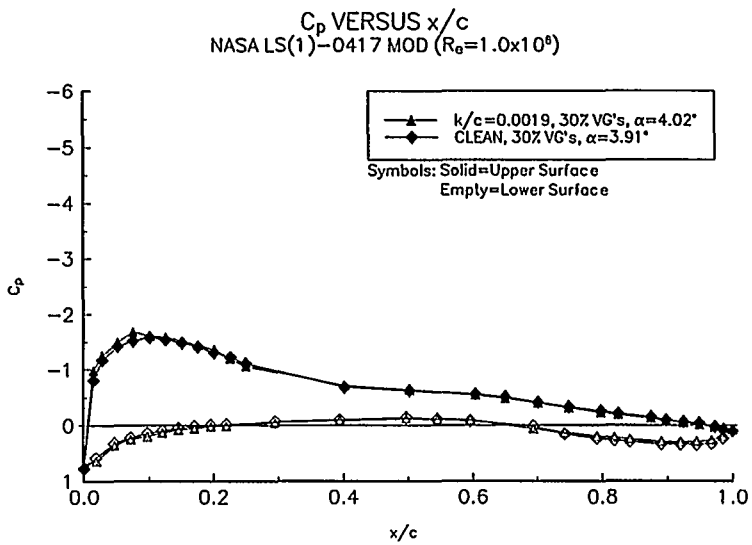

Figure 108. $\alpha = 4^\circ$

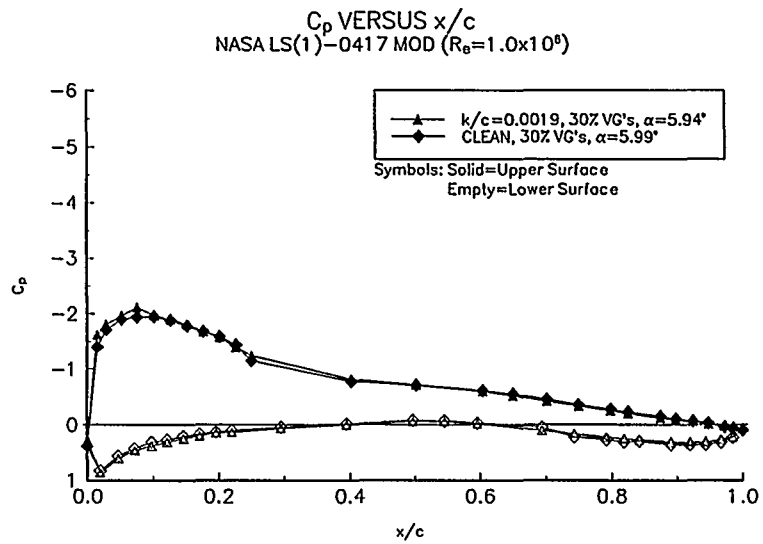

Figure 109. $\alpha = 6^\circ$

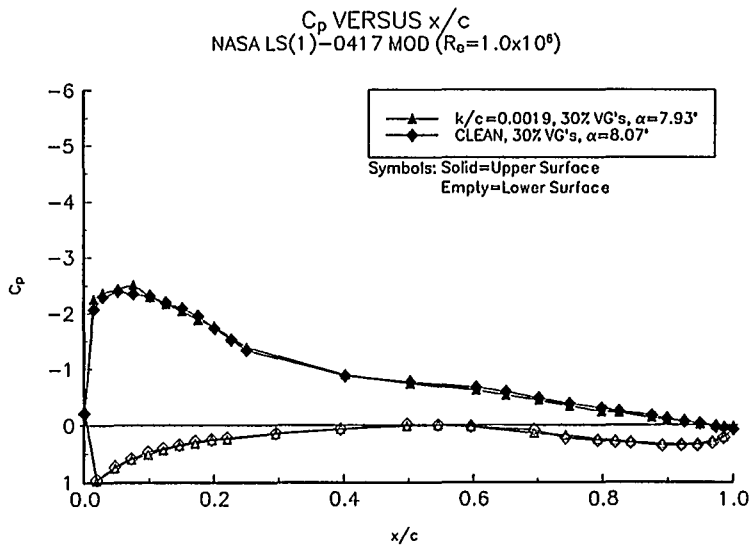

Figure 110. $\alpha = 8^\circ$

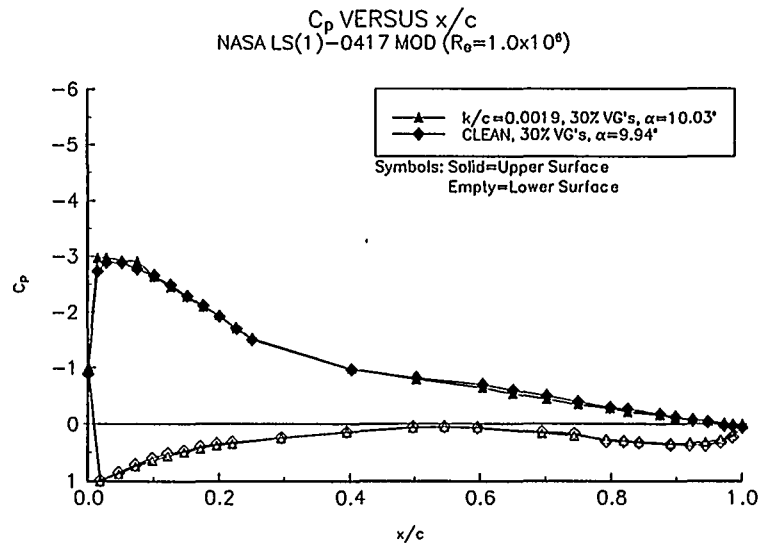

Figure 111. $\alpha = 10^\circ$

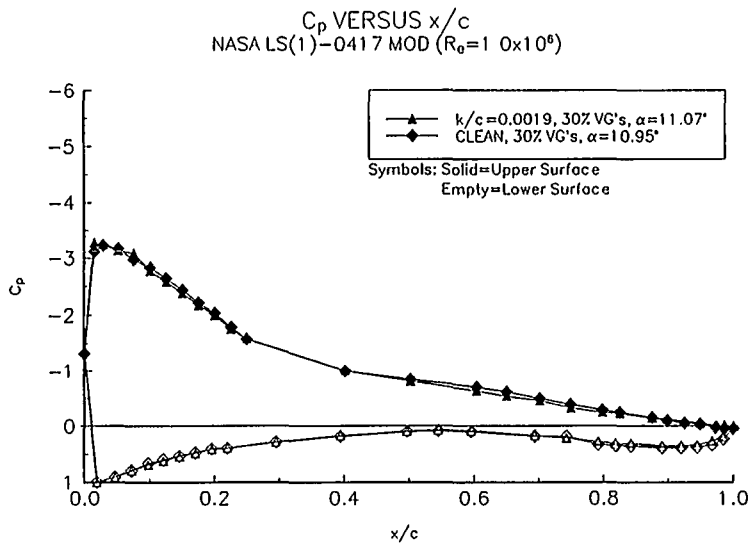

Figure 112. $\alpha = 11°$

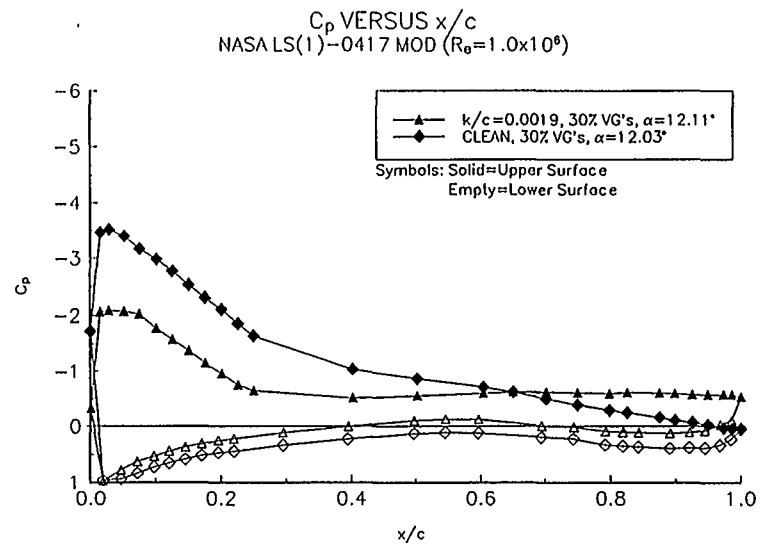

Figure 113. $\alpha = 12°$

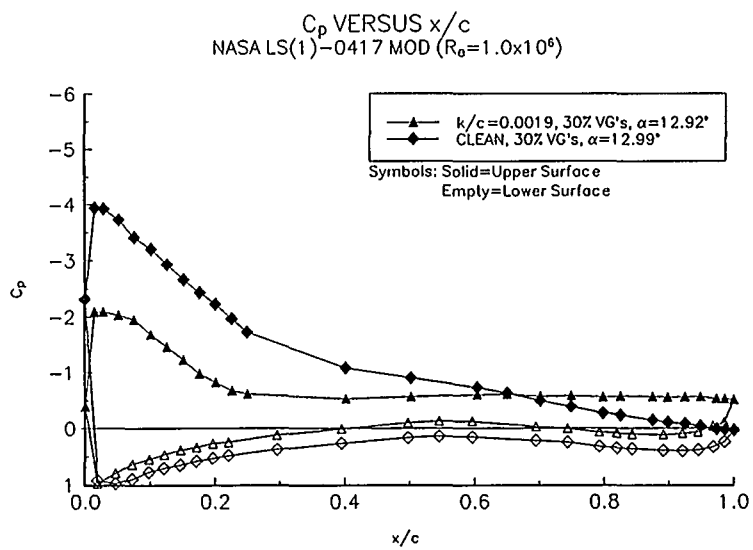

Figure 114. $\alpha = 13°$

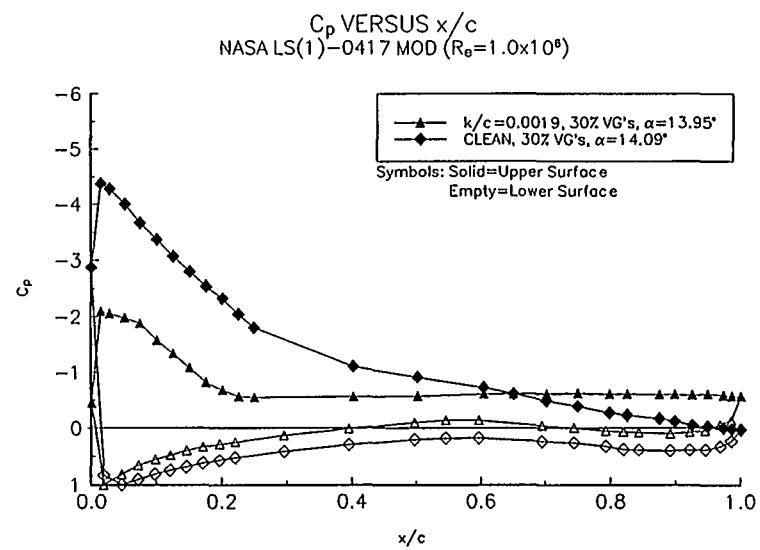

Figure 115. $\alpha = 14°$

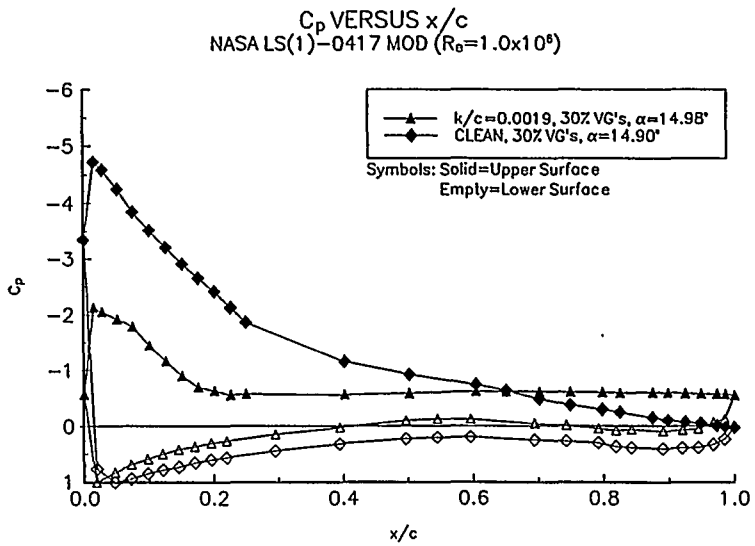

Figure 116. $\alpha = 15^\circ$

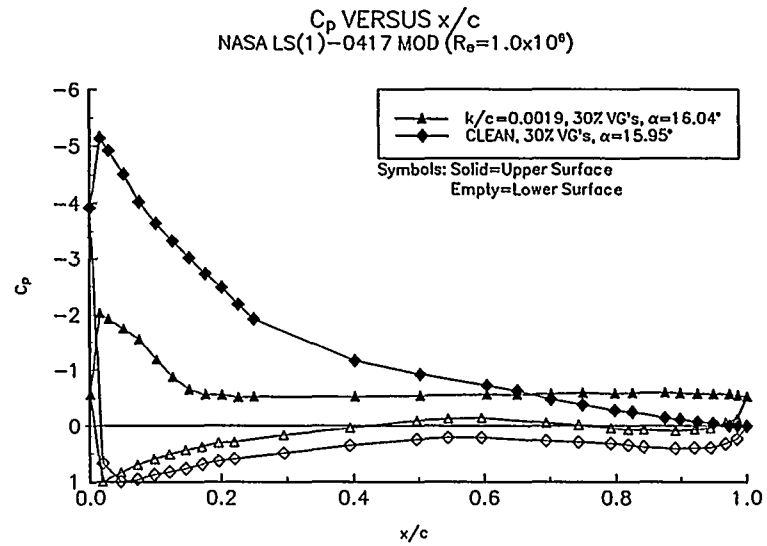

Figure 117. $\alpha = 16^\circ$

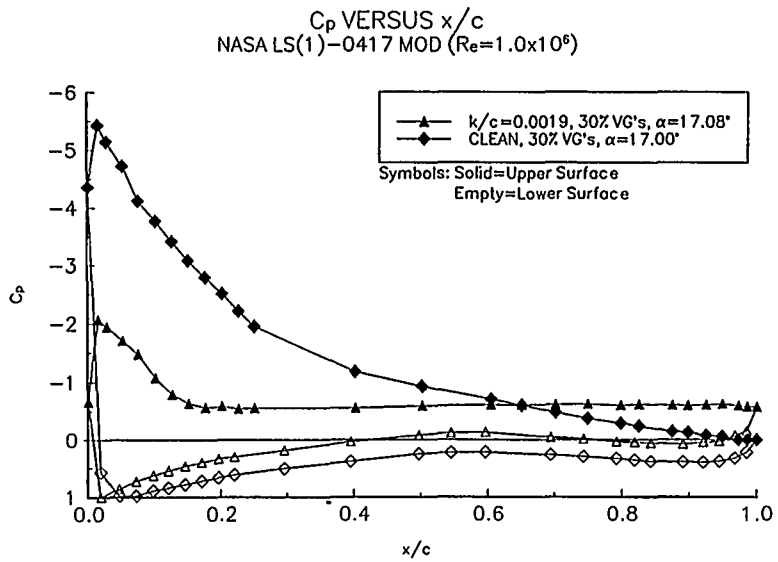

Figure 118. $\alpha = 17^\circ$

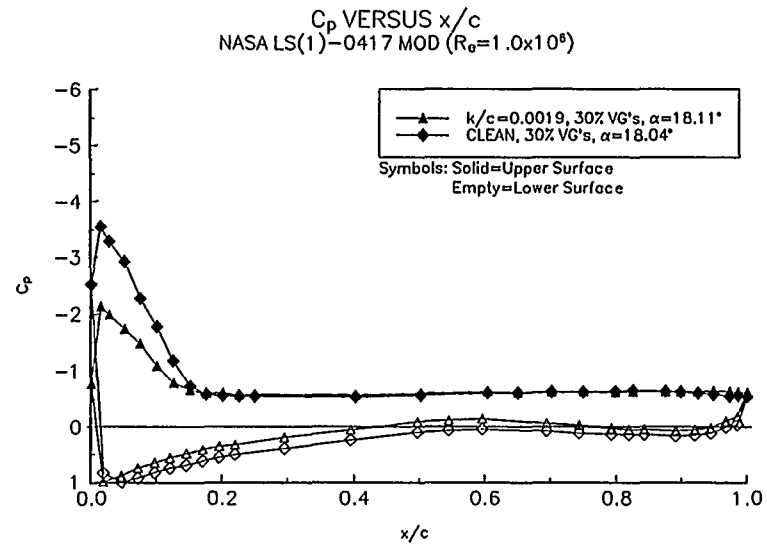

Figure 119. $\alpha = 18^\circ$

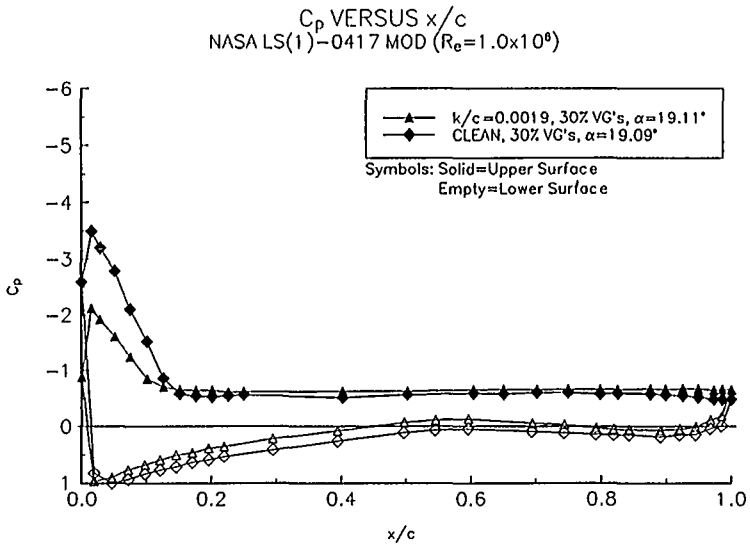

Figure 120. $\alpha = 19°$

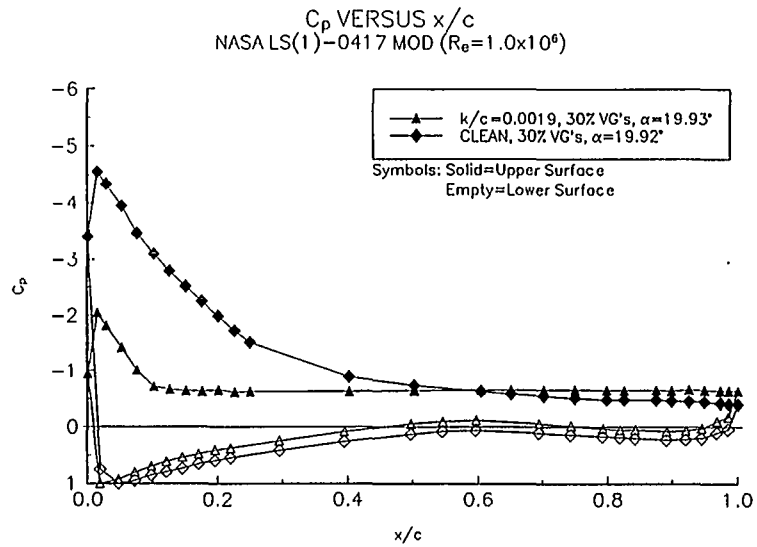

Figure 121. $\alpha = 20°$

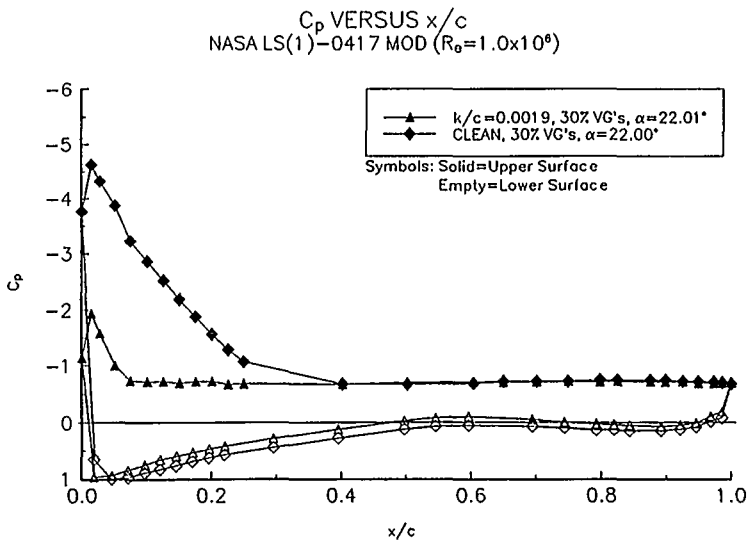

Figure 122. $\alpha = 22°$

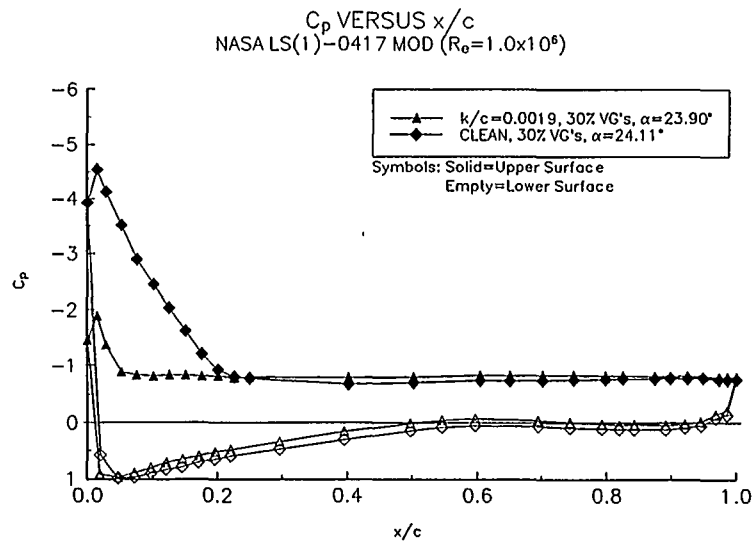

Figure 123. $\alpha = 24°$

Steady State Pressure Distributions

Re = 1.5 million

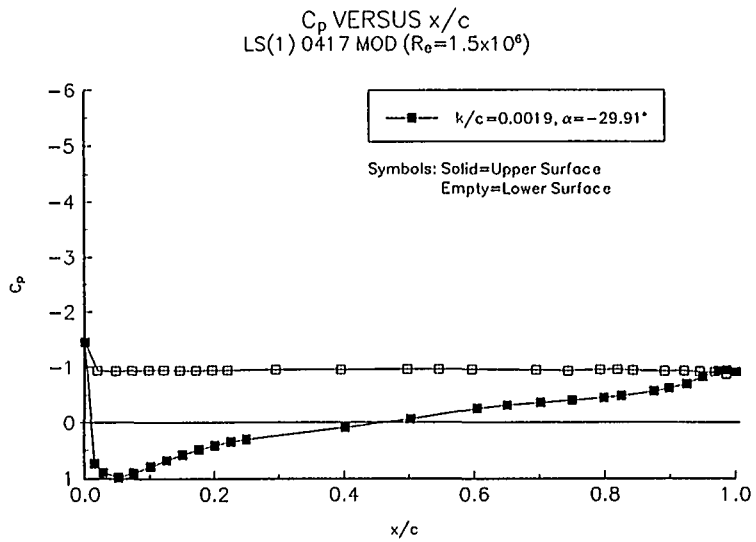

Figure 124. α = -30°

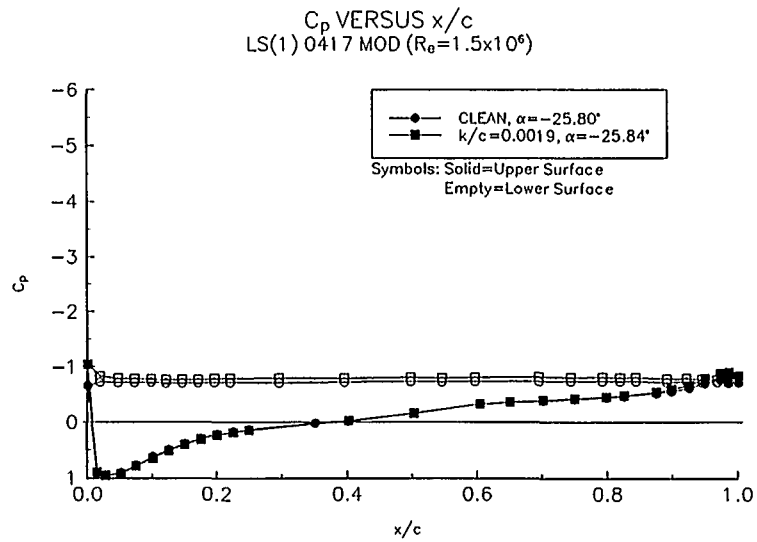

Figure 125. α = -26°

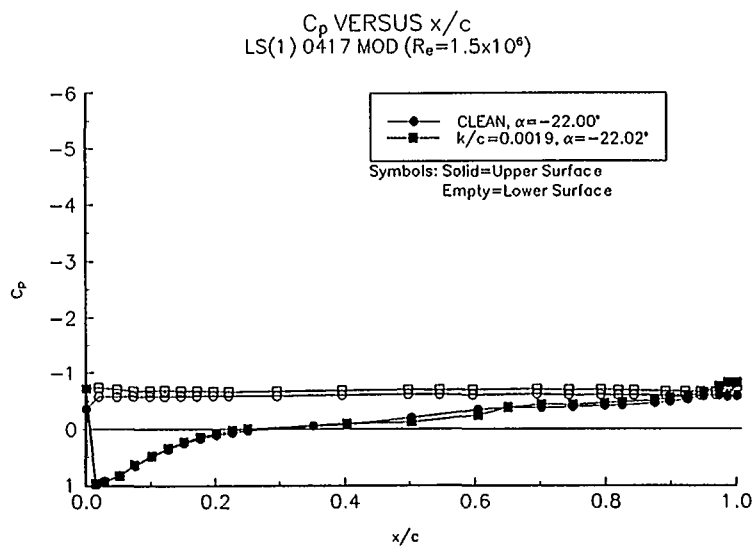

Figure 126. α = -22°

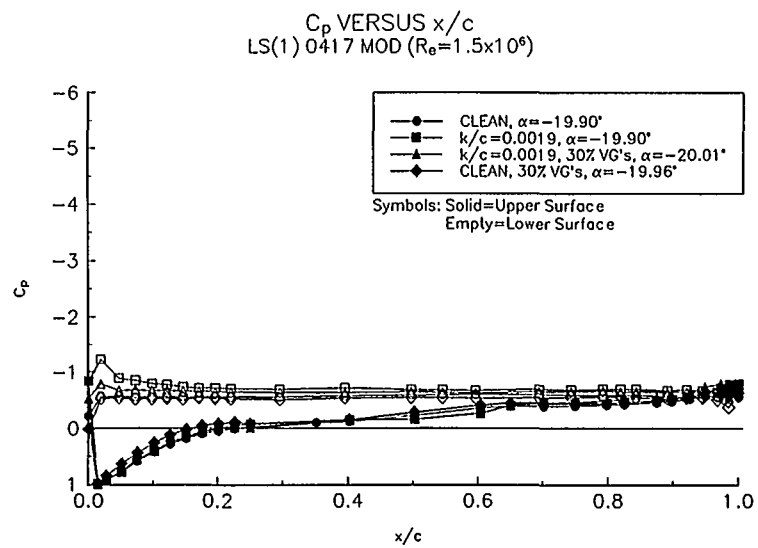

Figure 127. α = -20°

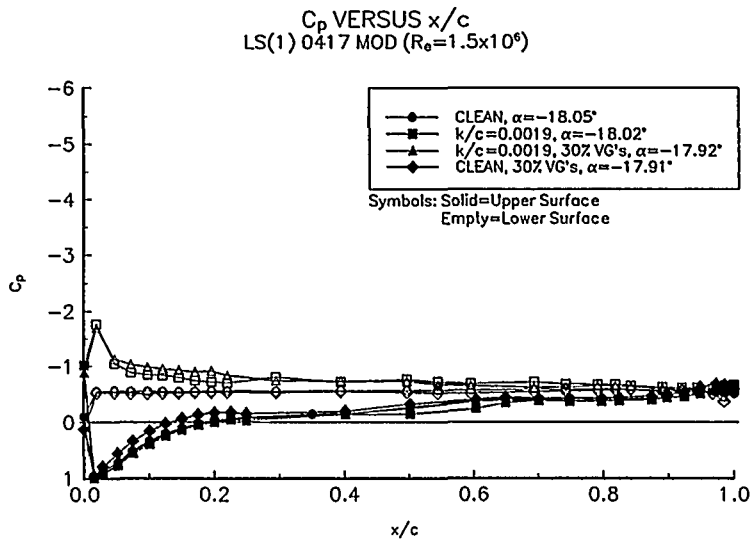

Figure 128. $\alpha = -18^\circ$

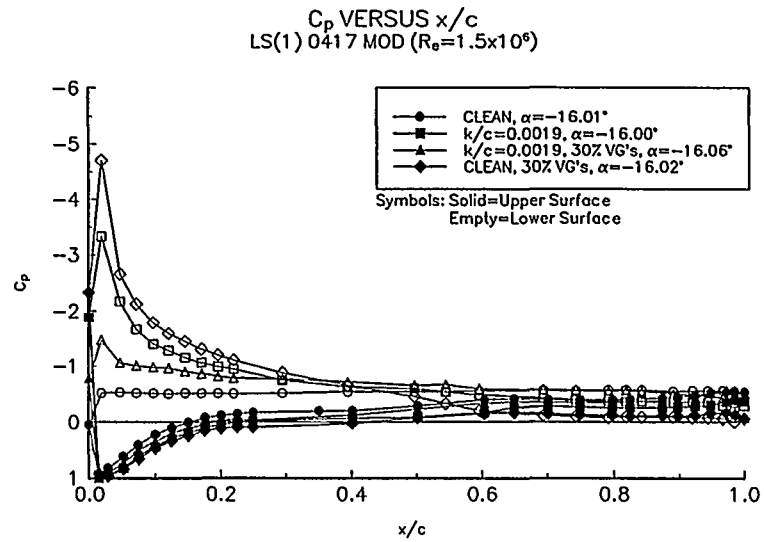

Figure 129. $\alpha = -16^\circ$

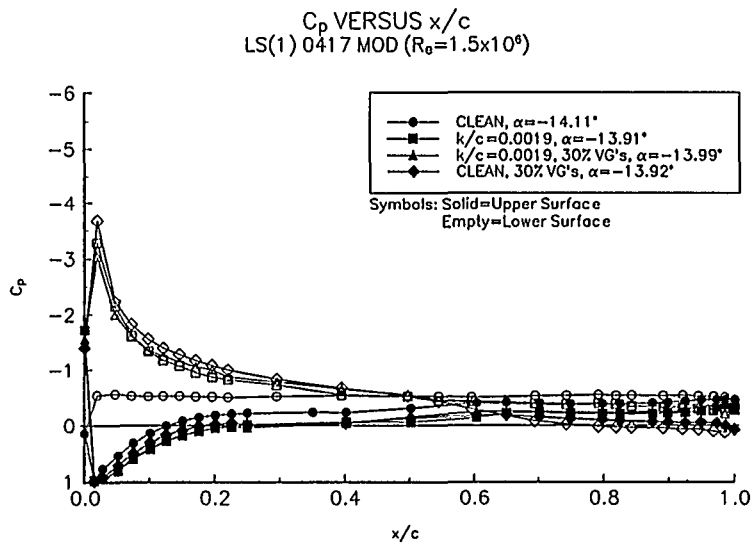

Figure 130. $\alpha = -14^\circ$

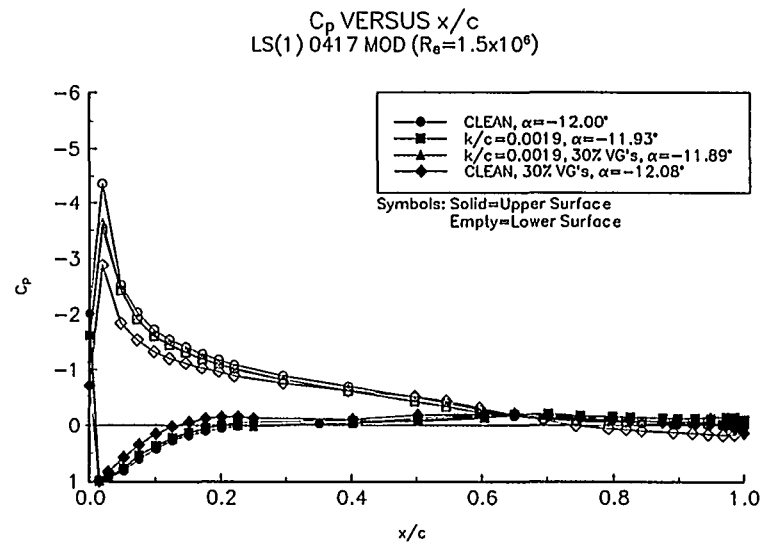

Figure 131. $\alpha = -12^\circ$

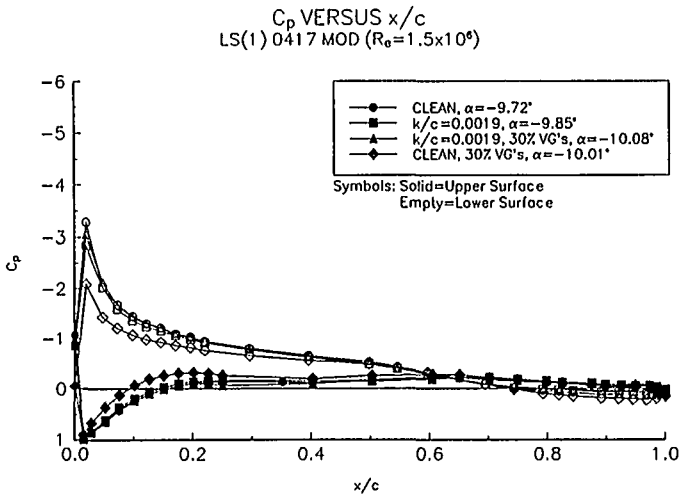

Figure 132. α = -10°

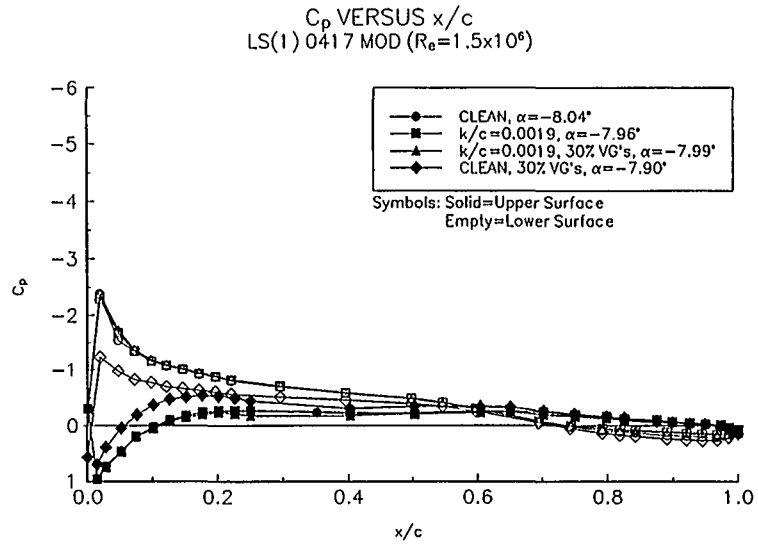

Figure 133. α = -8°

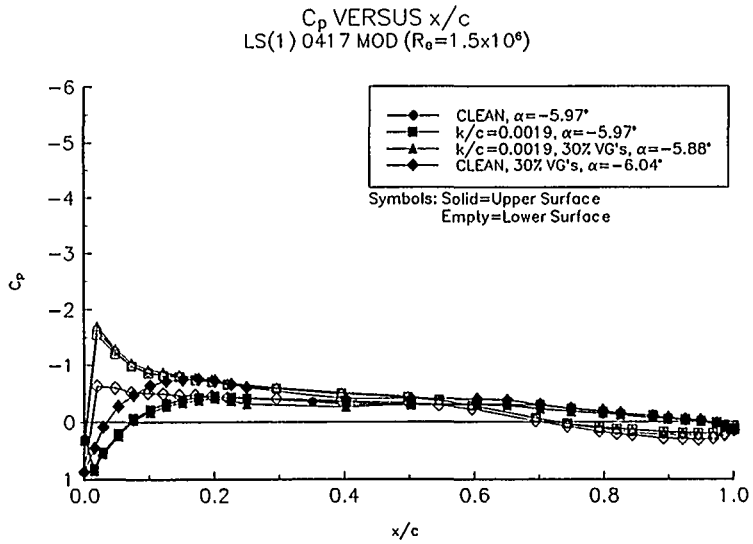

Figure 134. α = -6°

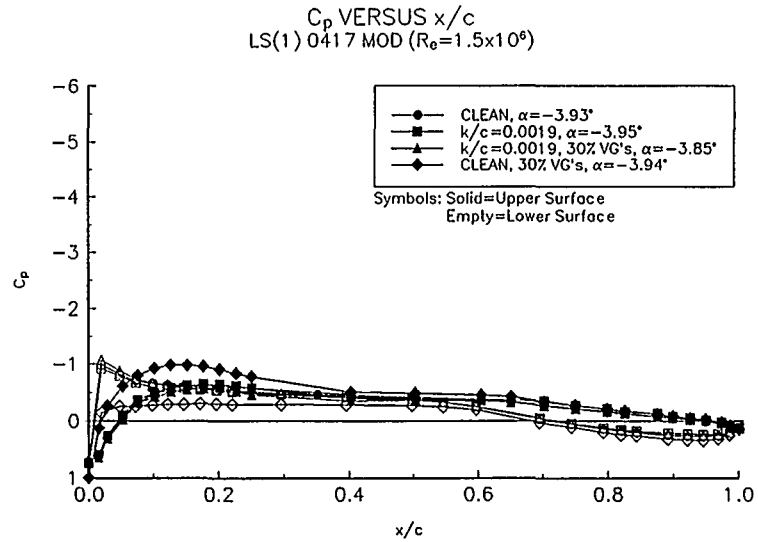

Figure 135. α = -4°

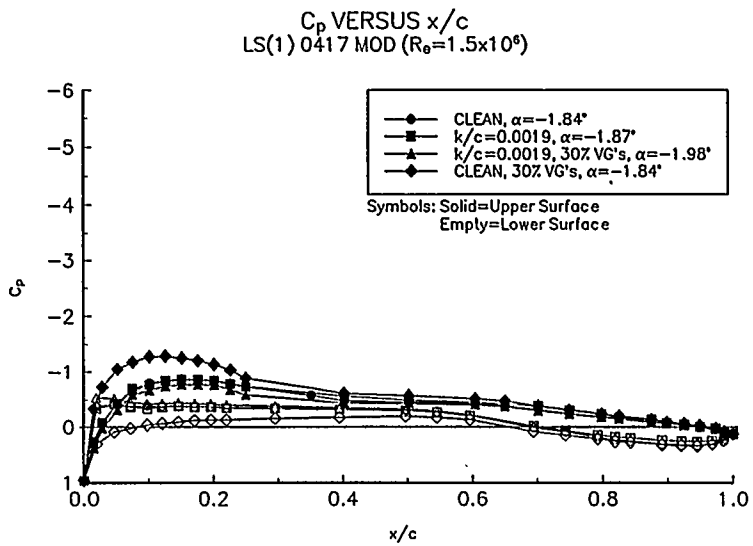

Figure 136. $\alpha = -2^\circ$

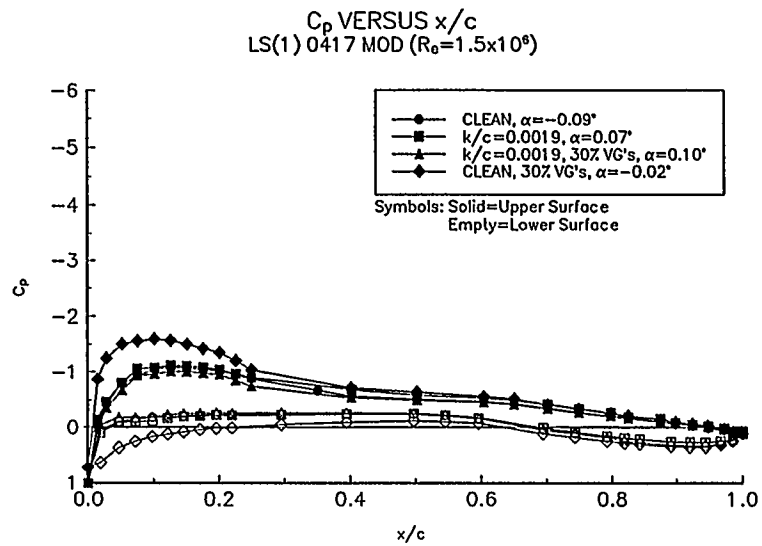

Figure 137. $\alpha = 0^\circ$

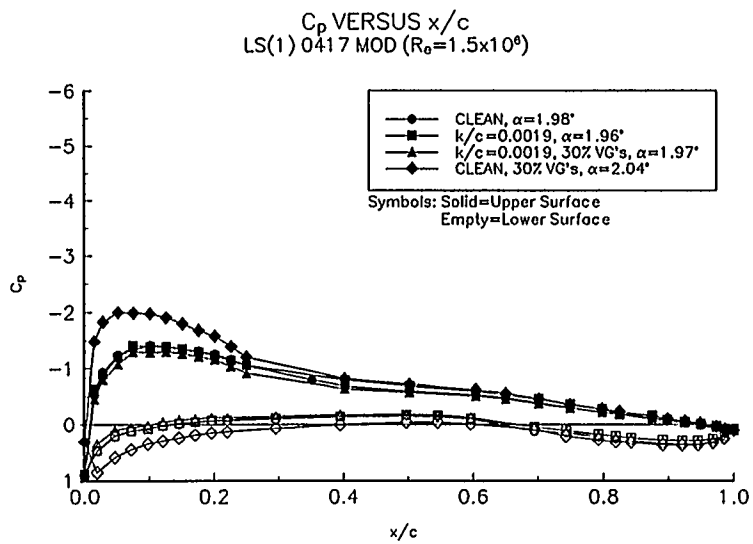

Figure 138. $\alpha = 2^\circ$

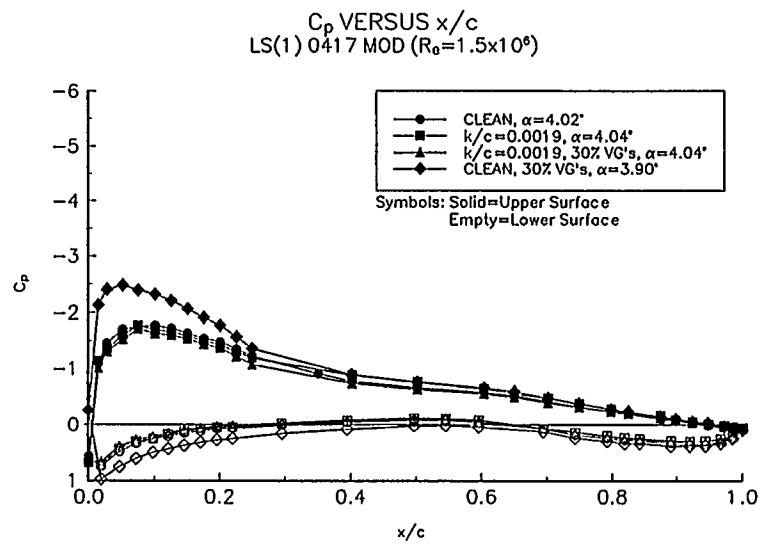

Figure 139. $\alpha = 4^\circ$

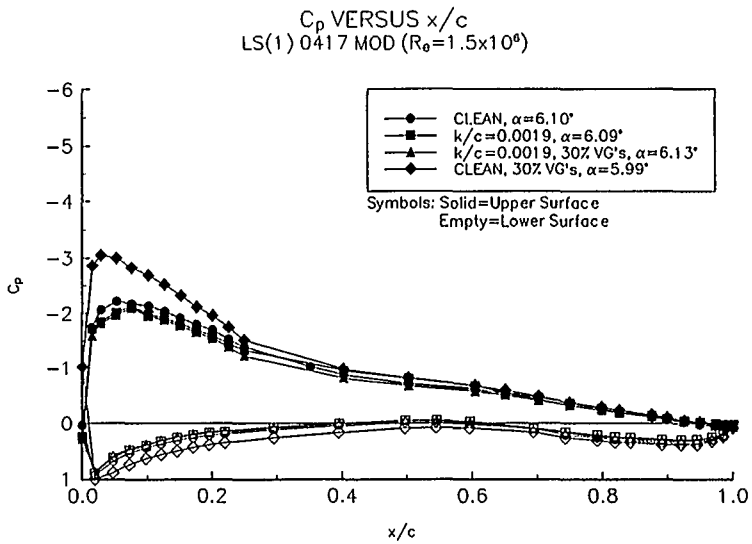

Figure 140. $\alpha = 6^\circ$

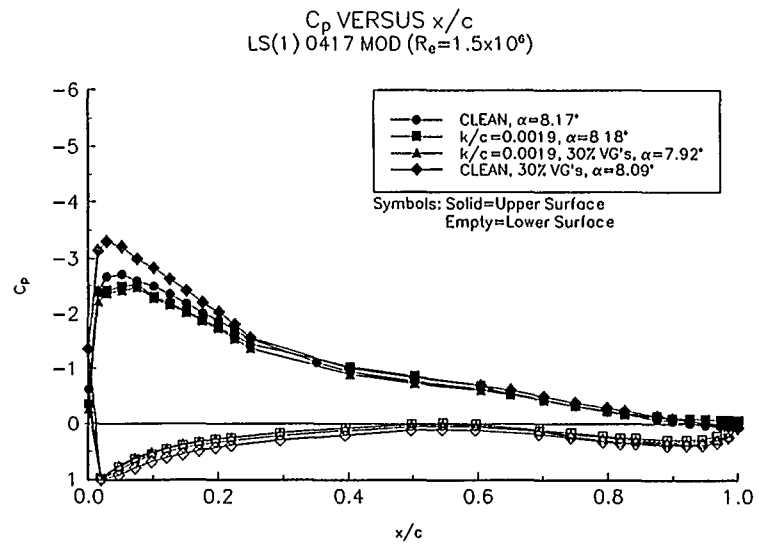

Figure 141. $\alpha = 8^\circ$

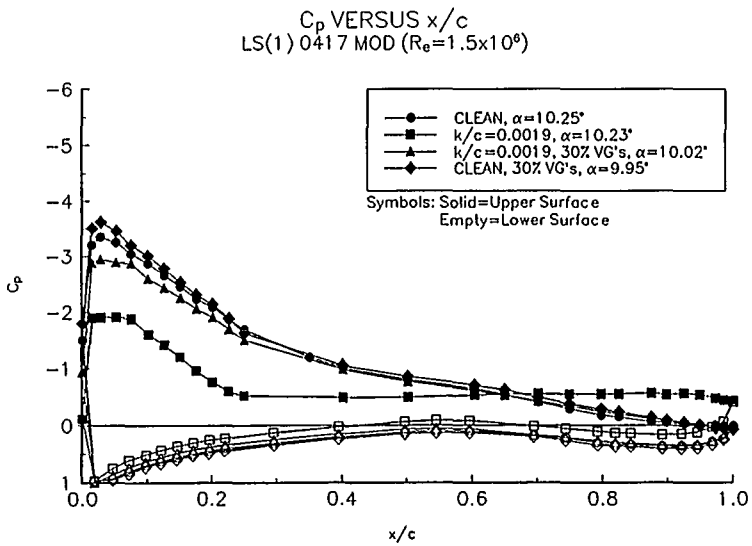

Figure 142. $\alpha = 10^\circ$

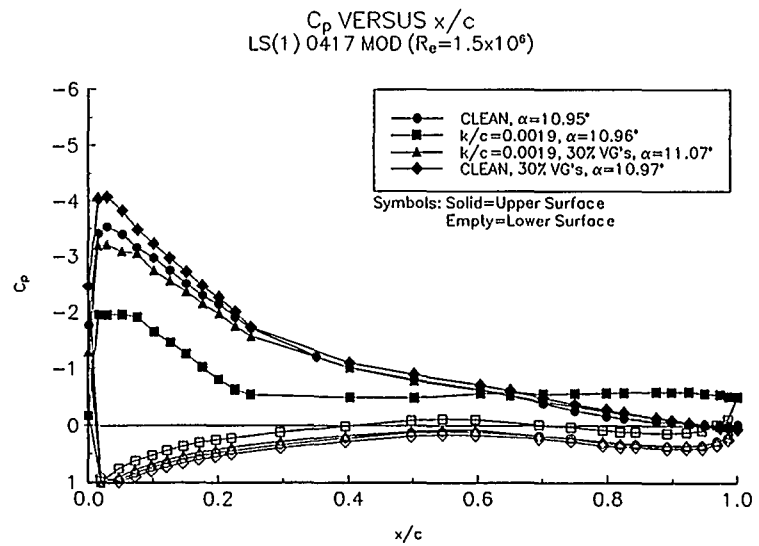

Figure 143. $\alpha = 11^\circ$

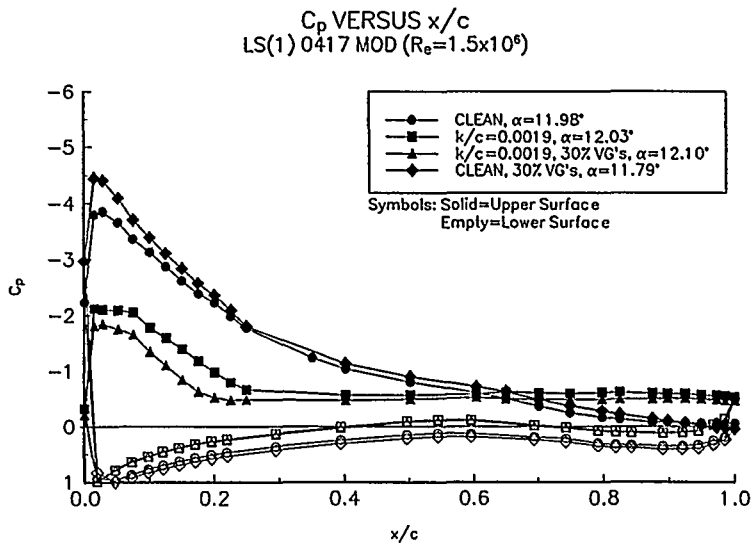

Figure 144. $\alpha = 12^\circ$

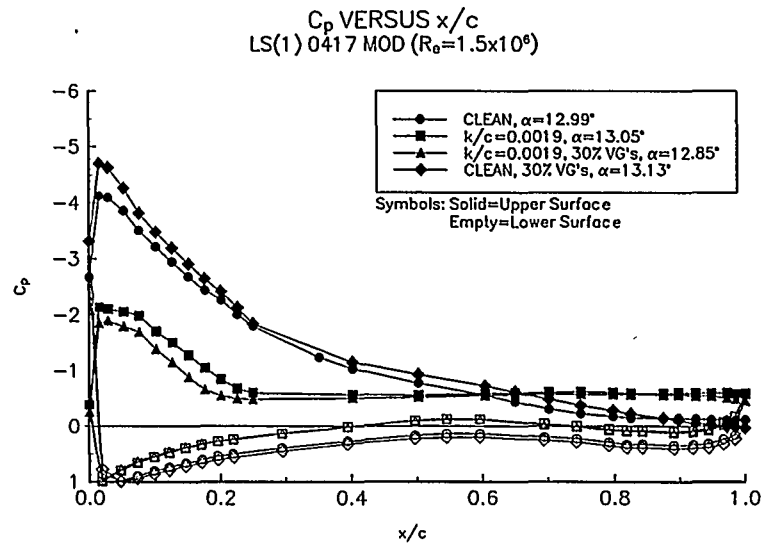

Figure 145. $\alpha = 13^\circ$

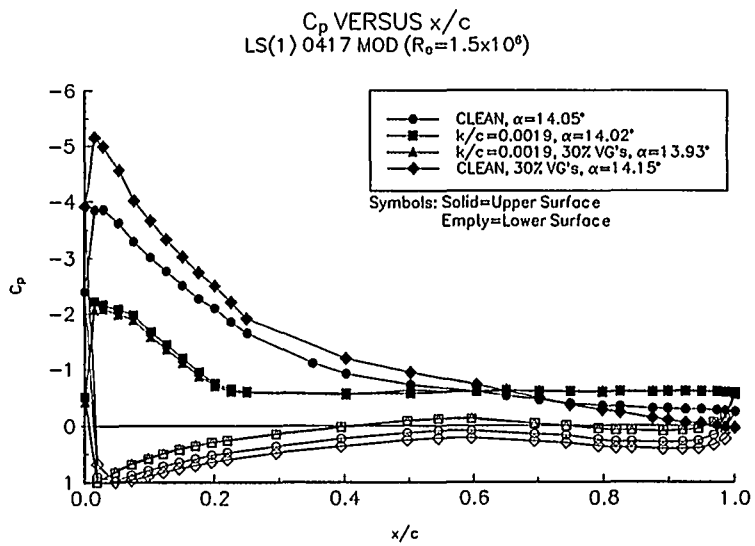

Figure 146. $\alpha = 14^\circ$

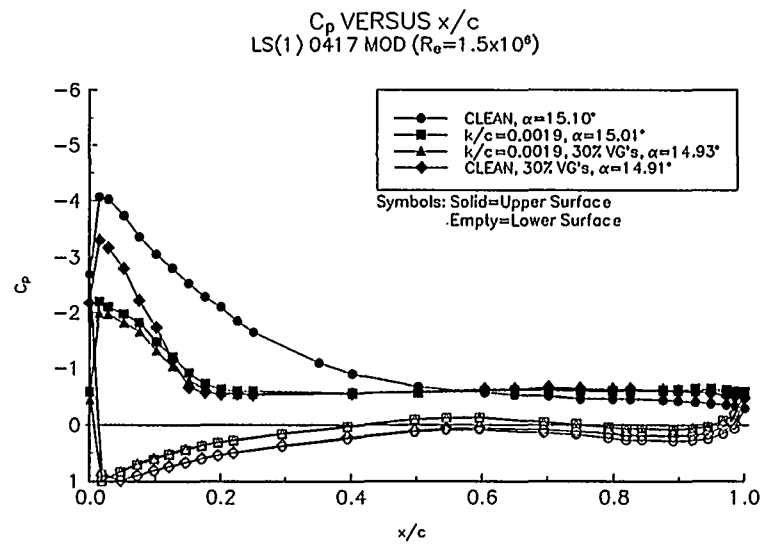

Figure 147. $\alpha = 15^\circ$

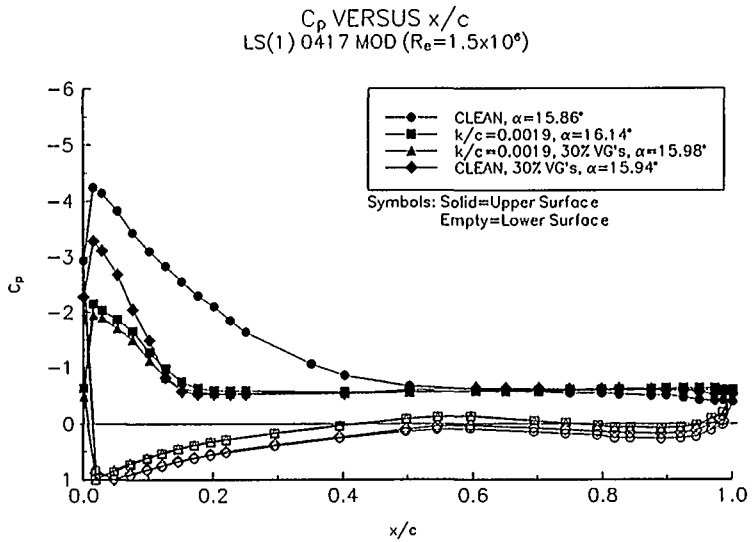

Figure 148. $\alpha = 16^\circ$

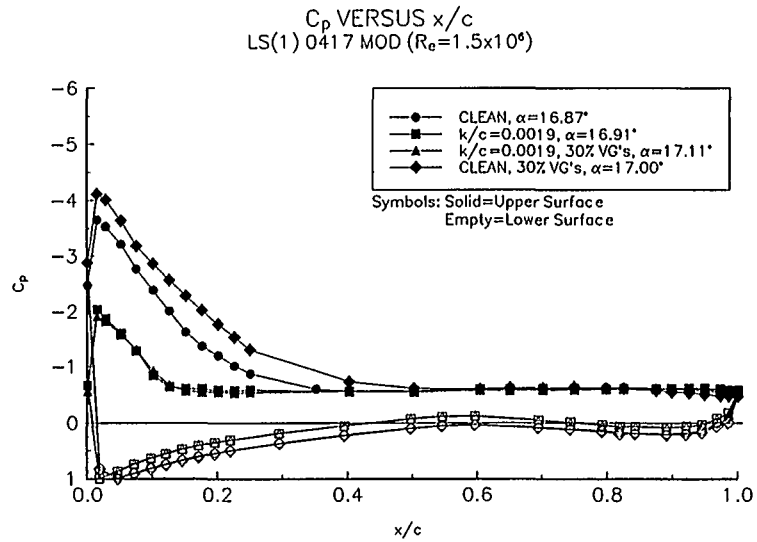

Figure 149. $\alpha = 17^\circ$

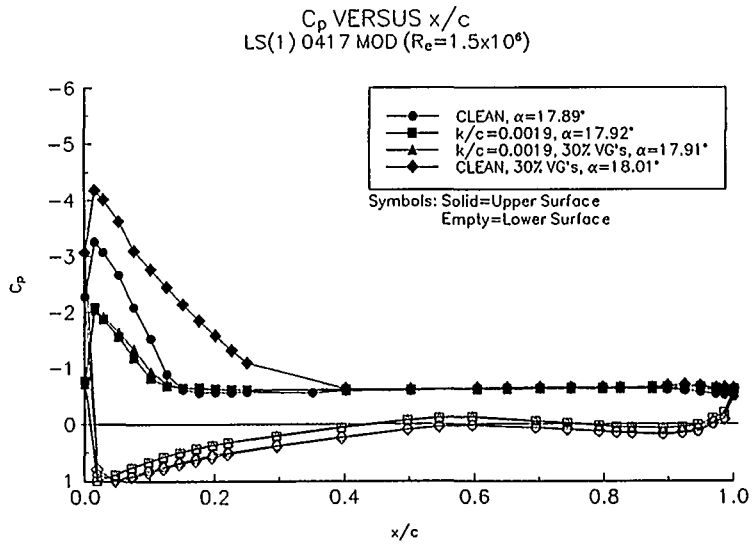

Figure 150. $\alpha = 18^\circ$

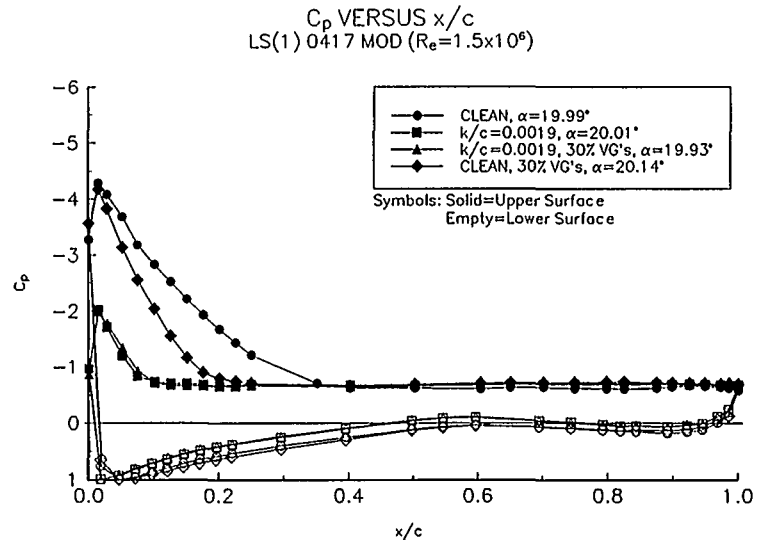

Figure 151. $\alpha = 20^\circ$

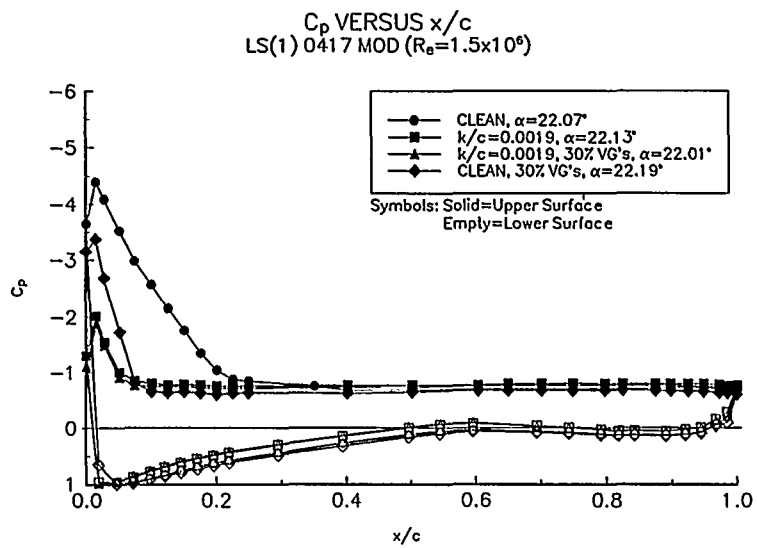

Figure 152. $\alpha = 22^\circ$

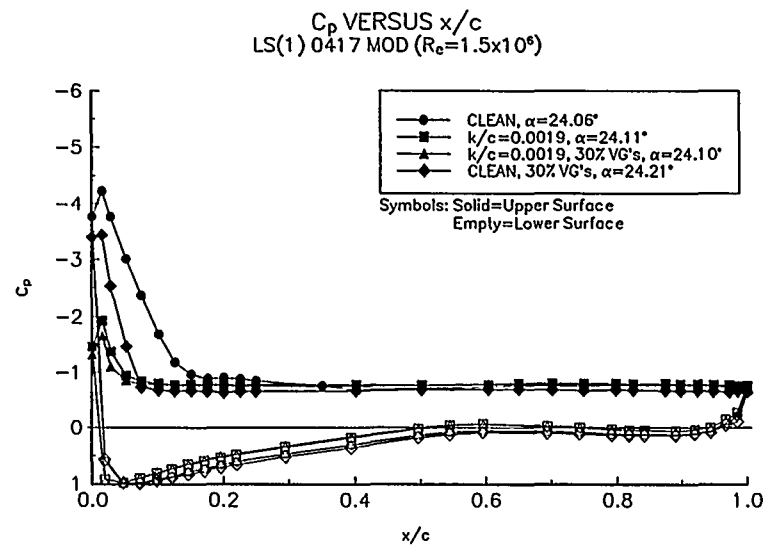

Figure 153. $\alpha = 24^\circ$

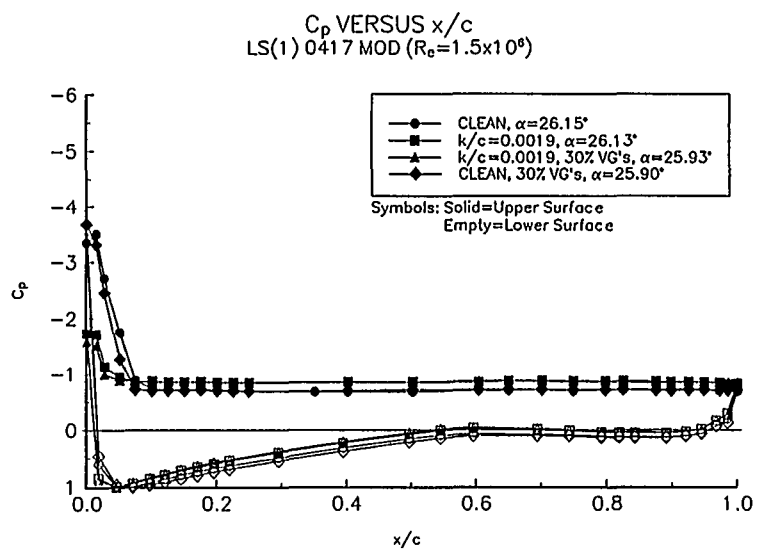

Figure 154. $\alpha = 26^\circ$

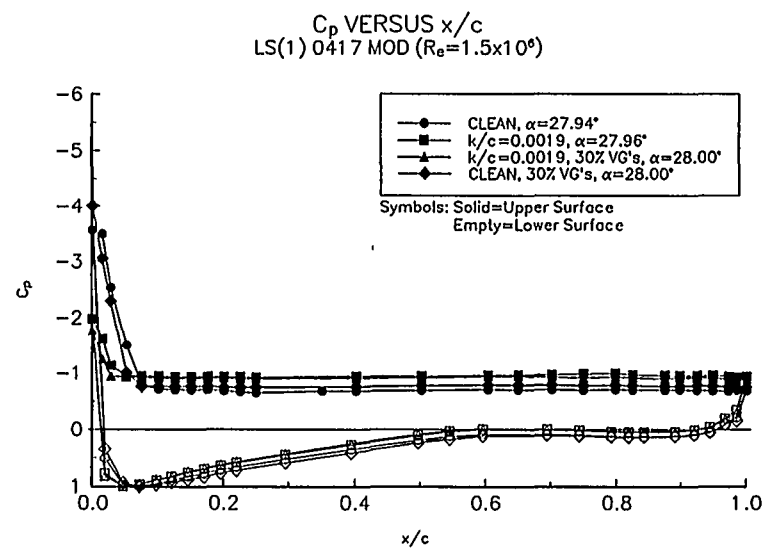

Figure 155. $\alpha = 28^\circ$

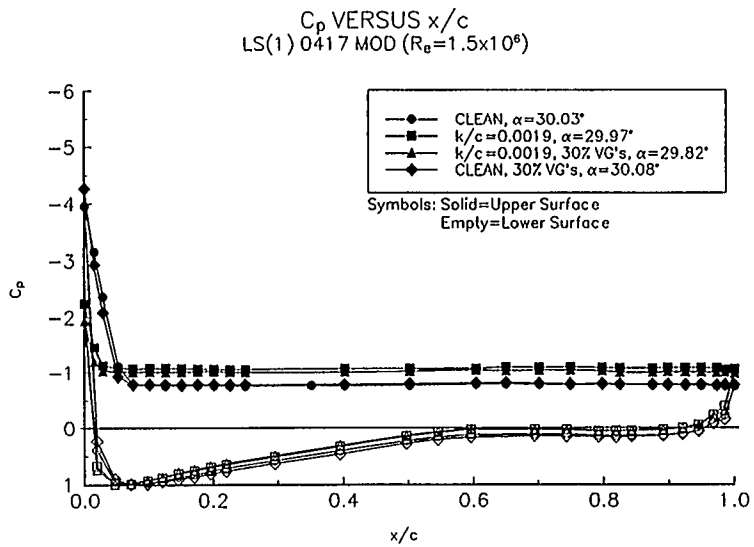

Figure 156. $\alpha = 30^\circ$

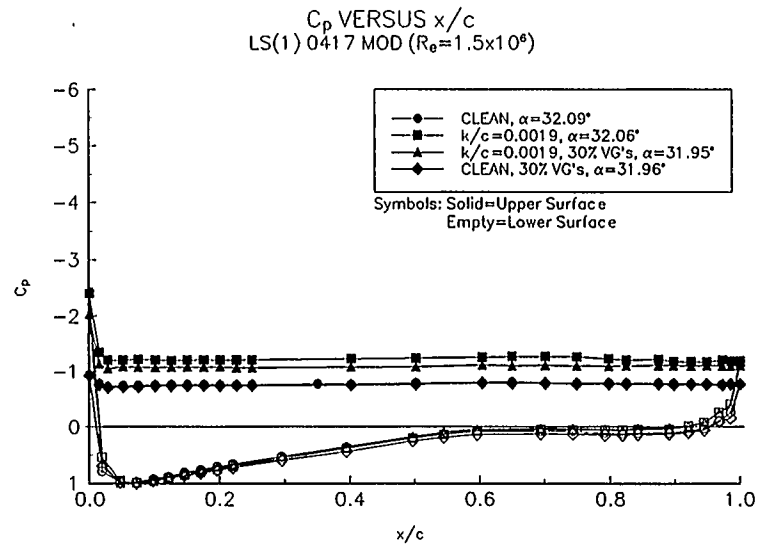

Figure 157. $\alpha = 32^\circ$

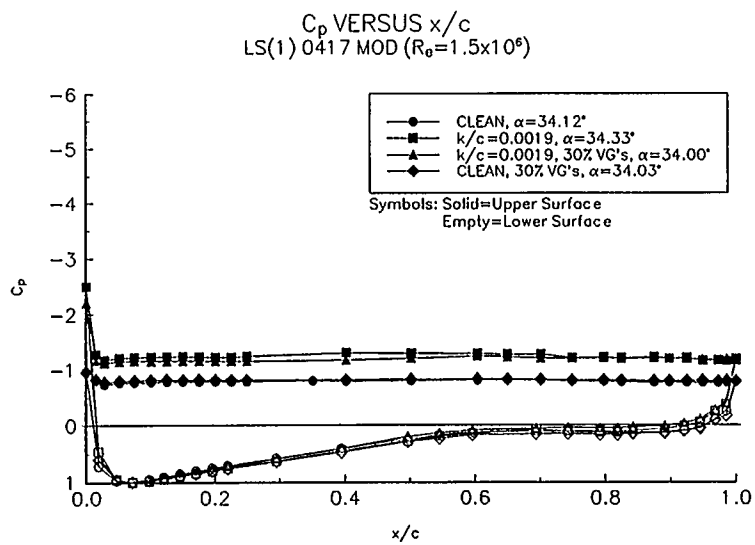

Figure 158. $\alpha = 34^\circ$

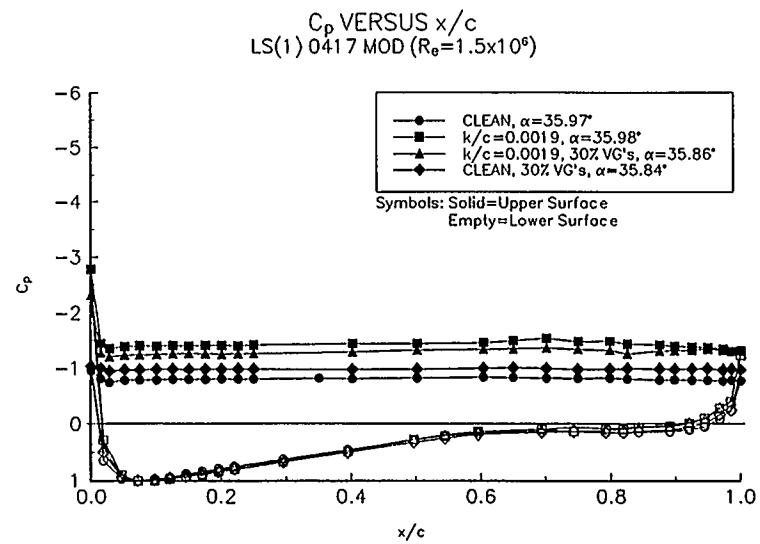

Figure 159. $\alpha = 36^\circ$

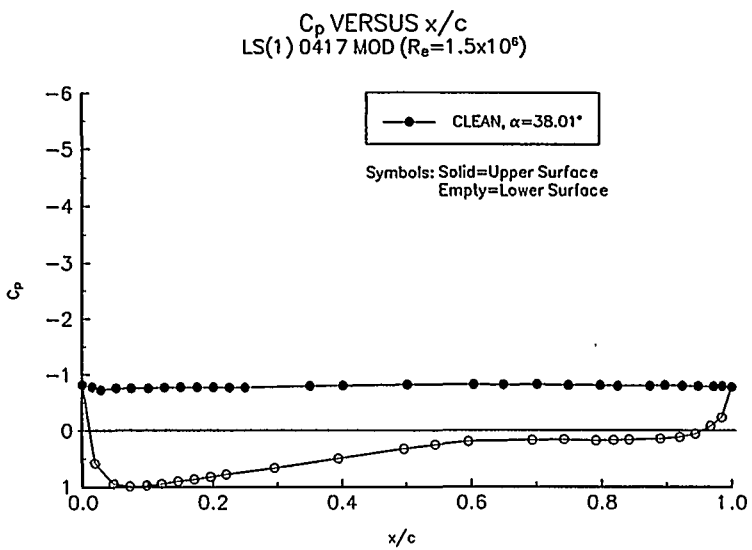

Figure 160. $\alpha = 38^\circ$

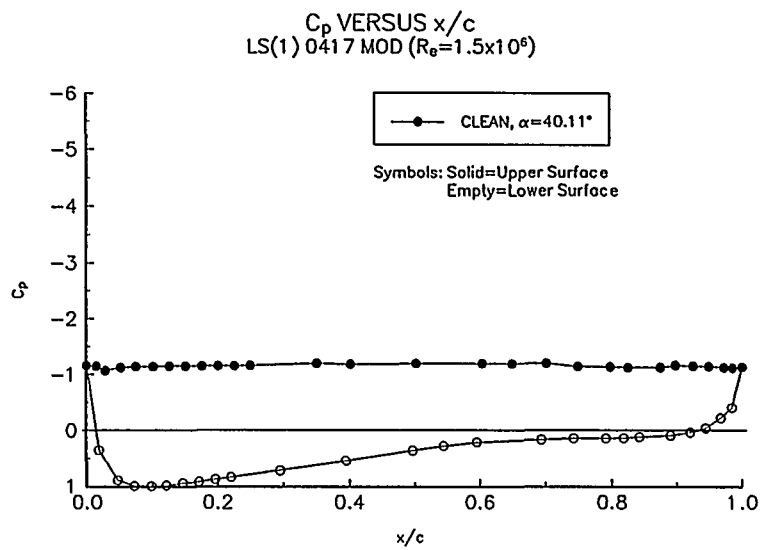

Figure 161. $\alpha = 40^\circ$

Steady State Pressure Distributions

Re = 2.0 million

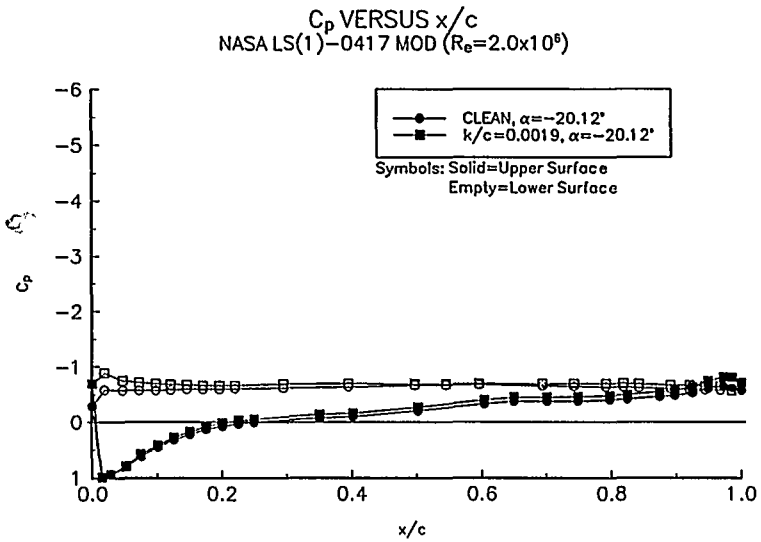

Figure 162. α = -20°

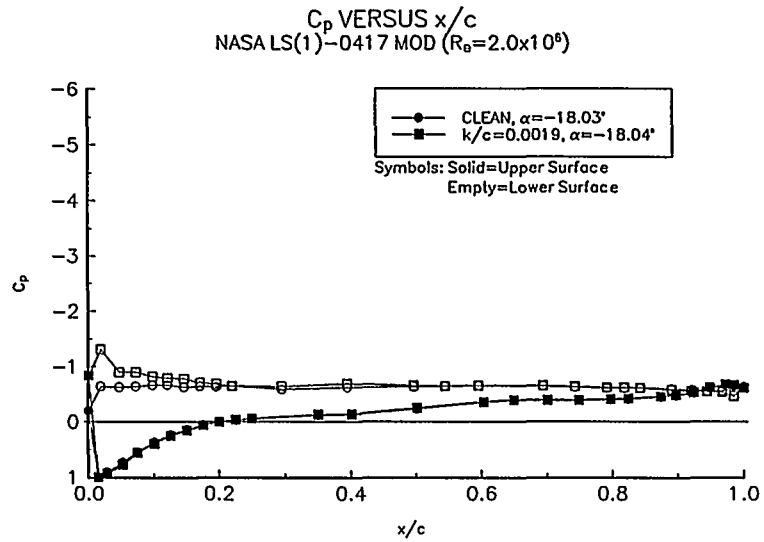

Figure 163. α = -18°

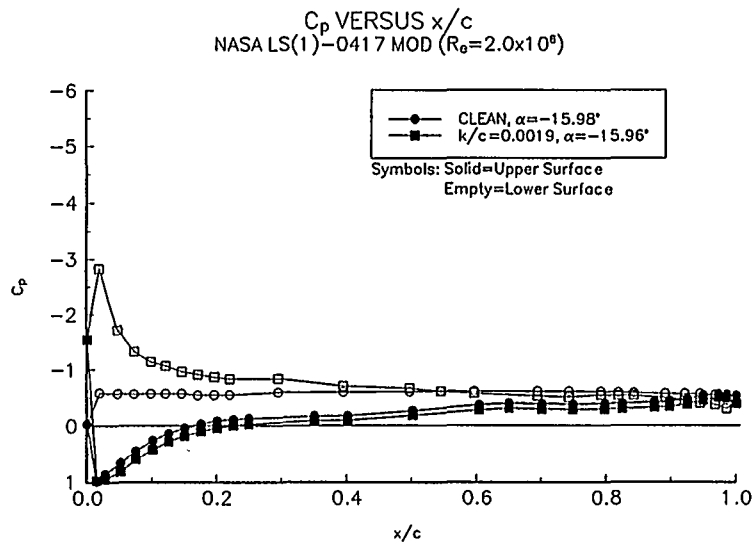

Figure 164. α = -16°

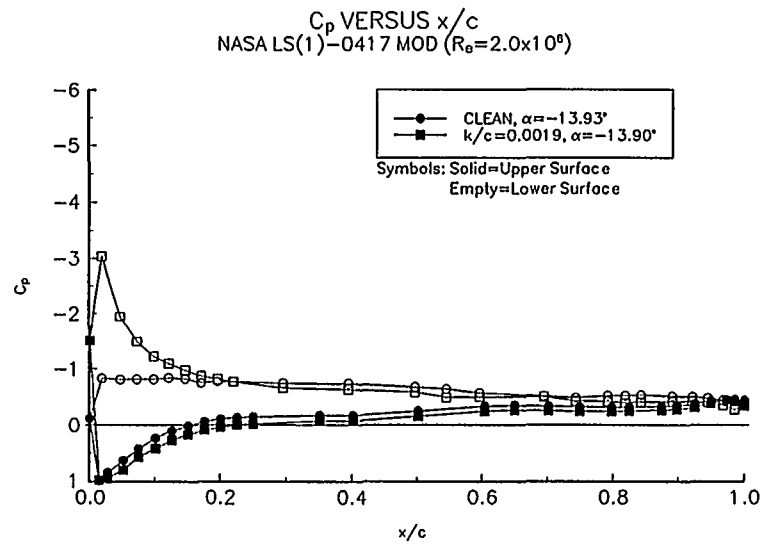

Figure 165. α = -14°

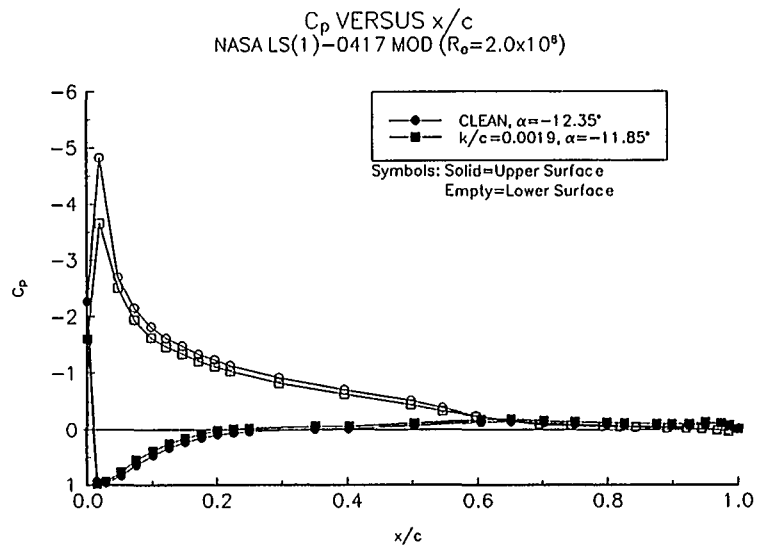

Figure 166. α = -12°

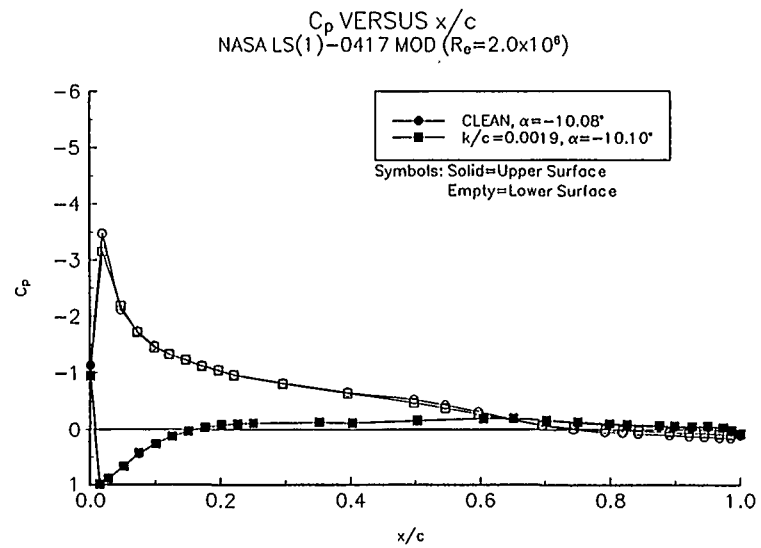

Figure 167. α = -10°

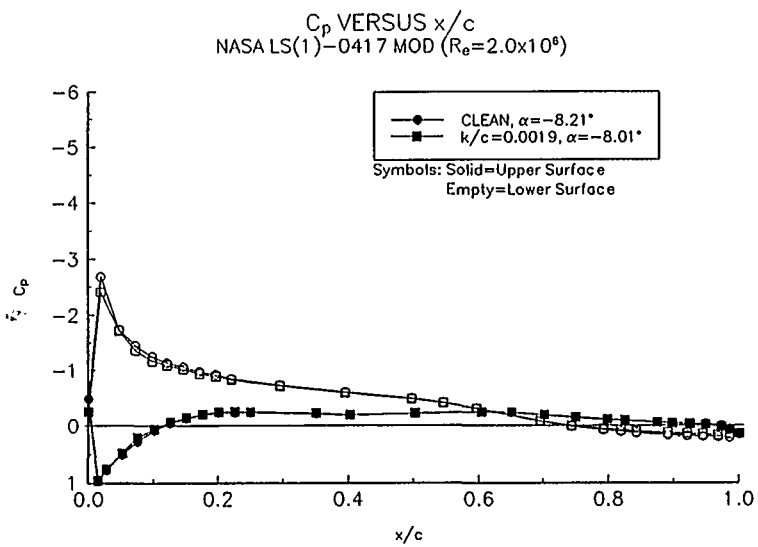

Figure 168. α = -8°

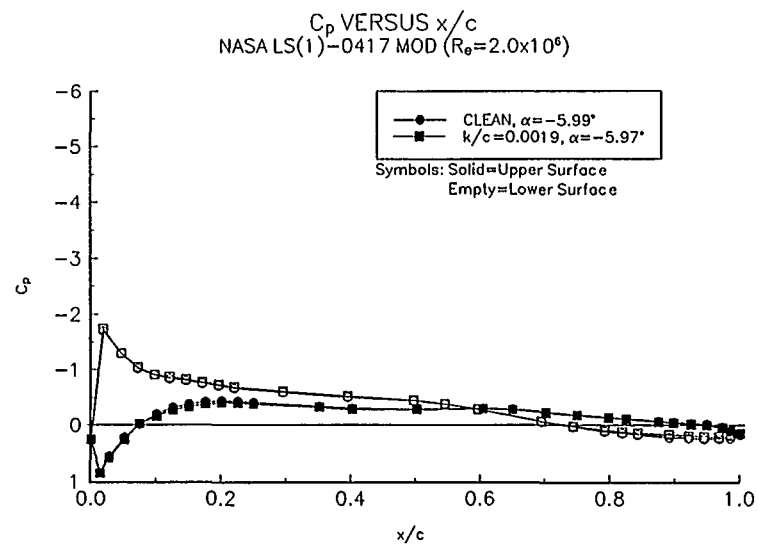

Figure 169. α = -6°

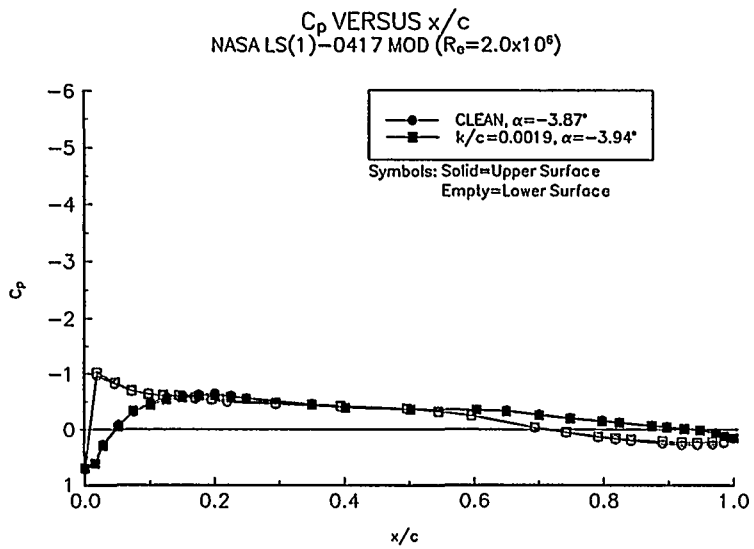

Figure 170. $\alpha = -4^\circ$

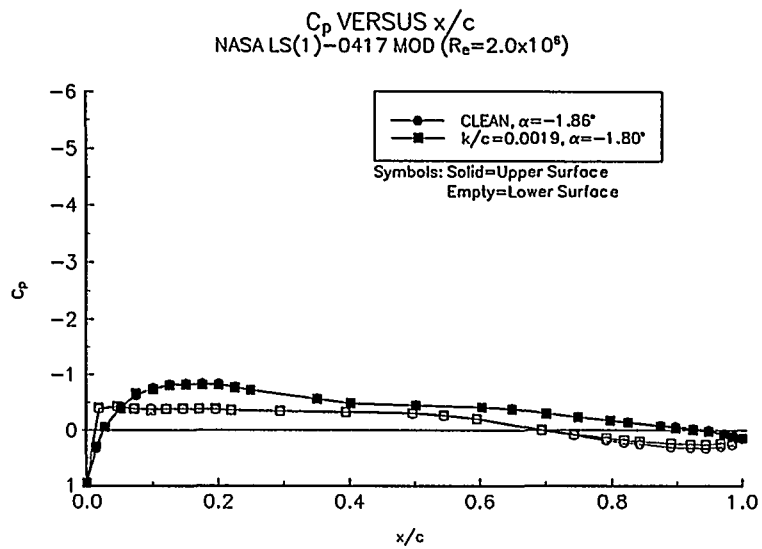

Figure 171. $\alpha = -2^\circ$

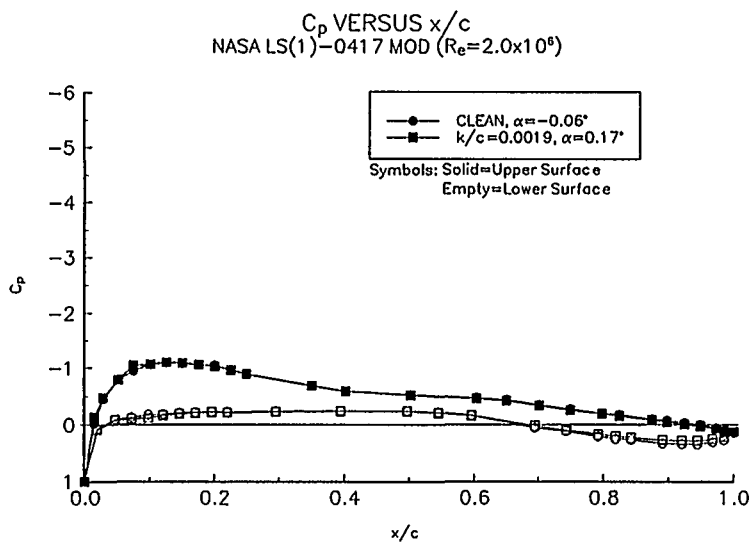

Figure 172. $\alpha = 0^\circ$

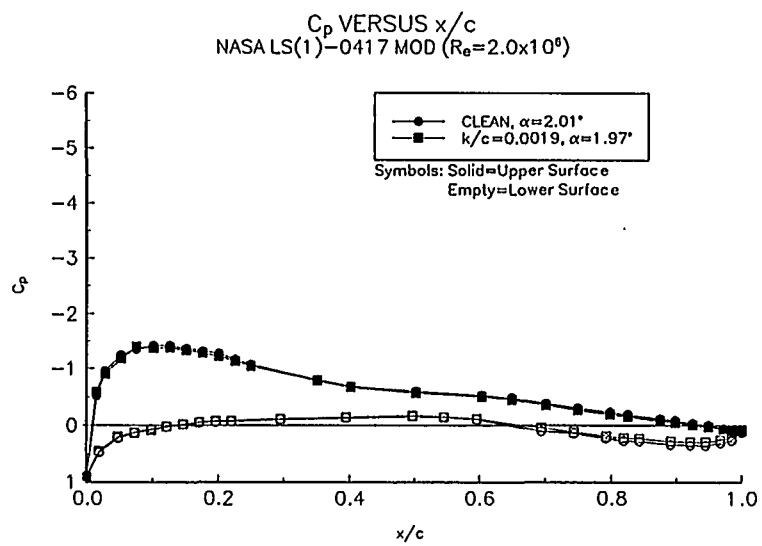

Figure 173. $\alpha = 2^\circ$

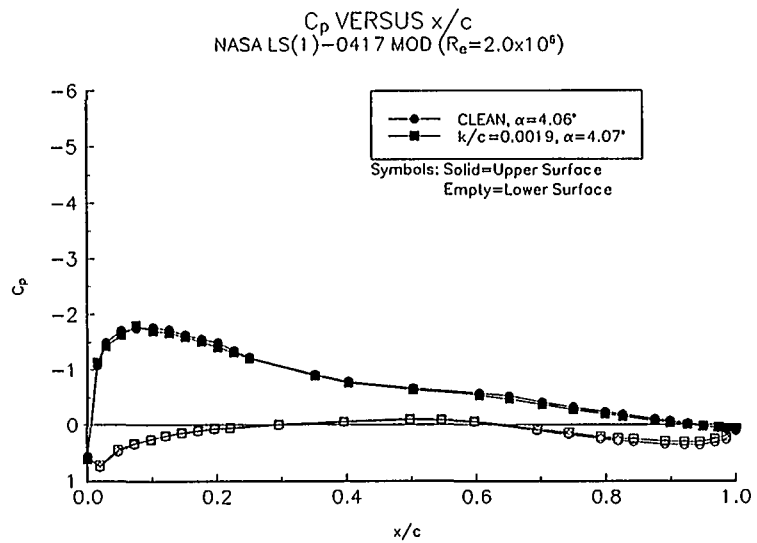

Figure 174. $\alpha = 4°$

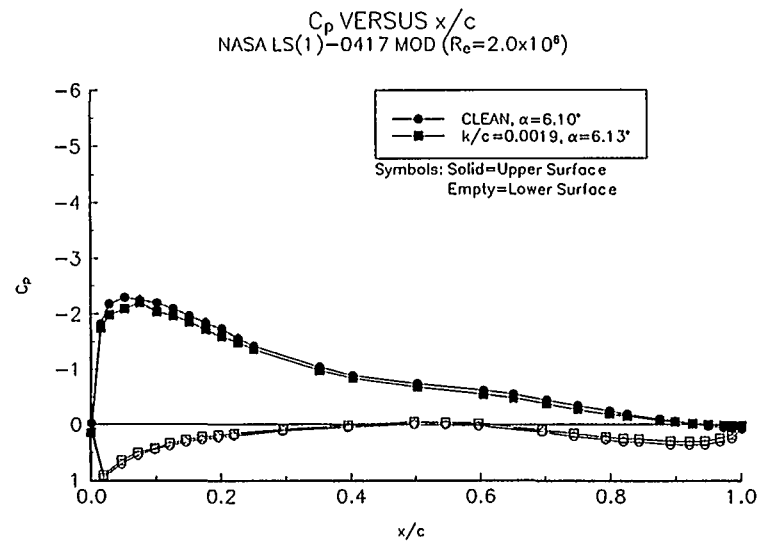

Figure 175. $\alpha = 6°$

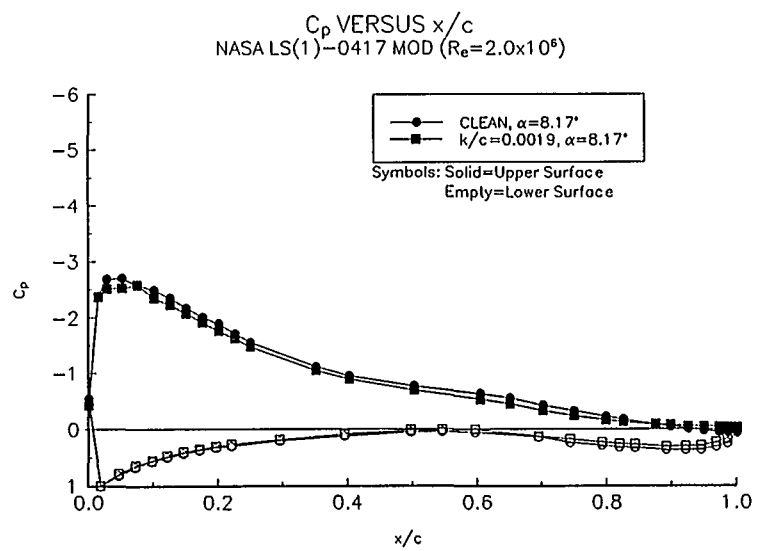

Figure 176. $\alpha = 8°$

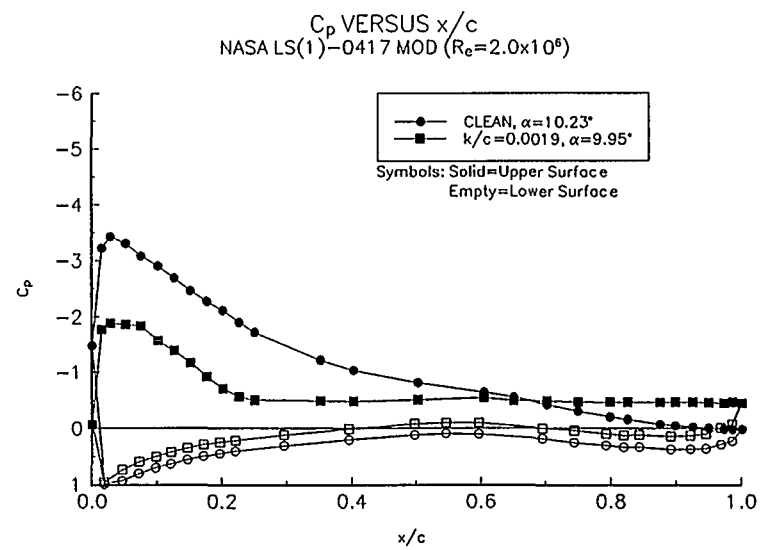

Figure 177. $\alpha = 10°$

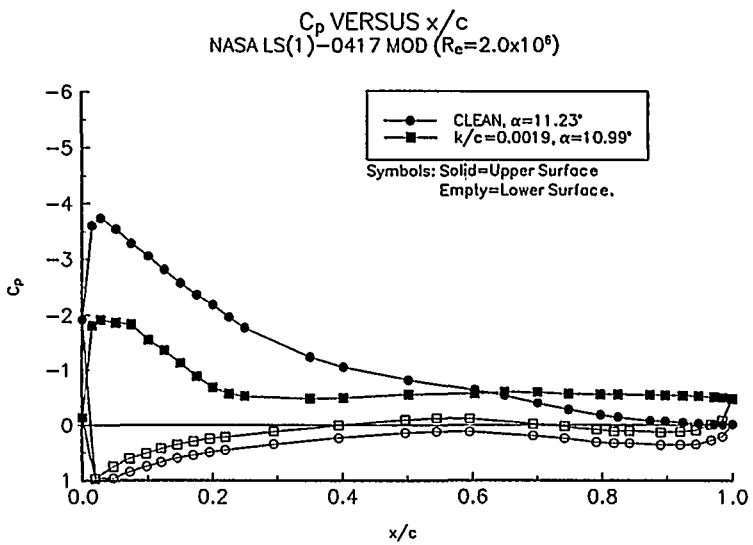

Figure 178. $\alpha = 11^\circ$

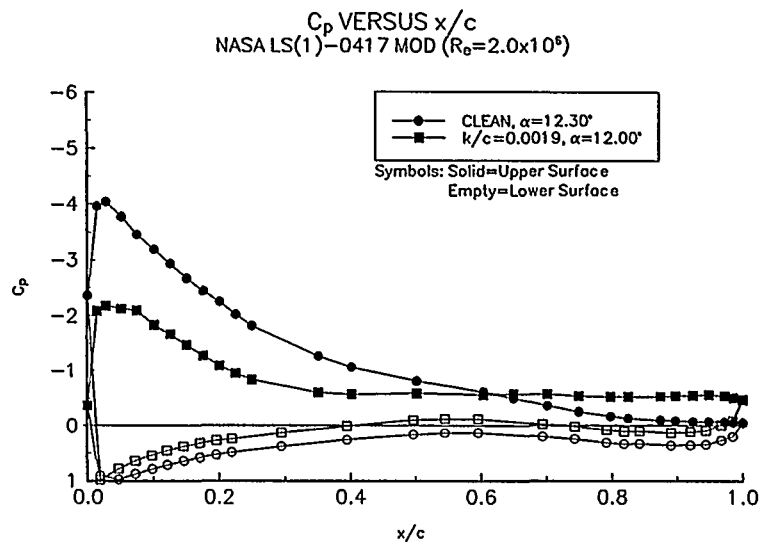

Figure 179. $\alpha = 12^\circ$

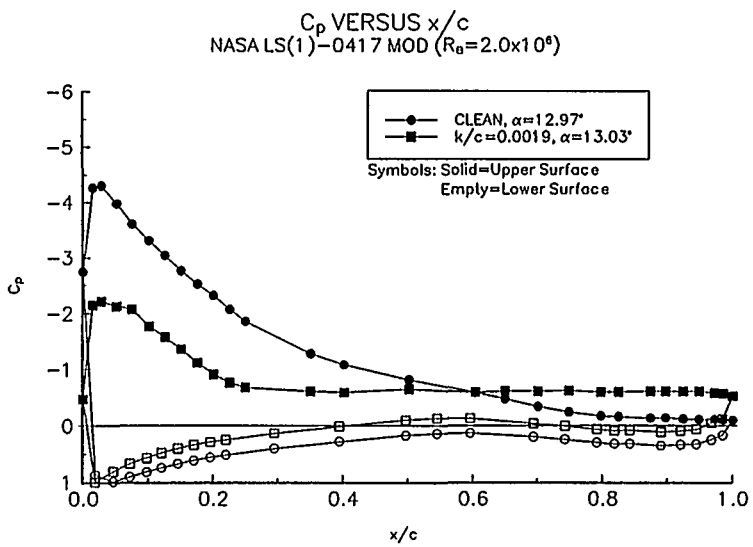

Figure 180. $\alpha = 13^\circ$

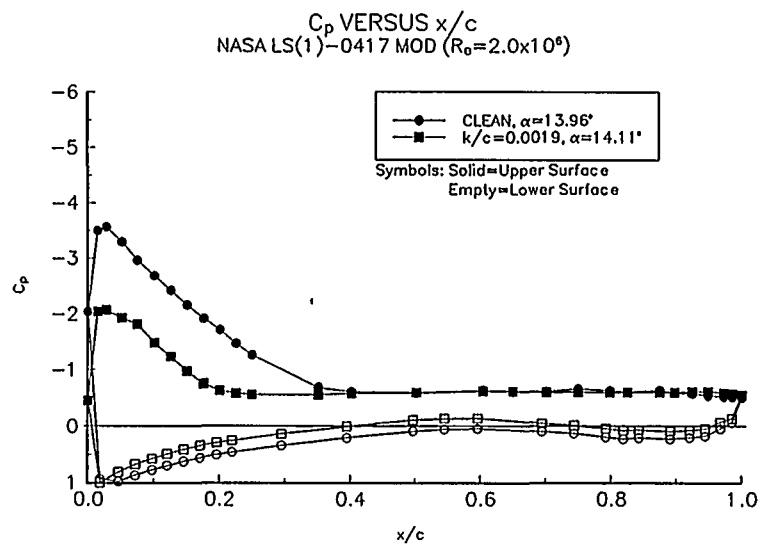

Figure 181. $\alpha = 14^\circ$

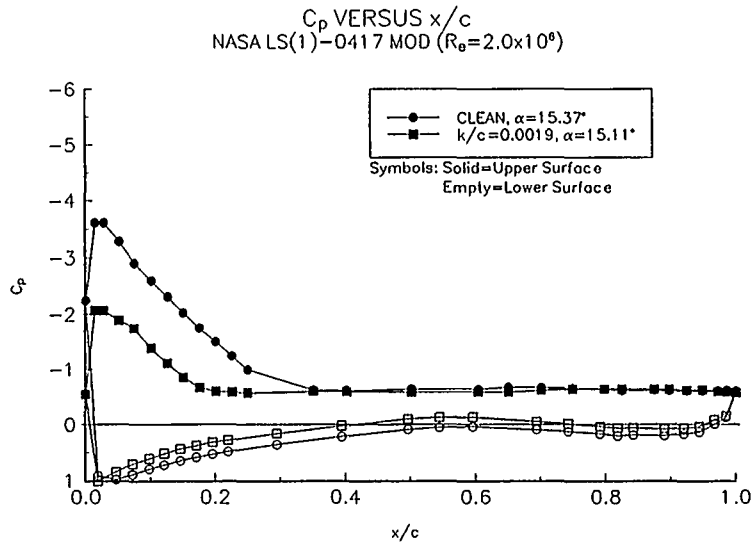

Figure 182. $\alpha = 15^\circ$

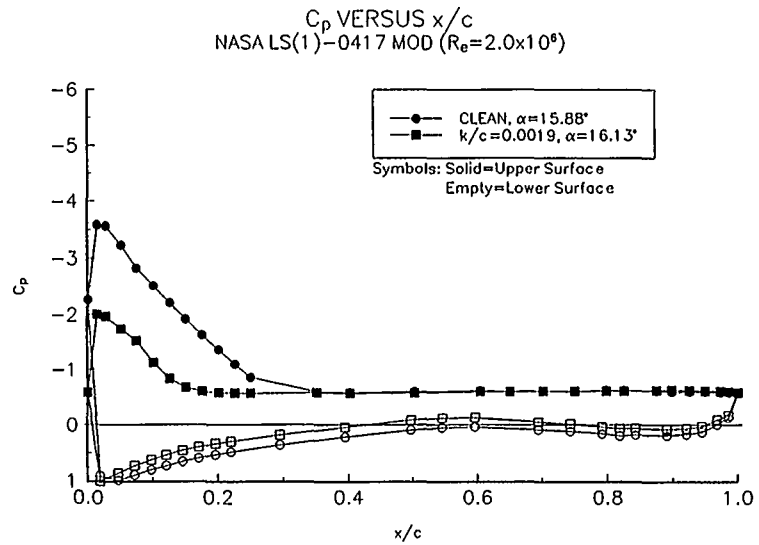

Figure 183. $\alpha = 16^\circ$

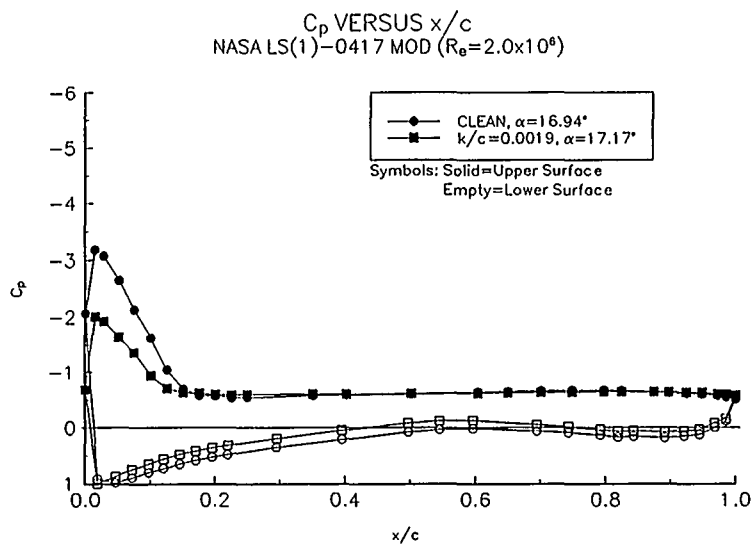

Figure 184. $\alpha = 17^\circ$

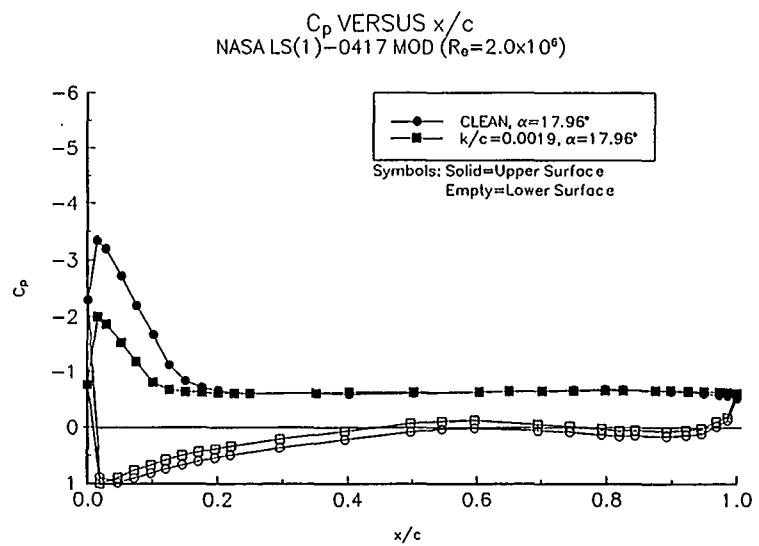

Figure 185. $\alpha = 18^\circ$

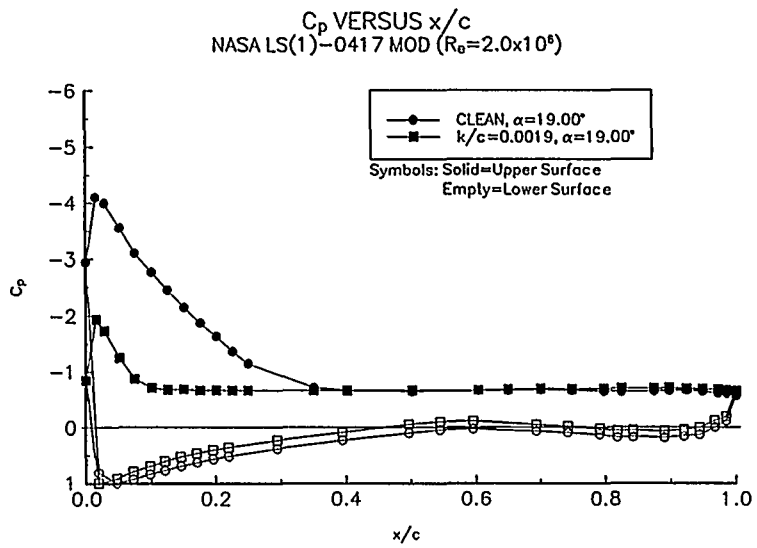

Figure 186. $\alpha = 19°$

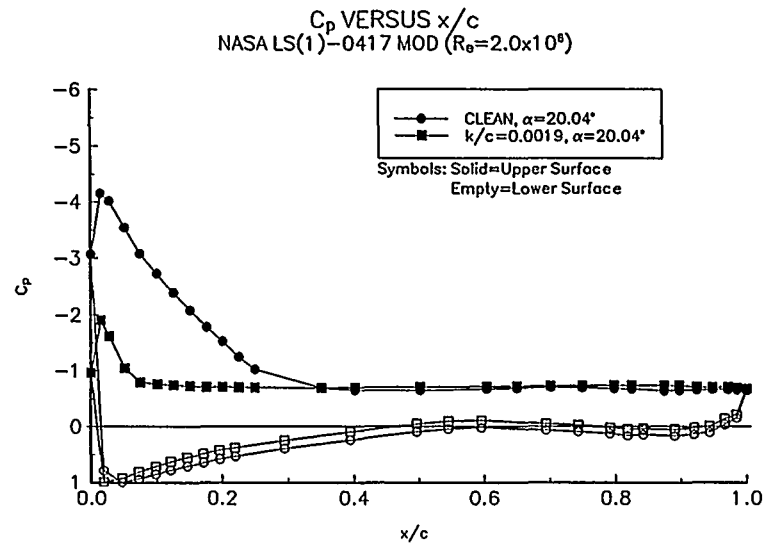

Figure 187. $\alpha = 20°$

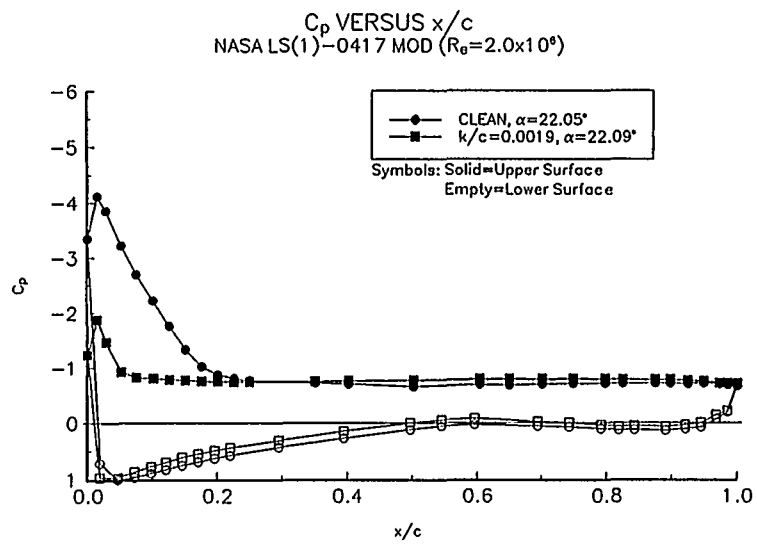

Figure 188. $\alpha = 22°$

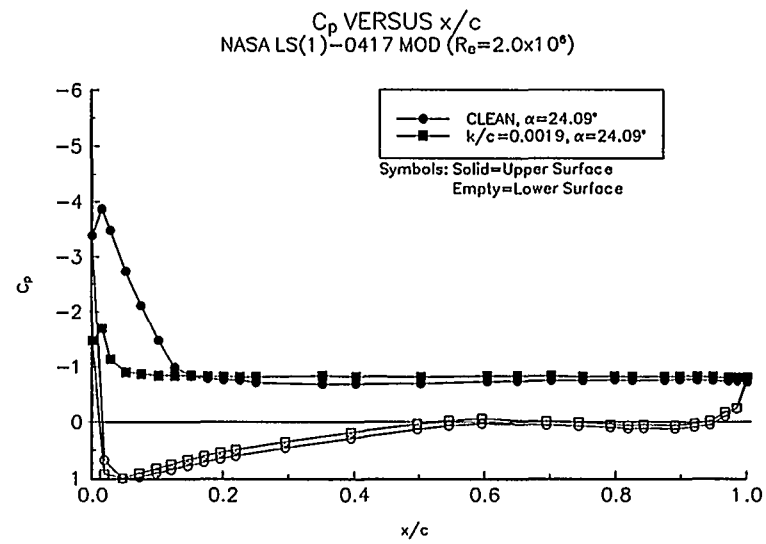

Figure 189. $\alpha = 24°$

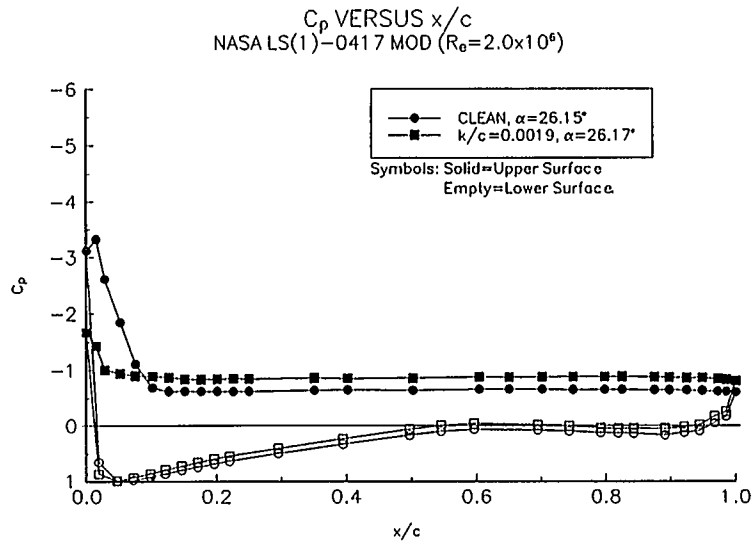

Figure 190. α = 26°

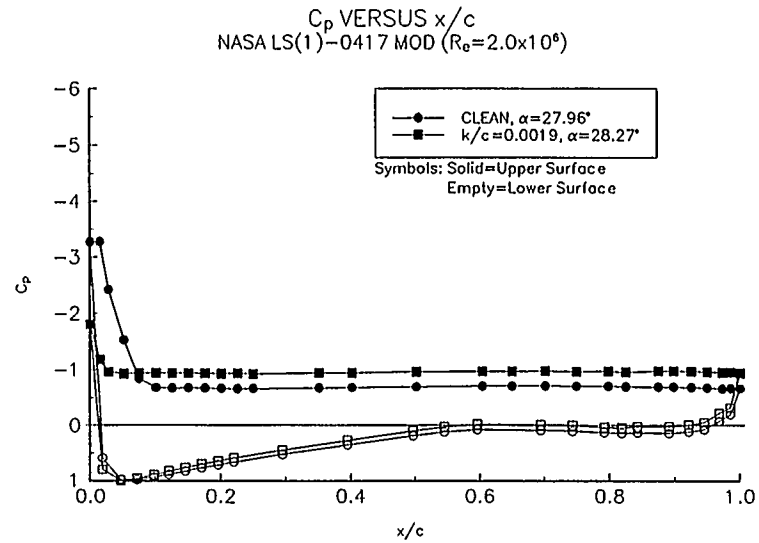

Figure 191. α = 28°

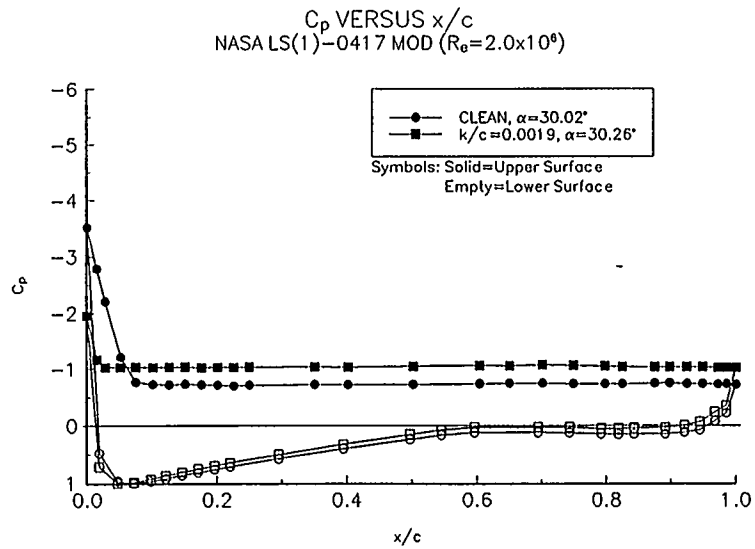

Figure 192. α = 30°

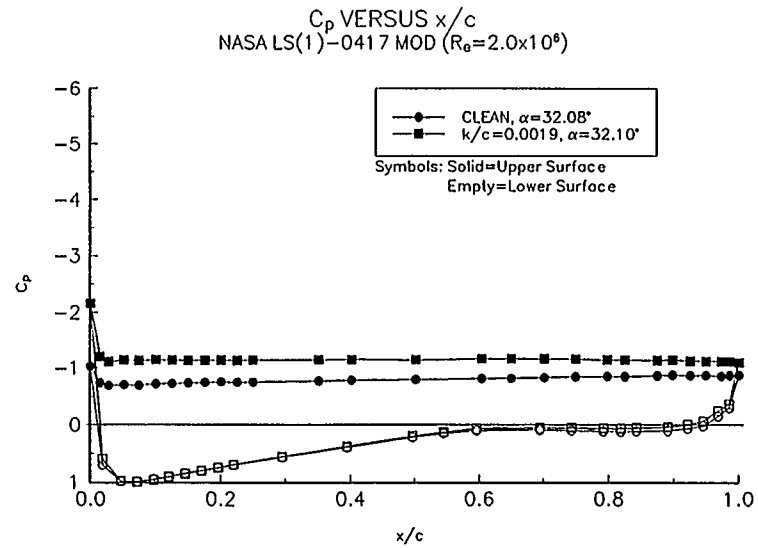

Figure 193. α = 32°

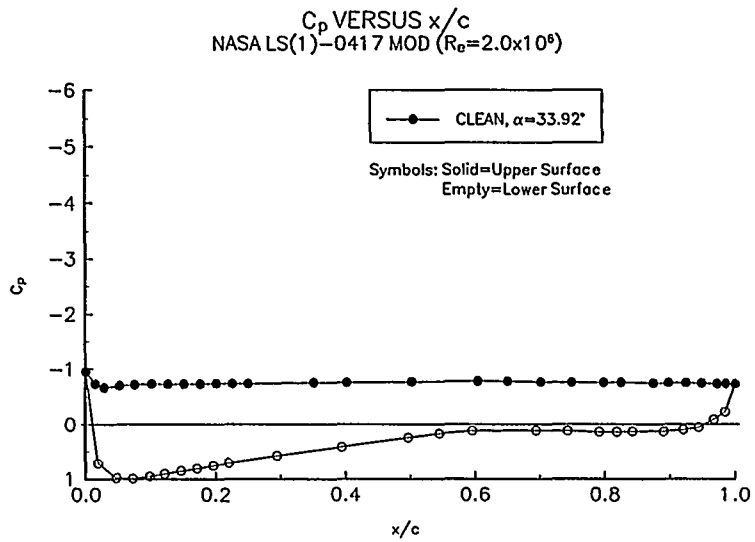

Figure 194. $\alpha = 34°$

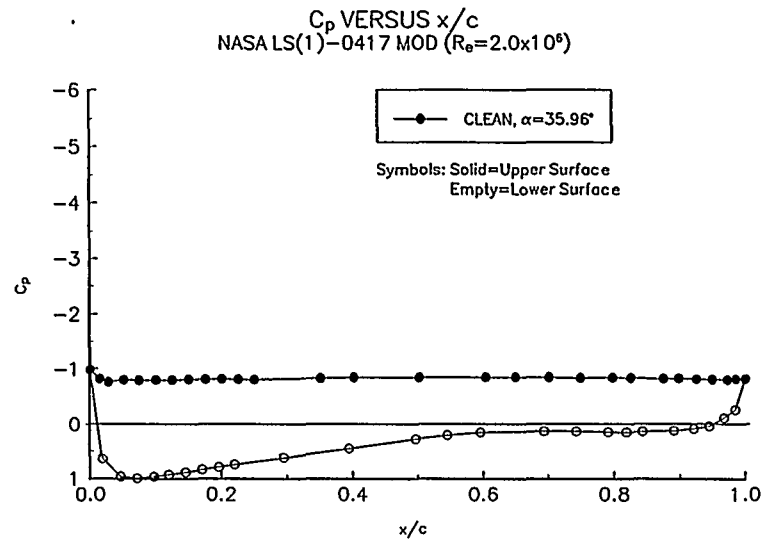

Figure 195. $\alpha = 36°$

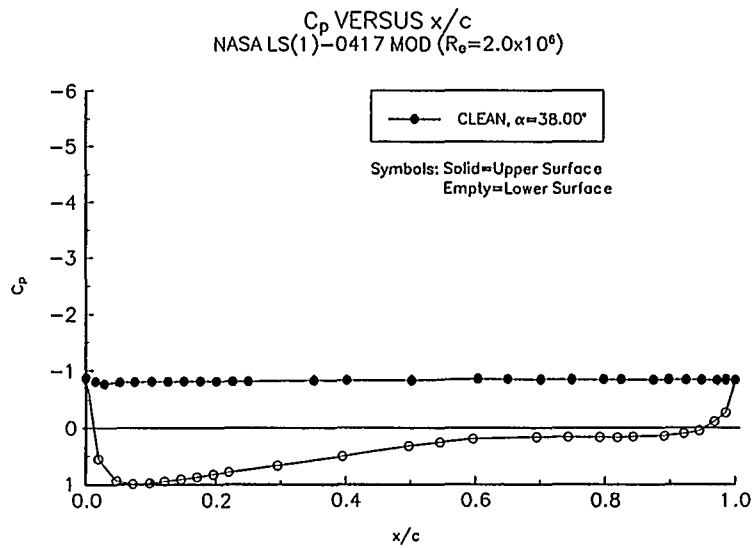

Figure 196. $\alpha = 38°$

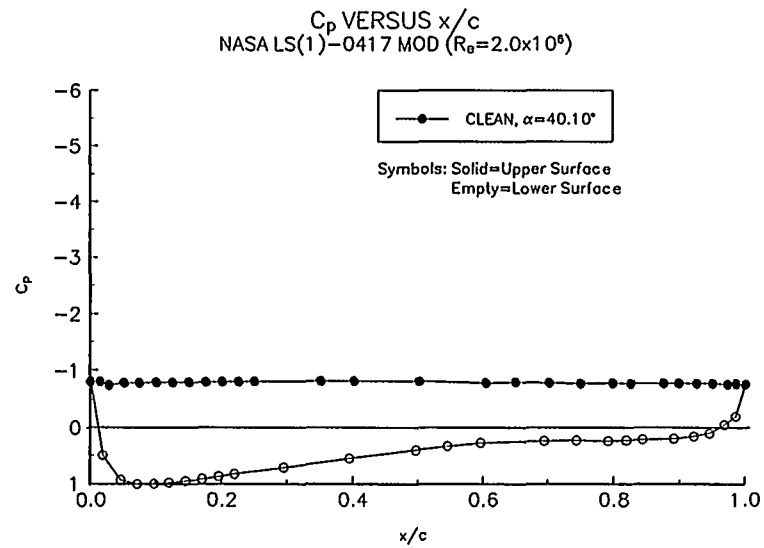

Figure 197. $\alpha = 40°$

REPORT DOCUMENTATION PAGE

Form Approved
OMB NO. 0704-0188

Public reporting burden for this collection of information is estimated to average 1 hour per response, including the time for reviewing instructions, searching existing data sources, gathering and maintaining the data needed, and completing and reviewing the collection of information. Send comments regarding this burden estimate or any other aspect of this collection of information, including suggestions for reducing this burden, to Washington Headquarters Services, Directorate for Information Operations and Reports, 1215 Jefferson Davis Highway, Suite 1204, Arlington, VA 22202-4302, and to the Office of Management and Budget, Paperwork Reduction Project (0704-0188), Washington, DC 20503.

1.	2. REPORT DATE	3. REPORT TYPE AND DATES COVERED
	December 1995	Subcontract Report

4. TITLE AND SUBTITLE
Effects of Surface Roughness and Vortex Generators on the LS(1)-0417MOD Airfoil

5. FUNDING NUMBERS
C:
TA: WE618120

6. AUTHOR(S)
R. L. Reuss, M. J. Hoffmann, G. M. Gregorek

7. PERFORMING ORGANIZATION NAME(S) AND ADDRESS(ES)
Dr. Gerald Gregorek
The Ohio State University
Aero & Astronautical Research
2300 West Case Road
Columbus, Ohio 43220
(614) 292-5491

8. PERFORMING ORGANIZATION REPORT NUMBER

9. SPONSORING/MONITORING AGENCY NAME(S) AND ADDRESS(ES)
National Renewable Energy Laboratory
1617 Cole Blvd.
Golden, CO 80401-3393

10. SPONSORING/MONITORING AGENCY REPORT NUMBER
TP-442-6474
DE96000495

11. SUPPLEMENTARY NOTES
NREL Technical Monitor: C. P. Butterfield

12a. DISTRIBUTION/AVAILABILITY STATEMENT
National Technical Information Service
U.S. Department of Commerce
5285 Port Royal Road
Springfield, VA 22161

12b. DISTRIBUTION CODE
UC-1211

13. ABSTRACT *(Maximum 200 words)*

An 18-inch constant-chord model of the LS(1)-0417MOD airfoil section was tested under two dimensional steady state conditions in the Ohio State University 7x10 Subsonic Wind Tunnel. The objective was to document section lift and moment characteristics under various model and air flow conditions. Surface pressure data was acquired at -60° through +230° geometric angles of attack, at a nominal 1 million Reynolds number. Cases with and without leading edge grit roughness were investigated. The leading edge roughness simulated blade conditions in the field. Additionally, surface pressure data were acquired for Reynolds numbers of 1.5 and 2.0 million, with and without leading edge grit roughness; the angle of attack was limited to a -20° to 40° range.

In general, results showed lift curve slope sensitivities to Reynolds number and roughness. The maximum lift coefficient was reduced as much as 29% by leading edge roughness. Moment coefficient showed little sensitivity to roughness beyond 50° angle of attack, but the expected decambering effect of a thicker boundary layer with roughness did show at lower angles.

Tests were also conducted with vortex generators located at the 30% chord location on the upper surface only, at 1 and 1.5 million Reynolds numbers, with and without leading edge grit roughness. In general, with leading edge grit roughness applied, the vortex generators restored 85 percent of the baseline level of maximum lift coefficient but with a more sudden stall break and at a higher angle of attack than the baseline.

14. SUBJECT TERMS
wind energy; horizontal-axis wind turbine; wind tunnel test data; wind turbine airfoil

15. NUMBER OF PAGES

16. PRICE CODE

17. SECURITY CLASSIFICATION OF REPORT	18. SECURITY CLASSIFICATION OF THIS PAGE	19. SECURITY CLASSIFICATION OF ABSTRACT	20. LIMITATION OF ABSTRACT
Unclassified	Unclassified	Unclassified	UL